The Faculty of Science

DISSERTATION

Defence held on 13/10/2022 in St Andrews
to obtain the degree of

DOCTEUR DE L'UNIVERSITÉ DU LUXEMBOURG

EN PHYSIQUE

AND

DOCTOR OF PHILOSOPHY
AT THE UNIVERSITY OF ST ANDREWS

IN PHYSICS

by

Andreas Nicolai Bock MICHELSEN
Born on 7 May 1994 in Esbjerg (Denmark)

INDUCED SUPERCONDUCTIVITY IN A
QUANTUM HALL EDGE STATE

Dissertation defence committee

Prof. Dr Thomas Schmidt, dissertation
supervisor
Professor, Université du Luxembourg

Dr Bernd Braunecker, dissertation
supervisor
Lecturer, University of St Andrews

Dr Jonathan Keeling, Chairman
Reader, University of St Andrews

Prof. Dr Ludger Wirtz, Vice Chairman
Professor, Université du Luxembourg

Prof. Annica Black-Schaffer
Professor, Uppsala University

Prof. Teemu Ojanen
Professor, Tampere University

Induced superconductivity in a quantum Hall edge state

Andreas Nicolai Bock Michelsen

University of
St Andrews

This thesis is submitted in partial fulfilment for the degree of

Doctor of Philosophy (PhD)

at the University of St Andrews

September 2022

Candidate's declaration

I, Andreas Nicolai Bock Michelsen, do hereby certify that this thesis, submitted for the degree of PhD, which is approximately 45,000 words in length, has been written by me, and that it is the record of work carried out by me, or principally by myself in collaboration with others as acknowledged, and that it has not been submitted in any previous application for any degree. I confirm that any appendices included in my thesis contain only material permitted by the 'Assessment of Postgraduate Research Students' policy.

I was admitted as a research student at the University of St Andrews in October 2018.

I received funding from an organisation or institution and have acknowledged the funder(s) in the full text of my thesis.

27/8 2022
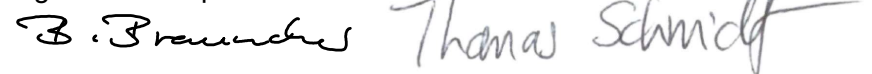
Date

Signature of candidate

Supervisor's declaration

I hereby certify that the candidate has fulfilled the conditions of the Resolution and Regulations appropriate for the degree of PhD in the University of St Andrews and that the candidate is qualified to submit this thesis in application for that degree. I confirm that any appendices included in the thesis contain only material permitted by the 'Assessment of Postgraduate Research Students' policy.

Date
25/8/2022

Signature of supervisor

Permission for publication

In submitting this thesis to the University of St Andrews we understand that we are giving permission for it to be made available for use in accordance with the regulations of the University Library for the time being in force, subject to any copyright vested in the work not being affected thereby. We also understand, unless exempt by an award of an embargo as requested below, that the title and the abstract will be published, and that a copy of the work may be made and supplied to any bona fide library or research worker, that this thesis will be electronically accessible for personal or research use and that the library has the right to migrate this thesis into new electronic forms as required to ensure continued access to the thesis.

I, Andreas Nicolai Bock Michelsen, confirm that my thesis does not contain any third-party material that requires copyright clearance.

The following is an agreed request by candidate and supervisor regarding the publication of this thesis:

Printed copy

No embargo on print copy.

Electronic copy

No embargo on electronic copy.

27/8 2022

Date   Signature of candidate

Date   Signature of supervisor

23/8/2022

Underpinning Research Data or Digital Outputs

Candidate's declaration

I, Andreas Nicolai Bock Michelsen, hereby certify that no requirements to deposit original research data or digital outputs apply to this thesis and that, where appropriate, secondary data used have been referenced in the full text of my thesis.

27/8 2022

Date   Signature of candidate

Abstract

In the search for non-Abelian anyonic zero modes for inherently fault-tolerant quantum computing, the hybridized superconductor – quantum Hall edge system plays an important role. Inspired by recent experimental realizations of this system, we describe it through a microscopic theory based on a BCS superconductor with Rashba spin-orbit coupling and Meissner effect at the surface, which is tunnel-coupled to a spin-polarized integer or fractional quantum Hall edge. By integrating out the superconductor, we arrive at an effective theory of the proximitized edge state and establish a qualitative description of the induced superconductivity.

We predict analytical relations between experimentally available parameters and the key parameters of the induced superconductivity, as well as the experimentally relevant transport signatures. Extending the model to the fractional quantum Hall case, we find that both the spin-orbit coupling and the Meissner effect play central roles. The former allows for transport across the interface, while the latter controls the topological phase transition of the induced p-wave pairing in the edge state, allows for particle-hole conversion in transport for weak induced pairing amplitudes, and determines when pairing dominates over fractionalization in the proximitized fractional quantum Hall edge.

Further experimental indicators are predicted for the system of a superconductor coupled through a quantum point contact with an integer or fractional quantum Hall edge, with a Pauli blockade which is robust to interactions and fractionalization as a key indicator of induced superconductivity. With these predictions we establish a more solid qualitative understanding of this important system, and advance the field towards the realization of anyonic zero modes.

Acknowledgements

General acknowledgements

I would first like to thank my supervisors Thomas Schmidt and Bernd Braunecker for giving me the opportunity to work on this project, for their close collaboration on all the work I have done, and for the wisdom concerning physics, research and life that they have imparted on me. I would also like to thank my close collaborators Patrik Recher, Edvin Idrisov and Nathan Harshman for the countless invaluable insights they have shared with me.

I want to thank Johan Ekström, who has been a wonderful friend and indispensable companion inside and outside of academia since I met him on my first day in Luxembourg, as well as our common friends Nora Paulus and Nijat Hajikhanov, who made the years in Luxembourg into such an excellent adventure.

I also want to thank my friends in St. Andrews, in particular Stephanie Matern for letting me take over her job, accommodations and friends when I arrived, Mari Cole for teaching me proper English and playing jazz with me, as well as Tobias Boorman and Joe Winter for being great friends to share an office and a pint with. A very special thanks goes out to Kristín Björg Arnardóttir, without whom I would never have survived the pandemic, and whose heartfelt support forms the very foundation of this thesis.

Furthermore, I must thank my family and friends in Denmark for their support, for helping me maintain my connection to home, and for hosting me on my many trips there.

Finally, as almost half the work on this thesis was done during the COVID-19 pandemic, I would like to express my sincere gratitude to everyone mentioned above for helping me continue my work during lockdowns, travel restrictions and quarantines.

Research Data/Digital Outputs access statement

The work presented in this paper is theoretical. No data were produced, and supporting research data are not required.

Contents

Introduction

"The old particles were the particles of the problem, and the new particles are the particles of the solution."

Jainendra Jain on quasiparticles,
in Composite Fermions *(2007)*

In the theory of condensed matter physics one applies quantum mechanics to systems consisting of a number of atoms on the order of Avogadro's number $N_A \sim 10^{23}$. Since quantum mechanical descriptions become notoriously complicated for any system of more than a couple of particles, some clever ideas are needed to succeed. For systems whose characteristic behavior arises from the collective dynamics of many strongly interacting particles, one particularly valuable idea is that of the quasiparticle. Instead of describing the collective dynamics in terms of each individual constituent particle, one can sometimes arrive at a simpler description by assigning a quasiparticle to describe just the collective behavior. Perhaps the simplest case of this is the phonon, which embodies the vibrations of an ion lattice, while the description of a missing electron in the Fermi sea as a quasiparticle (hole) lies at the very foundation of semiconductor theory.

Among the more exotic examples, we find the part electron, part hole quasiparticle characteristic of superconductivity [1], and the Laughlin quasiparticle of the fractional quantum Hall (QH) effect, which can be accurately described as a fraction of an electron [2]. This includes the accumulation of a fractional phase under exchange [3–5], i.e.

$$\psi(x_1, x_2) = e^{i\phi}\psi(x_2, x_1),$$

with ϕ a fraction of the fermionic phase ϕ_F. While all actual particles must be either bosons with $\phi_B = 0$ or fermions with $\phi_F = \pi$, the fractional exchange phase lies between these cases in an example of the more general exchange statistics of anyonic quasiparticles, or anyons. As shown by Leinaas and Myrheim [6], for particles in one and two dimensions any exchange phase is permitted, hence the "any" in anyon. Actual particles must exist in three dimensions, but quasiparticles are under no such obligation.

An important distinction is that between Abelian and non-Abelian anyons. In group theory, these labels refer to groups whose binary operation commutes (Abelian) or does not commute (non-Abelian). Similarly, there are Abelian anyons whose exchange simply
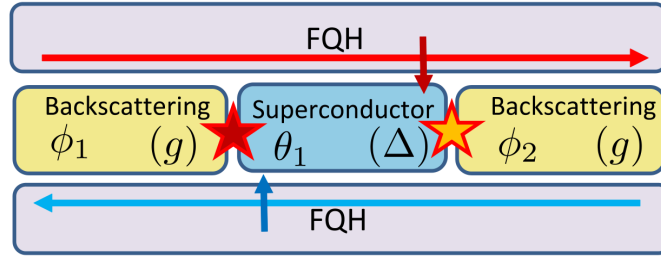
Figure 1.1: *A system of counter-propagating fractional QH edge states with a gap induced by either backscattering or superconductivity. At the domain wall between these topologically distinct gaps, the system is predicted to host non-Abelian zero modes (marked with stars) with generalized exchange statistics. Reproduced from Ref. [16].*

accumulates a phase, meaning exchanges commute, and non-Abelian anyons whose exchange amounts to a rotation within a degenerate subspace, meaning exchanges generally do not commute [7]. The experimental realization of non-Abelian anyons has been a topic of widespread interest since it was predicted that certain non-Abelian systems could form inherently fault-tolerant qubits [7,8]. In addition to academic efforts, the realization of qubits through non-Abelian anyons is currently also a key element in major industrial pursuits of large-scale quantum computing [9].

The main system of interest in the pursuit of non-Abelian anyons is one hosting domain walls between topologically distinct regions with gapped dispersions [10,11]. During the transition from one gapped system to another, the topological distinction forces a closing of the gap at the border between the systems. This implies the existence of localized degenerate states with zero energy at this border, also known as zero modes. These are protected from noise and perturbations, since breaking the degeneracy would require a breakdown of the topological distinction between the two regions.

To fully localize the zero modes, it is useful to use systems which are effectively one-dimensional, and whose domain walls are point-like. A useful source of such states is the QH effect, where a strong magnetic field causes a two-dimensional conductor to become insulating in the bulk with a persistent, chiral current running around the edge. This edge state is effectively one-dimensional and extremely robust to impurities in the material. Due to its chirality, a gap can only be induced in the coupling of two counter-propagating edges states, which can still be separated by a narrow trench. The topological nature of the gap can then be controlled by what material is in that trench.

In the simple case that they are separated by vacuum, tunneling across the trench will allow the states to backscatter, effectively hybridizing the two chiral states. The induced gap can be topologically distinguished from that of a superconductor (SC), which is due to the hybridization of particle and hole states. Thus, if we can make a segment of the QH edge superconducting, we would expect a zero mode between the superconducting region and the backscattering region. The superconducting QH edge can be achieved by placing a SC in the trench and taking advantage of the proximity effect, where the surface of the normal conductor near the interface experiences induced superconductivity due to its proximity to the SC. The result is a hybridization of the SC and normal conductor states, where we say that the normal conductor is proximitized. This effect has been theoretically known for decades [12], but the introduction of a strong magnetic field in order to induce the QH effect in the normal conductor complicates matters [13–15].

2

The system we have just described, and which is sketched in Fig. 1.1 for fractional QH edges, has indeed been predicted to host non-Abelian zero modes at the domain walls [16]. For edge states caused by the integer QH effect, these zero modes correspond to Majorana fermions, while for edge states caused by the fractional QH effect, the degeneracy increases, and the zero modes correspond to the more general parafermions [17]. Only recently has such systems become experimentally available, with fabrication techniques having improved enough that it is now possible to interface materials where a clear coexistence of superconductivity and QH effect is observed, along with transport across the interface [18–27]

The main focus of this thesis is the development of a theory which predicts the experimentally observed proximity effect from well-understood models of the SC and the QH effect in a framework which applies to both the integer and fractional QH effects. In addition to that, we will present various experimental signatures of induced superconductivity in a fractional QH edge, something which was only very recently achieved [27].

The system we will treat is that of a single edge state coupled to a SC, which in itself does not host any zero modes, but the understanding of which is an important element in understanding the composite system hosting zero modes. We will analytically predict how the experimental signatures of the proximity effect depends on parameters characterizing the constituent systems, such as the order parameter of the SC and the Landau level separation in the QH system. By doing this, we seek to further the understanding of how the hybridized SC-QH edge state depends on the presence of various underlying mechanisms including spin-orbit coupling and the Meissner effect, and to contribute with a deeper qualitative understanding of the problem, adding to the highly illuminating numerical and phenomenological treatments found in the literature [28–32].

Outline

The thesis is structured as follows.

In **Chapter 2** we introduce most of the background material needed to follow the thesis. The integer and fractional QH effects are described, and the BCS model in the presence of a strong magnetic field is discussed.

In **Chapter 3** the model of the integer QH-SC interface is presented, and reduced to an effective theory of the proximitized integer QH edge by integrating out the SC. The effective model is discussed with a focus on particle-hole mixing.

Chapter 4 consists of transport calculations involving the effective model. A carefully derived scattering formalism for particles and holes is used to predict the conditions for negative downstream resistance, which is a key experimental indicator of the proximity effect.

Chapter 5 extends the effective model to the case of the fractional QH edge state through the framework of a Tomonaga-Luttinger liquid. The effective pairing Hamiltonian is derived in terms of the bosonic fields of the Tomonaga-Luttinger liquid, and the derivation of transport signatures is sketched.

In **Chapter 6** we present work on the different system of a SC and a QH edge contacted through a point contact. A phenomenological model from the literature is used to derive the current and noise characteristics of the system.

Finally, in **Chapter 7** we conclude on the work presented.

List of publications

This thesis is based on the following papers co-authored by myself:

- Ref. [33]: A. B. Michelsen, T. L. Schmidt, E. G. Idrisov, *Current correlations of Cooper-pair tunneling into a quantum Hall system*, Phys. Rev. B **102** 125402 (2020)

- Ref. [34]: A. B. Michelsen, P. Recher, B. Braunecker, T. L. Schmidt, *Supercurrent-enabled Andreev reflection in a chiral quantum Hall edge state*, preprint under review with Phys. Rev. Research

Furthermore, the following paper was published during my work on this thesis, but is not included in the thesis itself:

- Ref. [35]: A. B. Michelsen, M. Valiente, N. T. Zinner, A. Negretti, *Ion-induced interactions in a Tomonaga-Luttinger liquid*, Phys. Rev. B **100** 205427 (2019)

Acronyms

2DEG two-dimensional electron gas

QH quantum Hall

SC superconductor

SOC spin-orbit coupling

Macroscopic quantum states

The main system of concern in this thesis consists of two elements: a material exhibiting the quantum Hall (QH) effect, and a superconductor (SC). Both of these are examples of "macroscopic quantum states", in the sense that they are both expressions of a macroscopic number of electrons condensing into a degenerate ground state at low temperatures.

To construct a model describing the hybridization of these two systems, we will start by modeling them separately, and then investigate the consequences of coupling them. This chapter will summarize the background material required to construct the separate models. In the case of the QH system, we will start by considering a finite two-dimensional electron gas (2DEG) in a strong magnetic field, which is a simple model of an integer QH system with a few important subtleties. The SC model will be based on the BCS model [36], which will be discussed in the context of an externally applied magnetic field. The models we present will generally be assumed to be at zero temperature.

2.1 A two-dimensional electron gas in a strong magnetic field

The quantization of conductance in a 2DEG in a strong magnetic field at low temperatures due to the QH effect is a startling example of quantization of a macroscopic observable robust to material impurities. So robust and exact is this quantization that it plays a fundamental role in the new SI unit definitions implemented in 2019 [37].

In this section we derive the quantum mechanical origin of the integer QH effect, and introduce important concepts and quantities for the following chapters. The fractional QH effect will not be treated until Chapter 5. Further reading on the integer QH effect can be found in sections 3.1, 3.2 and 14.1 of Ref. [38].

Let us first consider the case of an infinite plane of free electrons with a strong perpendicular magnetic field pointing out of the plane. We assume the field is strong enough to polarize the spins of the electrons in the up direction. The Hamiltonian of a non-relativistic electron with charge $-e$ moving in two dimensions in a perpendicular magnetic field of positive strength B_0 is given by minimal coupling

$$H_{\text{2DEG}} = \frac{1}{2m_e}\Big(\mathbf{q} + e\mathbf{A}\Big)^2, \tag{2.1}$$

where the square is in the sense of a dot-product, m_e is the electron mass, $\mathbf{q}$ is the two-dimensional momentum operator, and $\mathbf{A}$ is the vector potential. Note that we have chosen units where $\hbar = c = 1$. Let the magnetic field be uniform such that $\nabla \times \mathbf{A} = B_0 \mathbf{e}_z$, where $\mathbf{e}_z$ is the unit vector along the z-axis. We can freely choose the gauge of the vector potential, but the simplest choice is a gauge which reflects the geometry of the physical system. Since we will later introduce a straight edge, we will choose the Landau gauge

$$\mathbf{A} = -B_0(y - y_0)\mathbf{e}_x, \tag{2.2}$$

which leaves the Hamiltonian translationally invariant along the x-axis. The constant y_0 represents a remaining gauge freedom which will be fixed later. In this gauge, the x-momentum q_x is a good quantum number, and we can replace the operator with the eigenvalue in the Hamiltonian. We define the magnetic length

$$\ell \overset{\text{def}}{=} \sqrt{\frac{1}{eB_0}}, \tag{2.3}$$

which is the characteristic length scale of the system, and rewrite the Hamiltonian as

$$H_{\text{2DEG}} = \frac{1}{2m}\left[q_y^2 + \left(q_x - \frac{y - y_0}{\ell^2} \right)^2 \right]. \tag{2.4}$$

This is the Hamiltonian of a harmonic oscillator along the y-axis with frequency

$$\omega_c \overset{\text{def}}{=} \frac{eB_0}{m_e} = \frac{1}{\ell^2 m_e}, \tag{2.5}$$

which is also known as the cyclotron frequency. The evenly spaced eigenvalues of the Hamiltonian

$$E_n = \left(n + \frac{1}{2} \right)\omega_c, \qquad n = 0, 1, 2 \dots \tag{2.6}$$

are known as the Landau levels. An important characteristic of them is the lack of dependence on q_x, meaning that for a macroscopic number of allowed values of q_x, each level has a macroscopic degeneracy in q_x.

We can understand the role of the quantum number q_x better by looking at the Hamiltonian in Eq. (2.4). Here, q_x enters into the second term which acts as a harmonic potential centered around the *guiding center coordinate*

$$Y_{\text{gc}} \overset{\text{def}}{=} q_x \ell^2 + y_0. \tag{2.7}$$

The eigenfunctions of the Hamiltonian are [38],

$$\psi_{n,q_x}(x, y) = \frac{1}{\sqrt{2^n n!}(\pi \ell^2)^{1/4}} e^{iq_x x - \frac{1}{2}\left(\frac{y - Y_{\text{gc}}(q_x)}{\ell} \right)^2} H_n\left(\frac{y - Y_{\text{gc}}(q_x)}{\ell} \right), \tag{2.8}$$

where H_n is the nth Hermite polynomial. As we might have expected, they are plane waves along the x-dimension and exhibit Gaussian localization around Y_{gc} in the y-dimension. The intertwining of a state's y-position and x-momentum q_x will play an important role in our modeling of the edge interface.
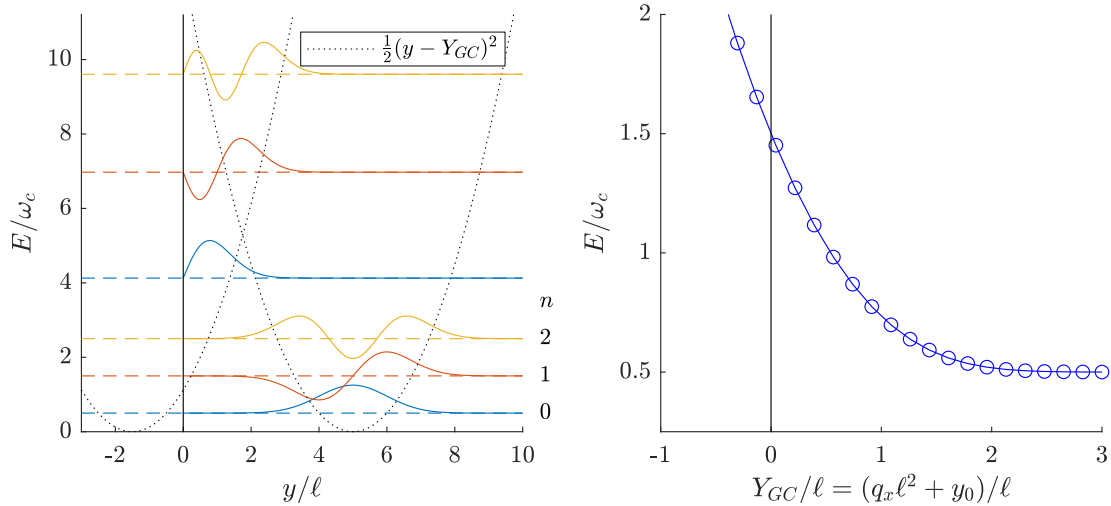
Figure 2.1: *Left: Numerical solutions to Eq. (2.9) with a hard wall at $y = 0$ (black line) for $n = 0, 1, 2$ at $Y_{gc} = -1\ell$ (edge state) and $Y_{gc} = 5\ell$ (bulk state). The dotted lines indicate the corresponding harmonic potential. Right: Dispersion relation corresponding to the numerical solutions for $n = 0$ (blue circles) with linear interpolation. See also the supplemental material of Ref. [41].*

2.2   Edge states

Let us now introduce an edge along the x-axis at $y = 0$, letting the 2DEG take up the semi-infinite plane of $y > 0$, with vacuum in the rest of space. In the laboratory, the 2DEG would naturally be finite in all dimensions, but we can assume that the dimensions of the 2DEG are much larger than ℓ, meaning the edges will not directly affect each other. We modify the Hamiltonian to include an edge potential, and rewrite it in terms of ℓ and ω_c,

$$H_{\text{2DEG}} = \frac{\omega_c}{2}\left[(q_y\ell)^2 + \frac{(y - Y_{\text{gc}})^2}{\ell^2}\right] + V_{\text{edge}}(y), \tag{2.9}$$

where the edge is a hard wall

$$V_{\text{edge}}(y) = \begin{cases} 0 \text{ for } y \geq 0, \\ \infty \text{ otherwise.} \end{cases} \tag{2.10}$$

The general problem of a harmonic potential with a barrier has been solved numerically, while the specific problem of an infinite barrier at the center of a harmonic potential (corresponding to $Y_{\text{gc}} = 0$) has been solved analytically [39, 40]. The solutions to the latter problem turn out to be the odd-n harmonic oscillator states of Eq. (2.8), which all have a node at the center of the potential, and thus obey the boundary condition of the hard wall.

We can develop an intuitive understanding of the effect of the edge by numerically calculating the y-dimension eigenvalues and eigenfunctions using the renormalized Numerov method, see Appendix A. As shown on the left of Fig. 2.1, the bulk eigenfunctions are simply the harmonic oscillator eigenfunctions, while the introduction of a hard edge "squeezes" the eigenfunctions and increases their energy. The energy eigenvalues for different values of q_x (or equivalently, different Y_{gc}) are shown on the right.

In other words, the presence of an edge induces a smooth, upwards curve in energy eigenvalues for states whose guiding center coordinate approaches the edge. Due to
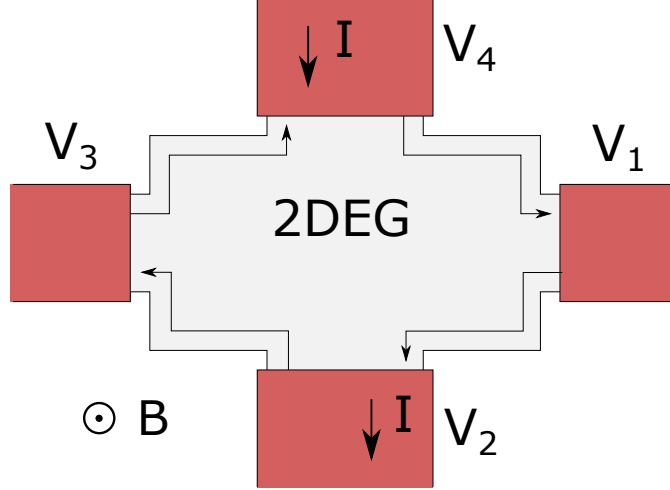
Figure 2.2: *An example of an experimental setup for measuring Hall conductance. Leads 1 and 3 are voltage leads, while leads 2 and 4 are current leads.*

the connection between Y_{gc} and q_x, the same upwards curve is found in the dispersion $E_n(q_x)$. If we consider the group velocity $v_g = \partial_{q_x} E(q_x)$, we see a remarkable feature of the quantum Hall effect: the bulk is insulating, $v_g = 0$, while the edge states carry a persistent current due to them all having $v_g < 0$. Since the above analysis applies to all sides of a real 2DEG, this current loops back around, and the material naturally remains charge neutral. However, this edge current has the peculiar feature that the electrons move without resistance, even in the presence of disorder. This ballistic transport of particles can be explained by the fact that for energies between the Landau levels there are no modes for the electron to backscatter into when they encounter impurities. The bulk allows no states with this energy, and the counter-propagating states are macroscopically far away, on the other side of the 2DEG. As we will see, this chiral transport of ballistic electrons around the edge of the 2DEG is what gives rise to the iconic quantization of conductance in the quantum Hall effect.

2.3 Transport through a QH system

Consider the setup presented in Fig. 2.2, where a 2DEG in a strong magnetic field is contacted with four terminals, with an applied current I passing from terminal 4 to terminal 2. Assuming that the current passes through M ballistic channels, we have the relation [42]

$$I = M\frac{e^2}{h}(V_4 - V_2), \tag{2.11}$$

where we have re-introduced the Planck constant for clarity. We can count the number of channels by counting the number of filled Landau levels: each filled Landau level adds one edge mode, with higher levels adding modes deeper in the bulk. Labeling the number of filled Landau levels as ν, also known as the filling factor, we conclude that the transversal resistance, or Hall resistance, as measured between terminals 1 and 3 will be $R_{13} = (V_3 - V_1)/I = h/(\nu e^2)$, while the longitudinal resistance as measured for example between terminals 2 and 3 must be zero, $R_{23} = 0$, due to the ballistic nature of the edge channels. Experimentally, this is indeed what is seen at very low temperatures ($\sim 1\text{K}$)
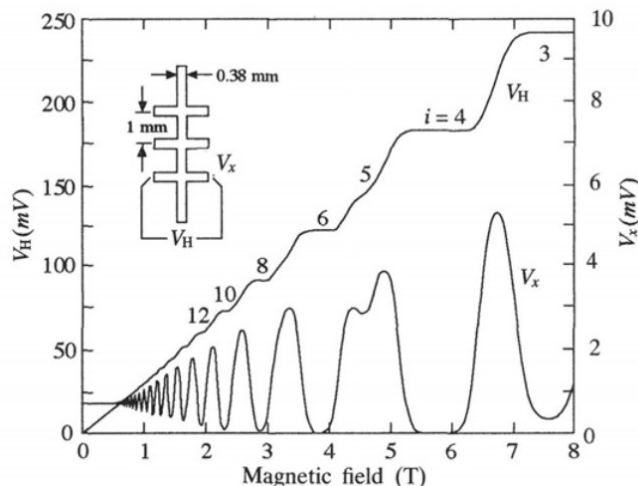
Figure 2.3: *Measurements of longitudinal and transverse voltages for a GaAs film showing QH plateaus at integer filling factors and temperature ∼ 1K. Reproduced from Ref. [44].*

and at strong magnetic fields, see Fig. 2.3. At higher temperatures, the quantization is lost due to electron-phonon scattering effects [43]. A more detailed discussion of transport through a QH system can be found in Chapter 3, where we will predict how these transport characteristics behave in the presence of superconducting correlations.

For samples of very high mobility and at very high magnetic fields [43], plateaus beyond the integer QH plateaus become visible, see Fig. 2.4. These occur at filling factors which are rational fractions, such as $\nu = 1/3$, and are clearly not accounted for by the theory presented thus far. Indeed, it turns out that one must allow for strong correlations between electrons to account for these fractional plateaus, as modeled by the wave function proposed by Laughlin [45], the Chern-Simons theory proposed by Wen [46] and beyond [38]. To an extent, these fractional states can be understood as collective electron states best described through fractional quasiparticles, with fractional charge and fractional exchange statistics. This makes the fractional QH edge an exciting candidate in the pursuit of parafermions, which can "borrow" the rich structure of the fractional edge state to go beyond the Majorana fermion.

Since we will not concern ourselves with the fractional QH edge until Chapter 5, further discussion on the matter can be found there.

2.4   The BCS superconductor model

Among the startling effects of materials at extremely low temperatures, perhaps the most well-known is superconductivity. For a wide range of materials, sufficiently strong cooling makes their electric resistance drop to zero, and sees them perfectly expelling any external magnetic fields. Such behavior is predicted in materials where the repulsive Coulomb interaction among electrons is competing with an attractive interaction, typically from electron-phonon coupling. At low temperatures, the attractive interaction wins out, causing a phase transition into superconductivity. This phase transition can be understood as electrons pairing up to form bosonic Cooper pair states, which can then condense into a degenerate ground state. Further reading on superconductivity can be found in Refs. [1, 47].
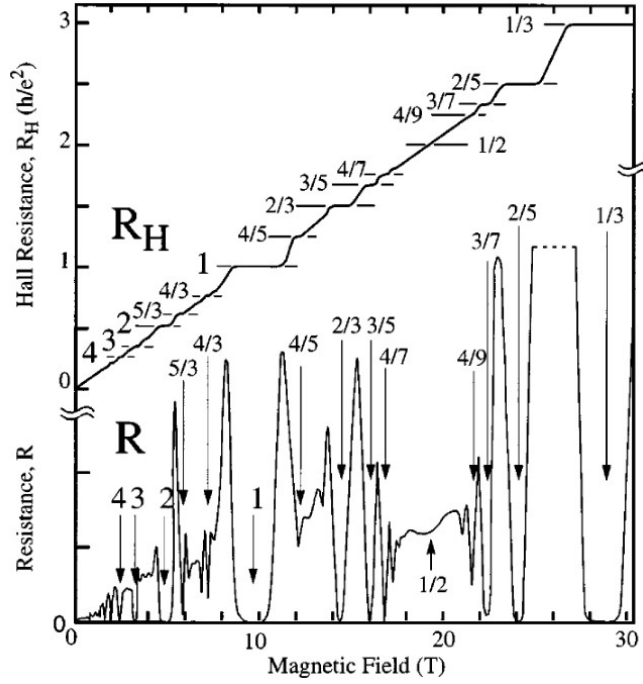
Figure 2.4: *Measurements of longitudinal and transverse resistance for a GaAs/AlGaAs heterojunction showing QH plateaus at fractional filling factors. Reproduced from Ref. [43].*

We will be modeling a SC exhibiting conventional superconductivity, where the attractive interaction between electrons is mediated primarily by phonons. This type of SC can be accurately modeled by the theory developed by Bardeen, Cooper and Schrieffer (BCS) [36]. They showed that by considering an interacting electron system under a mean-field approximation, superconductivity can be accounted for using the effective non-interacting second-quantization Hamiltonian

$$H_{\text{BCS}} = \sum_{\mathbf{k},\sigma} \left[\epsilon_{\mathbf{k}} c^{\dagger}_{\mathbf{k},\sigma} c_{\mathbf{k},\sigma} + \left(\Delta_0 c^{\dagger}_{\mathbf{k},\uparrow} c^{\dagger}_{-\mathbf{k},\downarrow} + \text{h.\,c.} \right) \right], \tag{2.12}$$

where $c_{\mathbf{k},\sigma}$ is the annihilation operator of an electron with momentum $\mathbf{k}$ and spin σ with kinetic energy

$$\epsilon_{\mathbf{k}} = \frac{\mathbf{k}^2}{2m_s} - \mu_s, \tag{2.13}$$

where m_s is the mass of the superconducting electrons and μ_s is the chemical potential. The complex superconducting order parameter Δ_0 generally depends on momentum, but in the simplest model it is assumed to be constant. At non-zero temperatures, the parameter indicates the phase of the system, only attaining non-zero values below a critical temperature.

An important signature of superconductivity is the mixing of particles and holes. For a non-superconducting system, we can write the free electron Hamiltonian as a free hole Hamiltonian by exchanging the electron fields and exploiting the symmetric summation over $\mathbf{k}$

$$H = \sum_{\mathbf{k},\sigma} \epsilon_{\mathbf{k}} c^{\dagger}_{\mathbf{k},\sigma} c_{\mathbf{k},\sigma} = \sum_{\mathbf{k},\sigma} -\epsilon_{-\mathbf{k}} c_{-\mathbf{k},\sigma} c^{\dagger}_{-\mathbf{k},\sigma} + \text{const.} \tag{2.14}$$
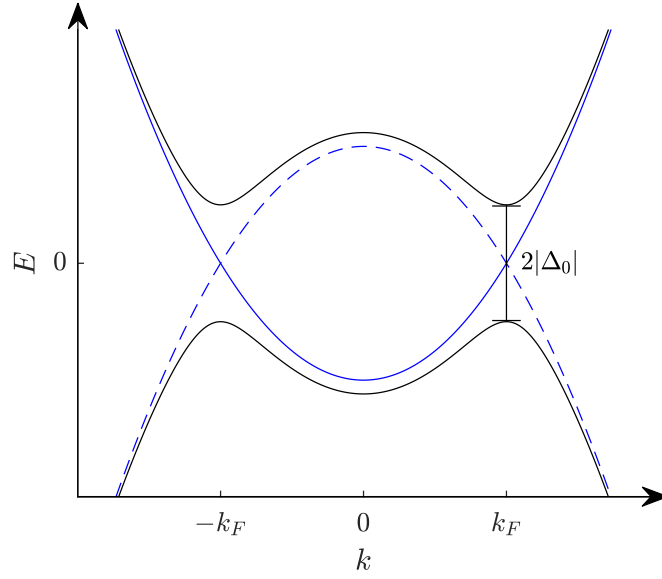
Figure 2.5: *The dispersion of the BCS Hamiltonian in Eq. (2.18) for zero Δ_0 (blue) and non-zero Δ_0 (black). Without superconductivity, the particle dispersion (full blue line) and hole dispersion (dashed blue line) are distinct. Non-zero Δ_0 opens an energy gap and hybridizes the particle and hole dispersions.*

If we interpret $c_{-\mathbf{k},\sigma}$ as the creation operator of a hole in the Fermi sea with kinetic energy $-\epsilon_{-\mathbf{k}}$, we see that describing the system in terms of holes and describing it in terms of particles are equivalent approaches up to a constant, which we can ignore as long as the energy scale is not fixed. Now let us diagonalize the BCS Hamiltonian Eq. (2.12) through the Bogoliubov transformation

$$\begin{pmatrix} \gamma_{\mathbf{k},1} \\ \gamma^{\dagger}_{-\mathbf{k},2} \end{pmatrix} = \begin{pmatrix} u^{*}_{\mathbf{k}} & -v_{\mathbf{k}} \\ v^{*}_{\mathbf{k}} & u_{\mathbf{k}} \end{pmatrix} \begin{pmatrix} c_{\mathbf{k},\uparrow} \\ c^{\dagger}_{-\mathbf{k},\downarrow} \end{pmatrix}, \tag{2.15}$$

where $u_{\mathbf{k}}, v_{\mathbf{k}}$ are complex numbers with amplitudes,

$$|u_{\mathbf{k}}|^2 = \frac{1}{2}\left(1 + \frac{\epsilon_{\mathbf{k}}}{\sqrt{\epsilon_{\mathbf{k}}^2 + |\Delta_0|^2}}\right), \tag{2.16}$$

$$|v_{\mathbf{k}}|^2 = \frac{1}{2}\left(1 - \frac{\epsilon_{\mathbf{k}}}{\sqrt{\epsilon_{\mathbf{k}}^2 + |\Delta_0|^2}}\right), \tag{2.17}$$

and phases such that $\arg(u_{\mathbf{k}}) + \arg(v_{\mathbf{k}}) = \arg(\Delta_0)$. This results in the diagonal Hamiltonian

$$H_{\text{BCS}} = \pm \sum_{\mathbf{k},j=1,2} \sqrt{\epsilon_{\mathbf{k}}^2 + |\Delta_0|^2}\, \gamma^{\dagger}_{\mathbf{k},j}\gamma_{\mathbf{k},j}. \tag{2.18}$$

The dispersion $E_{\text{BCS}}(\mathbf{k}) = \pm\sqrt{\epsilon_{\mathbf{k}}^2 + |\Delta_0|^2}$ is plotted in Fig. 2.5 both for the superconducting and non-superconducting cases, with the negative dispersion corresponding to an exchange of the γ operators. We see that the quasiparticles given by the operator $\gamma_{\mathbf{k}}$ are

11
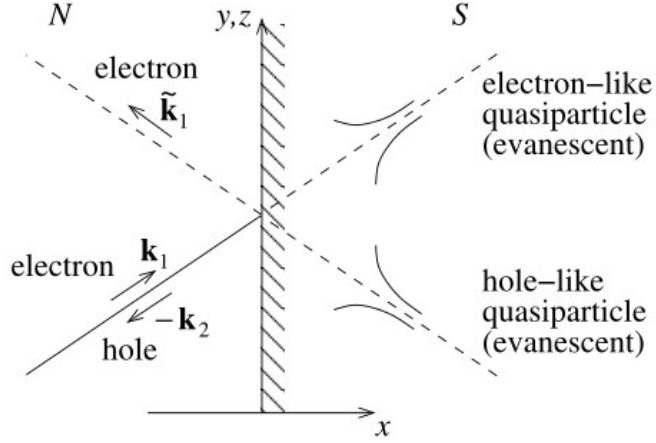
Figure 2.6: *An electron wave impinging from the N side on an NS interface at energies within the SC gap is either reflected normally, or reflected as a hole through Andreev reflection. Reproduced from Ref. [1].*

superpositions of particles and holes. Specifically, for $|\Delta_0| = 0$, we see that

$$\gamma_{\mathbf{k},1} \propto \begin{cases} c_{\mathbf{k},\uparrow} \text{ for } \epsilon_{\mathbf{k}} > 0, \\ c^\dagger_{-\mathbf{k},\downarrow} \text{ for } \epsilon_{\mathbf{k}} < 0. \end{cases} \tag{2.19}$$

That is, if we define the amplitude $k = |\mathbf{k}|$ and the Fermi momentum $k_F = \sqrt{2m_s\mu_s}$, the operator $\gamma^\dagger_{\mathbf{k}}$ creates a hole if $k < k_F$ and creates an electron if $k > k_F$. However, for non-zero Δ_0 we see a smooth interpolation between the two cases, with perfect mixing between electron and hole at $k = k_F$. As we can see in Fig. 2.5, the hybridization between electron and hole states leads to avoided crossings between the particle and hole dispersions, opening up an energy gap of width $|\Delta_0|$ from zero. Throughout the thesis, the order parameter Δ_0 may be referred to as the SC gap or the pairing amplitude, depending on context.

At energies within the gap there are no single electron states. All the electrons have paired up and condensed into a collective state, and it requires an energy of at least $2|\Delta_0|$ to break up such a Cooper pair. At energies $E > |\Delta_0|$ we find quasiparticle states consisting of electron/hole mixtures, and for $E \gg |\Delta_0|$ the states are almost entirely electron-like.

2.4.1 The NS junction

To accurately model transport between a normal system (N) and a superconducting system (S), i.e. across an NS junction, the quasiparticle nature of the SC excitations must be taken into account. In the framework of single particle mechanics, such transport was modeled by Blonder, Tinkham and Klapwijk [48] using a generalized semiconductor model. An important result from this work is the process of Andreev reflection. At energies within the gap, a single electron wave function impinging from the N side onto an NS junction is forbidden from transmitting into the superconductor by the lack of single electron states. It does, however, still transmit evanescently into the SC, which results in a non-zero amplitude of being reflected as a hole rather than an electron in a process known as Andreev reflection, see Fig. 2.6. The fact that the process changes the total charge on the N side by $2e$ hints at the physical interpretation: the impinging

electron is absorbed into the SC condensate along with another electron, forming a Cooper pair.

The amplitude of this process can be found by wave-matching across the interface, i.e. by solving the Schrödinger equation on both sides of the interface and requiring continuity of the wave function [49]. For example, with an interface at $y = 0$ and the wave functions $\psi_\pm(y)$ in the $y > 0$ and $y < 0$ regions, respectively, continuity of the wave function requires

$$\psi_+(0) = \psi_-(0). \tag{2.20}$$

This method has been applied to the case of a SC-QH interface in previous work [13, 14], but since this thesis considers a second quantization model of the interface, the method does not apply. It does, however, form the basis of the numerical Numerov method used to calculate the edge dispersion of the QH edge, see Fig. 2.1 and Appendix A, and will play an important role in Chapter 4 where we will consider the transport across an NSN junction, where a superconducting segment is found between to normal segments. As discussed in that chapter, however, under certain boundary conditions Eq. (2.20) does not hold, but is superseded by the requirement of continuity of the probability current across the junction, as implied by the unitary evolution of quantum states [50].

2.5 The London theory of SC electrodynamics

In the presence of an externally applied magnetic field $B_0\mathbf{e}_z$, a SC will expel the field such that no flux penetrates it in a case of perfect diamagnetism. For modeling the bulk of a BCS SC, one usually does not take magnetic effects into account, but since we will be considering the interface between a SC and a QH edge state, it is important to accurately model the surface of the SC. To do this, we must take the effects of the externally applied magnetic field into account, which we will do through a phenomenological theory of the electrodynamics of the SC, namely London theory [1]. Under the assumption that the electrons in the SC form a normal fluid with uniform density n_n and a superfluid with uniform density n_s, which is insensitive to scattering, the theory predicts the magnetic field

$$\mathbf{B}(y) = B_0 e^{y/\lambda}\mathbf{e}_z \tag{2.21}$$

for a SC taking up the half-space $y \leq 0$, where λ is the London penetration depth

$$\lambda \overset{\text{def}}{=} \sqrt{\frac{m_s}{4\pi e^2 n_s}}. \tag{2.22}$$

In other words, the magnetic field is exponentially suppressed inside the SC with a characteristic length scale λ. To account for the magnetic field in the SC Hamiltonian, we will consider the vector potential $\mathbf{A} = \mathbf{A}_L$ in the London gauge [51],

$$\mathbf{A}_L(y) = -B_0\lambda e^{y/\lambda}\mathbf{e}_x \tag{2.23}$$

which is the unique gauge for which

$$\boldsymbol{\nabla} \cdot \mathbf{A_L} = 0, \tag{2.24}$$
$$\mathbf{A}_L = 0 \text{ in the SC bulk,} \tag{2.25}$$
$$\mathbf{A}_L \cdot \mathbf{n} = 0, \tag{2.26}$$

where $\mathbf{n}$ is the normal vector to the SC surface. This gauge has the unique property that $\mathbf{A}_L$ is directly related to the supercurrent density $\mathbf{j}_s$ through the London equation

$$\mathbf{j}_s = -\frac{n_s e^2}{m_s} \mathbf{A}_L. \tag{2.27}$$

From this we can see that the magnetic field induces a non-zero supercurrent at the SC surface, which vanishes exponentially with the magnetic field into the SC. This is the Meissner current which is responsible for the expulsion of the magnetic field.

We can now write up the position space BCS Hamiltonian in the presence of a magnetic field,

$$H_{\text{BCS}} = \sum_\sigma \int d^3\mathbf{r} \left[c_\sigma^\dagger(\mathbf{r}) \left(\frac{[-i\boldsymbol{\nabla} + e\mathbf{A}]^2}{2m_s} - \mu_s \right) c_\sigma(\mathbf{r}) + \left(\Delta_0 c_\uparrow^\dagger(\mathbf{r}) c_\downarrow^\dagger(\mathbf{r}) + \text{h. c.} \right) \right], \tag{2.28}$$

where $c_\sigma(\mathbf{r})$ annihilates an electron with spin σ at a point $\mathbf{r}$. At this point, it is practical to express the Meissner current in terms of the supercurrent carrier momentum $\mathbf{k}_s$, which relates to the current density as [47]

$$\mathbf{j}_s = \frac{n_s e}{m_s} \mathbf{k}_s, \tag{2.29}$$

which means $\mathbf{k}_s = -e\mathbf{A}_L$. Specifically, Eq. (2.23) implies

$$\mathbf{k}_s(y) = e B_0 \lambda e^{y/\lambda} \mathbf{e}_x, \tag{2.30}$$

for $y \leq 0$.

2.5.1 Surface current

Let us assume that we wish to describe the surface current in a region where the vector potential varies very slowly, i.e. that it changes on a length scale greater than the size of a Cooper pair, and thus the Cooper pair experiences an approximately constant vector potential. Concretely this would correspond to $\lambda \gg \xi$, where the superconducting coherence length ξ is the characteristic length scale of a Cooper pair [47]. Then we can approximate $\mathbf{A}(y) \simeq \mathbf{A}(0)$ near the edge, corresponding to a constant supercurrent momentum $\mathbf{k}_s = e B_0 \lambda \mathbf{e}_x$. Under this approximation, the Hamiltonian in Eq. (2.28) reduces to

$$H_{\text{BCS}}^{\text{surface}} = \sum_\sigma \int d^3\mathbf{r} \left[c_\sigma^\dagger(\mathbf{r}) \left(\frac{[-i\boldsymbol{\nabla} - k_s \mathbf{e}_x]^2}{2m_s} - \mu_s \right) c_\sigma(\mathbf{r}) + \left(\Delta_0 c_\uparrow^\dagger(\mathbf{r}) c_\downarrow^\dagger(\mathbf{r}) + \text{h. c.} \right) \right]. \tag{2.31}$$

Temporarily re-introducing hats to mark operators, the x-component of the kinetic energy term in the Hamiltonian is

$$\hat{c}_\sigma^\dagger(x) \left(\frac{(\hat{k}_x - k_s)^2}{2m_s} - \mu_s \right) \hat{c}_\sigma(x). \tag{2.32}$$

Let us then define the unitary transformation $\hat{U}(x) = e^{-i k_s \hat{x}}$ such that $\hat{U}^\dagger \hat{U} = 1$. We can then write Eq. (2.32) as

$$\hat{c}_\sigma^\dagger(x) \hat{U}^\dagger \hat{U} \left(\frac{(\hat{k}_x - k_s)^2}{2m_s} - \mu_s \right) \hat{U}^\dagger \hat{U} \hat{c}_\sigma(x). \tag{2.33}$$

Expanding $\hat{U}(x)$ we find

$$\hat{U}^\dagger(\hat{k}_x - k_s)\hat{U} = \hat{k}_x - k_s + [-ik_s\hat{x}, \hat{k}_x - k_s] + \frac{1}{2!}[-ik_s\hat{x}, [-ik_s\hat{x}, \hat{k}_x - k_s]] + \dots, \quad (2.34)$$

where $[\cdot, \cdot]$ is the commutator. Applying the canonical commutator $[\hat{x}, \hat{k}_x] = i$, we see that all the nested commutators in the expansion drop out, and we find

$$\hat{U}(\hat{k}_x - k_s)\hat{U}^\dagger = \hat{k}_x - k_s - ik_s[\hat{x}, \hat{k}_x] = \hat{k}_x. \quad (2.35)$$

Such a $\hat{U}$ is known as a shift operator, and we are using the fact that the position operator $\hat{x}$ is the generator of momentum translation, much like how momentum is the generator of position translation [50]. Once again dropping the hats, we can perform the unitary transformation $c_\sigma(\mathbf{r}) \to U(x)c_\sigma(\mathbf{r})$, after which the Hamiltonian Eq. (2.28) becomes

$$H_{\text{BCS}}^{\text{surface}} = \sum_\sigma \int d^3\mathbf{r} \left[c_\sigma^\dagger(\mathbf{r}) \left(-\frac{1}{2m_s}\boldsymbol{\nabla}^2 - \mu_s \right) c_\sigma(\mathbf{r}) + \left(\Delta_0 e^{2ik_s x} c_\uparrow^\dagger(\mathbf{r})c_\downarrow^\dagger(\mathbf{r}) + \text{h. c.} \right) \right]. \quad (2.36)$$

In other words, the current can be described through a plane wave factor on the SC pairing amplitude [47, 52]. Assuming translational invariance in x and z, as well as approximate translational invariance along $y < 0$, we can label the states by their momentum and Fourier transform the Hamiltonian to find

$$H_{\text{BCS}}^{\text{surface}} = \sum_{\delta\mathbf{k},\sigma} \left[\epsilon_{\mathbf{k}_s+\delta\mathbf{k}} c_{\mathbf{k}_s+\delta\mathbf{k},\sigma}^\dagger c_{\mathbf{k}_s+\delta\mathbf{k},\sigma} + \left(\Delta_0 c_{\mathbf{k}_s+\delta\mathbf{k},\uparrow}^\dagger c_{\mathbf{k}_s-\delta\mathbf{k},\downarrow}^\dagger + \text{h. c.} \right) \right], \quad (2.37)$$

where we have changed variables to $\delta\mathbf{k} = \mathbf{k} - \mathbf{k}_s$. This makes it clear that the Meissner current corresponds to pairing at the surface occurring between electrons with a total center-of-mass momentum of $2\mathbf{k}_s$.

2.5.2 Doppler shift

Diagonalizing Eq. (2.37) yields the dispersion

$$E_{\text{current},\pm}(\mathbf{k}) = \frac{\mathbf{k} \cdot \mathbf{k}_s}{m_s} \pm \sqrt{|\Delta_0|^2 + (\epsilon_{\mathbf{k}} + E_s)^2}, \quad (2.38)$$

where we have defined the supercurrent energy $E_s = k_s^2/(2m_s)$ which is usually small compared to μ_s and thus often ignored [47]. The dispersion is sketched in Fig. 2.7 with negative k_s. Comparing to Eq. (2.18), we see that the current has an important effect on the dispersion, namely the introduction of a term which is linear in $\mathbf{k}$. This term is known as the Doppler shift, and predicts the breakdown of superconductivity at applied magnetic fields beyond a critical field value B_c corresponding to high currents [53]. If we assume that $k_s \ll k_F$, we can ignore E_s and approximate the minimum energy of an excitation into the upper band as found at $k = k_F$, such that

$$\min\left(E_{\text{current},+}(\mathbf{k}) \right) = |\Delta_0| - \frac{k_F k_s}{m_s}. \quad (2.39)$$

When this minimum excitation energy is zero or negative, there are single particle states at all energies, and superconductivity has broken down, see Fig. 2.7. In particular, at

15
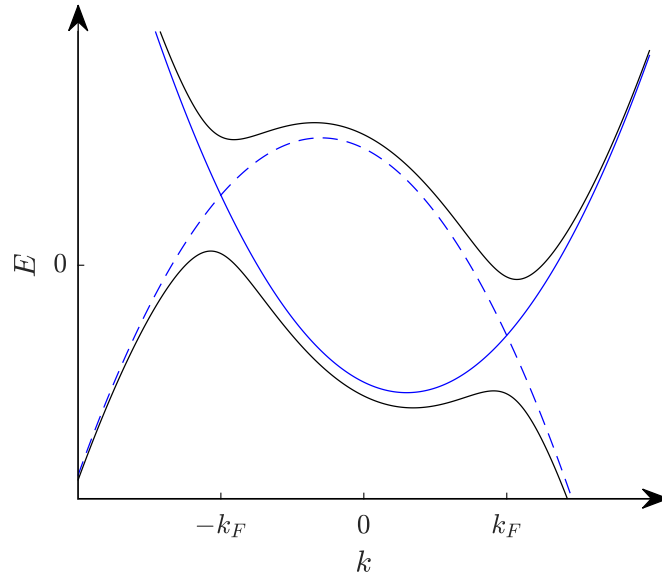
Figure 2.7: *The current induced by a magnetic field tilts the dispersion at the SC surface through the Doppler shift, see Eq. (2.38), with sufficiently large fields causing the gap to close as shown. The blue lines indicate the $\Delta_0 = 0$ case, with a full line for the electron dispersion, and a dashed line for the hole dispersion. The black line indicates the $\Delta_0 \neq 0$ case.*

this point single electron / hole tunneling into the SC would be allowed for any energy, suppressing Andreev reflection. To avoid this breakdown, we must then assume

$$k_s < \frac{|\Delta_0|m_s}{k_F}, \tag{2.40}$$

which guarantees a gap in the SC. This corresponds to assuming that the magnetic field is less than the critical field, $B_0 < B_c$ [47].

2.6   Summary

To model the hybridized SC-QH edge system, we first establish separate models for the QH edge and the SC. The integer QH state is derived from a 2DEG in a strong magnetic field, and we show that in the Landau gauge, the eigenstates are plane waves with well defined momentum q_x along the interface, and harmonic oscillator states in the y-direction, with the two dimensions connected through the fact that the guiding center coordinate Y_{gc} of the harmonic oscillator state is determined by the x momentum q_x. We show that introducing edges to the 2DEG causes chiral edge states to form, with backscattering suppressed by the macroscopic distance between the edges.

The transport characteristics of an QH system, i.e. quantized Hall resistance and zero longitudinal resistance, are described in terms of ballistic transport through these edge states. In later chapters we will see that the introduction of a superconductor changes these characteristics.

An s-wave SC is described through the BCS model, and the eigenstates are shown to be mixtures of particle-like states and hole-like states. This mixing will be the main mechanism behind induced superconductivity in the QH edge, as well as the main experimental indicator. At the SC-QH interface, transport can occur due to Andreev reflection, which causes an impinging electron to reflect as a hole.

The presence of a strong magnetic field induces a surface current in the SC due to the Meissner effect. This is described through the London theory of SC electrodynamics, and it is shown that it can be accounted for by considering the electron pairing at the SC surface to happen for electron states with a center-of-mass momentum $k_s = eB_0\lambda$. This causes a Doppler shift of the gapped SC dispersion at the surface, from which we deduce a limit on the SC momentum beyond which quasiparticle tunneling takes the place of Andreev reflection. Since we wish to model Andreev reflection, we will assume that the supercurrent momentum is beneath this limit, which will let us avoid unphysical singularities in the theory in the next chapter.

In the next chapter, the two systems will be coupled and an effective theory of the integer quantum Hall edge state with induced superconductivity will be derived.

Induced superconductivity in the integer quantum Hall state

We now turn our attention to the system sketched in Fig. 3.1 where a superconductor (SC) and a quantum Hall (QH) edge state hybridize through the proximity effect. We can understand the effect in a semiclassical picture, where electrons form skipping orbits along the edge of the two-dimensional electron gas (2DEG), and are converted into holes at the SC-QH interface due to Andreev reflection. In a more accurate quantum mechanical model, the QH edge state is a plane wave along the SC-QH interface, with the SC inducing superconducting correlations into the edge state resulting in mixing of particle and hole states [13,14]. In the previous chapter, we summarized the general theory behind an integer QH edge and a SC surface in the presence of a magnetic field. In this chapter we introduce the specific models of the two systems we will use to develop an effective theory of the QH edge with induced SC correlation. We introduce a specific analytical approximation of the QH edge dispersion, discuss the presence of spin-orbit coupling (SOC) at the SC surface, and couple the two systems through a tunneling coupling. We then integrate out the SC fields to arrive at an effective theory of the proximitized QH edge.
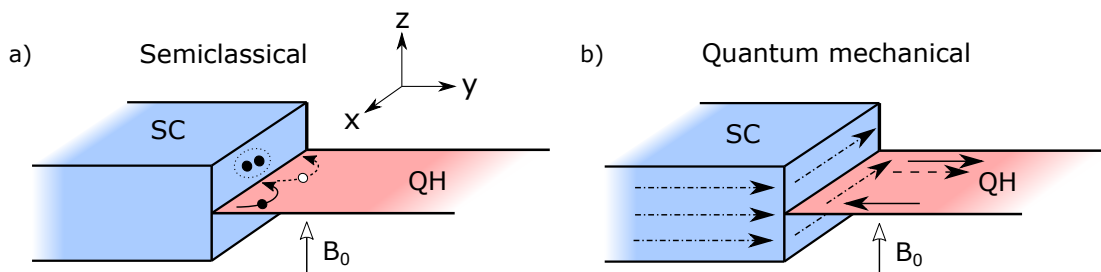
Figure 3.1: *A sketch of the QH-SC interface. a) In the semiclassical picture, electrons perform skipping cyclotron orbits along the edge of the QH due to the applied magnetic field. At the QH-SC interface, the electrons can reflect into holes through Andreev reflection. b) In the quantum mechanical picture, the QH edge state is a plane wave state oscillating between electron-like and hole-like states due to hybridization with the SC surface state. This may result in a hole being emitted at the end of the interface.*

3.1 The QH edge dispersion

We consider again the Hamiltonian of a free electron in a magnetic field with vector potential $\mathbf{A}$, see Eq. (2.1), but now with an added constant energy shift U_0,

$$H_{\text{2DEG}} = \frac{1}{2m_e}\left(\mathbf{q} + e\mathbf{A}\right)^2 + V_{\text{edge}}(y) - U_0, \tag{3.1}$$

where $V_{\text{edge}}(y)$ models a hard wall at $y = 0$. The energy shift U_0 allows us to explicitly account for constant shifts induced by the SC as we will see later. To develop a many-body Hamiltonian of the total SC-QH system, we need to transform this Hamiltonian into a second quantization Hamiltonian. Since the integer QH effect hosts quasi-one-dimensional spin-polarized electron edge states, we can model the lowest filling factor edge state through the Hamiltonian

$$H_{\text{edge}} = \sum_q E_q \psi_q^\dagger \psi_q, \tag{3.2}$$

where ψ_q is the annihilation operator of a spinless one-dimensional QH edge electron with momentum q, and E_q is the corresponding dispersion. As discussed in Section 2.2, this dispersion does not have an exact analytical form, but we can approximate it with one. To do this, we will first fix the gauge of the total vector potential of the system. In the SC region $y < 0$, we will use the London gauge

$$\mathbf{A}_{\text{SC}}(y) = -B_0 \lambda e^{y/\lambda} \Theta(-y)\mathbf{e}_x \tag{3.3}$$

where B_0 is the applied magnetic field, λ is the London penetration length and $\Theta(y)$ is the Heaviside step function. Meanwhile, in the QH region $y > 0$ we have the Landau gauge

$$\mathbf{A}_{\text{QH}}(y) = -B_0(y - y_0)\Theta(y)\mathbf{e}_x, \tag{3.4}$$

where y_0 is a remaining gauge freedom. Since $\mathbf{B} = \mathbf{\nabla} \times \mathbf{A}$, it is clear that the total vector potential formed by Eqs. (3.3) and (3.4) must have a continuous derivative to avoid unphysical skips in the magnetic field. This fixes the remaining gauge freedom to $y_0 = -\lambda$, yielding the total vector potential [14]

$$\mathbf{A}(y) = -B_0\left[\lambda e^{y/\lambda}\Theta(-y) + (y + \lambda)\Theta(y)\right]\mathbf{e}_x. \tag{3.5}$$

Upon fixing the gauge we then have that the QH states are centered around the guiding center coordinate in the y-dimension

$$Y_{\text{gc}} = q_x \ell - \lambda. \tag{3.6}$$

We can now formulate an analytical approximation of the QH state dispersion. Inspired by Ref. [41], we approximate the dispersion with a half-parabola. Given the magnetic length $\ell = \sqrt{1/(eB_0)}$ and the cyclotron frequency $\omega_c = eB_0/m$, we can assume that

- the approximate ground state dispersion goes as the square of q_x,

- that we have the exact solution $E = 3\omega_c/2 - U_0$ at $Y_{\text{gc}} = 0$ [40],
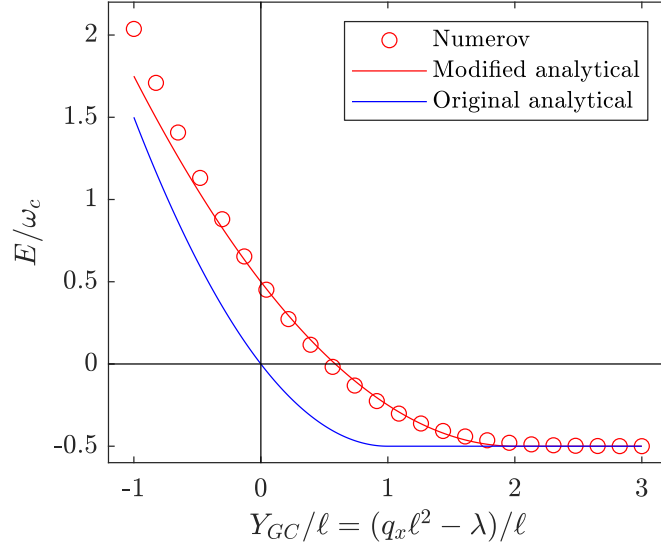
Figure 3.2: *The QH dispersion with $E_F = \omega_c/2$ as calculated numerically with the Numerov method (red circles), along with the analytical approximation of Ref. [41] (blue line) and the modified analytical approximation in Eq. (3.7) (red line).*

- that we reach the bulk solution $E = \omega_c/2 - U_0$ for $Y_{gc} > 2\ell$.

Under these assumptions we arrive at the approximation for the ground state energy band

$$E_q = \frac{\omega_c}{4\ell^2} \Theta\Big(2\ell - [q\ell^2 - \lambda]\Big)\Big(2\ell - [q\ell^2 - \lambda]\Big)^2 - E_F. \tag{3.7}$$

where we have fixed the energy shift

$$U_0 = \omega_c/2 + E_F, \tag{3.8}$$

such that the Fermi energy is measured relative to the bulk ground state energy $\omega_c/2$. The dispersion is shown in Fig. 3.2. There it is compared with the approximation from Ref. [41], which we have modified by the substitutions $\ell \to 2\ell$ inside the square and the Heaviside function, as well as $\omega_c/2\ell^2 \to \omega_c/4\ell^2$ as the front factor. The original expression fits numerical results well at large filling factors $E_F \gg \omega_c$, while our expression is more accurate the lowest filling factor $0 \le E_F \le \omega_c$. With this dispersion we can define the Fermi momentum such that $E_{q_F} = 0$, as well as the Fermi velocity

$$q_F(E_F) = \frac{2}{\ell}\left(1 + \frac{\lambda}{2\ell} - \sqrt{\frac{E_F}{\omega_c}}\right), \tag{3.9}$$

$$v_F(E_F) = \partial_q E_q|_{q=q_F} = -\ell\sqrt{E_F\omega_c} = -\sqrt{\frac{E_F}{m_e}}. \tag{3.10}$$

At this point one might be puzzled by the appearance of λ, which is a material-specific SC parameter, in Eqs. (3.7) and (3.9) which describe the QH edge. This is a consequence of the choice of gauge in Eq. (3.5). In particular, the gauge independent quantities E_F and v_F do not depend on λ.

In the rest of the chapter, as well as in Chapter 4, we will assume the QH edge to be described by the Hamiltonian in Eq. (3.2) which has the dispersion in Eq. (3.7) with

Fermi energy $0 \leq E_F \leq \omega_c$ corresponding to being at filling factor $\nu = 1$ and thus having a single edge state.

3.2 The SC surface

We consider the surface of a SC in a magnetic field as described by the Hamiltonian in Eq. (2.37), namely

$$H_{\text{BCS}}^{\text{surface}} = \sum_{\delta\mathbf{k},\sigma} \left[\epsilon_{\mathbf{k}_s+\delta\mathbf{k}} c_{\mathbf{k}_s+\delta\mathbf{k},\sigma}^\dagger c_{\mathbf{k}_s+\delta\mathbf{k},\sigma} + \left(\Delta_0 c_{\mathbf{k}_s+\delta\mathbf{k},\uparrow}^\dagger c_{\mathbf{k}_s-\delta\mathbf{k},\downarrow}^\dagger + \text{h. c.} \right) \right], \qquad (3.11)$$

where $c_{\delta\mathbf{k},\sigma}$ is the annihilation operator for a SC electron with momentum $\delta\mathbf{k}$ and spin σ, $\mathbf{k}_s$ is the supercurrent momentum, and we have the energy

$$\epsilon_{\mathbf{k}_s+\delta\mathbf{k}} = \frac{(\mathbf{k}_s + \delta\mathbf{k})^2}{2m_s} - \mu_s \qquad (3.12)$$

as well as the superconducting order parameter Δ_0. We recall that this Hamiltonian was derived under the assumption that the vector potential varies slowly within the relevant region. We will model the coupling between QH and SC as a tunnel coupling for energies within the SC gap, which involves the splitting of a Cooper pair into two electrons. The characteristic length scale of a Cooper pair is the superconducting coherence length ξ [47], and so we will consider the SC region $-\xi < y < 0$ as the relevant surface region in the context of tunneling. Then the Hamiltonian of Eq. (3.11) is a good approximation when $\lambda \gg \xi$. How well does that that correspond to the typical experimental situation?

The exact values of λ and ξ in an experimental context depend on many external parameters including temperature, pressure, crystallic structure of the material and the overall geometry, in particular the thickness of the SC [54, 55], but order-of-magnitude analysis is still feasible. If we consider the superconductor NbN at a thickness of ~ 100 nm, which is a high-field SC applied in key experiments on induced superconductivity in quantum Hall edge states [22, 27], it is estimated that it has a penetration length of $\lambda_{\text{NbN}} \sim 300$ nm [54–56], and a coherence length between $\xi_{\text{NbN}} \sim 5$ nm [56, 57] and $\xi_{\text{NbN}} \sim 50$ nm [22]. Another important SC material is MoRe [20, 24], where it is estimated that the penetration length is $\lambda_{\text{MoRe}} \sim 900$ nm [56], while the coherence length is between $\xi_{\text{MoRe}} \sim 8$ nm [56] to $\xi_{\text{MoRe}} \sim 160$ nm [24]. In conclusion, for comparable experiments we will expect λ to be no less than about an order of magnitude larger than ξ, meaning that between $y = 0$ and $y = -\xi$, the supercurrent momentum $k_s(y)$ should decrease less than 10%.

3.2.1 Spin-orbit coupling

In describing Andreev reflection through the model presented so far, we are facing an important issue. While the s-wave SC condensate consists of pairs of electrons with opposite spin, the QH edge is spin-polarized. For two QH edge electrons to pair up and enter the SC condensate, we require a physical process allowing the electrons to flip their spins [58]. A good candidate for such a mechanism is Rashba spin-orbit coupling (SOC), which is a coupling of spin and momentum with origins in the symmetries of low-dimensional systems [59]. The SOC may be inherent to the 2DEG [15]. However, the observation of induced superconductivity in a QH edge across a NbN-graphene

interface [22] motivates us to consider the situation where a 2DEG with vanishing SOC (graphene) inherits its spin-flip mechanism from a SC with strong SOC (NbN).

To model this situation, we follow Ref. [60], which models Rashba SOC at the x, z plane surface of a three dimensional s-wave SC through the Hamiltonian

$$H_{\text{SOC}} = \alpha \sum_k [k_z + ik_x] c^\dagger_{\mathbf{k},\uparrow} c_{\mathbf{k},\downarrow} + \text{h. c.,} \qquad (3.13)$$

where α is the real SOC amplitude with units of velocity. This Hamiltonian couples up and down spins at the SC surface, and upon shifting the momentum as discussed in Section 2.5.1 we arrive at the final description of the SC surface by adding it to Eq. (3.11),

$$H_{\text{sc}} = \sum_{\delta\mathbf{k},\sigma} \left[\epsilon_{\mathbf{k}_s+\delta\mathbf{k}} c^\dagger_{\mathbf{k}_s+\delta\mathbf{k},\sigma} c_{\mathbf{k}_s+\delta\mathbf{k},\sigma} + \left(\Delta_0 c^\dagger_{\mathbf{k}_s+\delta\mathbf{k},\uparrow} c^\dagger_{\mathbf{k}_s-\delta\mathbf{k},\downarrow} + \text{h. c.} \right) \right.$$
$$\left. + \left(\alpha[\delta k_z + i(\delta k_x + k_s)] c^\dagger_{\mathbf{k}_s+\delta\mathbf{k},\uparrow} c_{\mathbf{k}_s+\delta\mathbf{k},\downarrow} + \text{h. c.} \right) \right]. \quad (3.14)$$

In the rest of the chapter, as well as in Chapters 4 and 5, we will assume that this Hamiltonian describes the SC surface region relevant in a tunneling context.

3.3 Tunneling

Having presented models for both the QH edge and the SC, the final element needed is a coupling between the two systems. Modeling weak single-electron tunneling across the QH-SC interface within a limited range in the y and z dimensions allows us to describe the coupling between the edge state electrons and the SC condensate caused by Andreev reflection. We will assume the tunneling to be local in the fields $\psi(x), c(\mathbf{r})$ and that it conserves the spin of the electrons involved. Assuming without loss of generality that the QH edge is polarized in the spin up direction, the tunneling Hamiltonian is then given by

$$H_{\text{tunn}} = \gamma\sqrt{w_z w_y} \int_{-L_x/2}^{L_x/2} dx [\psi^\dagger(x) c_\uparrow(x, 0, 0) + \text{h. c.}]$$
$$= \Gamma \sum_{q,\mathbf{k}} \delta_{q,k_x} (\psi^\dagger_q c_{\mathbf{k},\uparrow} + \text{h. c.}), \qquad (3.15)$$

where the second line is the momentum space Hamiltonian resulting from a Fourier transform of the position space Hamiltonian on the first line. We have defined the effective tunneling amplitude

$$\Gamma = \gamma\sqrt{\frac{w_z w_y}{L_z L_y}} \qquad (3.16)$$

where γ is the tunneling amplitude in units of energy, $w_{y,z}$ are the effective tunneling ranges in the y and z directions, and $L_{y,z}$ are the total lengths of the SC in the y and z dimensions. The presence of the Kronecker delta δ_{q,k_x} means that the tunneling preserves the x-momentum of the electrons involved, which is implied by the assumption of local tunneling and translation invariance in the x direction.

It is worth pointing out that the Andreev reflection caused by this tunneling is qualitatively different from that typically described in single particle theories, and
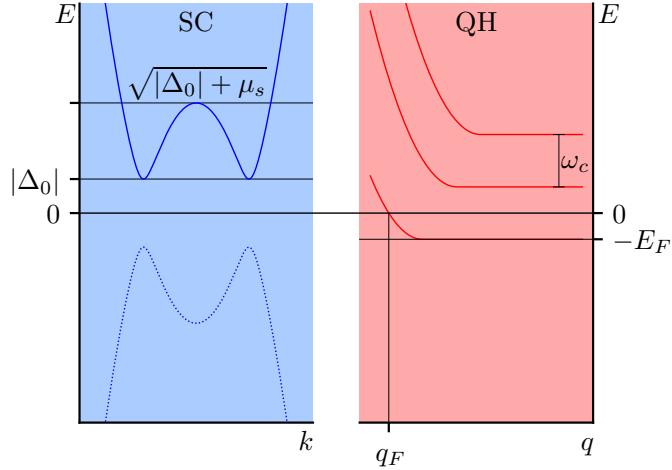
Figure 3.3: *The energy scales in the SC (blue) and QH (red) regions. All energies are measured with respect to the center of the SC gap. Energies are not to scale, e.g. $|\Delta_0| \ll \mu_s$.*

thus from the mechanism sketched in Fig. 2.6. In the single particle picture, Andreev reflection depends on the evanescent penetration of electron waves into the SC, an effect not described by the presented tunneling Hamiltonian. As explored in Chapter 4, this distinction will turn out to have a profound effect on the importance of the Meissner current at the SC surface, which only causes relatively minor corrections in the single particle picture [14, 15].

3.4 The full model

The full model of the QH-SC interface which will be treated in this and the following chapter then consists of the combined QH edge Hamiltonian in Eq. (3.2), the SC Hamiltonian in Eq. (3.14) and the tunneling Hamiltonian in Eq. (3.15),

$$H = H_{\text{edge}} + H_{\text{sc}} + H_{\text{tunn}}. \tag{3.17}$$

Before moving forward, it is worth considering the different energy scales involved in these Hamiltonians. We will measure all energies with respect to the center of the SC gap, with the main energy scales sketched in Fig. 3.3. At the top of the energy hierarchy, we have the SC chemical potential, which for a metallic SC is on the order of $\mu_s \sim 1\,\text{eV}$. Several orders of magnitude below that we have the SC gap with typical values of $|\Delta_0| \sim 1\,\text{meV}$. To model Andreev reflection, we must assume that the gap is large enough that the edge state does not couple to quasiparticle states beyond the gap. First of all, this implies that neither the Meissner current nor the Rashba SOC are strong enough to suppress the gap. The former corresponds to assuming

$$k_s \ll \frac{|\Delta_0| m_s}{k_F}, \tag{3.18}$$

as discussed in Section 2.5.2. The latter can be achieved by assuming $\alpha k_F \ll |\Delta_0|$, meaning that the SOC energy is small near the narrowest point of the gap $k = k_F$. The weak tunneling model presented in the previous section has its origins in a linear expansion in γ, which means we have implicitly assumed $\gamma \ll |\Delta_0|$, and thus $\Gamma \ll |\Delta_0|$ since $\gamma \geq \Gamma$.

24

In the QH region, the energy scale is determined by the applied magnetic field through $\omega_c = eB_0/m_e$. Experiments on induced superconductivity in a QH edge at filling factor $\nu = 1$ typically apply magnetic fields on the order of $B_0 \sim 10$ T [22, 24], yielding $\omega_c \simeq 1$ meV and $\ell \sim 1$ nm.

The assumption that the vector potential varies slowly corresponds to estimating

$$\mathbf{k}_s = \mathbf{A}(y = 0) = eB_0\lambda\mathbf{e}_x. \tag{3.19}$$

Assuming that the SC material is NbN or MoRe, we have $\lambda \sim 600$ nm as discussed in Section 3.2. Further assuming that the effective mass of the SC charge carrier is the electron mass, $m_s = m_e$, we can evaluate the assumption Eq. (3.18),

$$\frac{eB_0\lambda}{|\Delta_0|m_e/\sqrt{2m_e\mu_s}} \sim 10^3. \tag{3.20}$$

Thus, under the current assumptions the theory would predict that the applied magnetic field is far above the critical field B_c of the SC, which from Eq. (3.18) is predicted to be $B_c \sim 1$ mT. While Doppler-shift induced breakdown of superconductivity at this magnetic field scale has been observed for geometries of Nb SC's on a InAs 2DEG [61], it is clear that the theory does not capture the high-field behavior of the SC's which have been observed to induce superconductivity into the $\nu = 1$ QH state, which requires large fields. A central feature of the SC description is the assumption of homogeneity, both in the London theory which assumes uniform supercurrent carrier density n_s and the assumption that a slowly varying vector potential $\mathbf{A}$ is enough to assume plane wave solutions in the SC.

It is clear from this discussion that we should not expect accurate quantitative predictions of experimental outcomes from the theory as presented, but rather turn to it for phenomenological predictions whose scale should match experimental data given correctly adjusted effective parameters, such as a large effective mass in the SC $m_s \gg m_e$.

3.5 Diagonalisation

Given the total model of the system, we can start deriving an effective theory of the proximitized QH edge. This will be done by integrating out the SC fields in the context of a path integral. Before that, however, we will diagonalize the SC Hamiltonian to make the future path integral more tractable. Since the SOC is weak, we first consider the limit of vanishing SOC, $\alpha \to 0$, and then add the SOC perturbatively to first order, which significantly simplifies the calculation.

3.5.1 Bogoliubov transformation

The SC surface Hamiltonian in the limit of vanishing SOC is

$$H_{\text{SC},\,\alpha=0} = \sum_{\delta\mathbf{k},\sigma} \left[\epsilon_{\mathbf{k}_s+\delta\mathbf{k}} c^\dagger_{\mathbf{k}_s+\delta\mathbf{k},\sigma} c_{\mathbf{k}_s+\delta\mathbf{k},\sigma} + \left(\Delta_0\, c^\dagger_{\mathbf{k}_s+\delta\mathbf{k},\uparrow} c^\dagger_{\mathbf{k}_s-\delta\mathbf{k},\downarrow} + \text{h.\,c.} \right) \right]. \tag{3.21}$$

This type of Hamiltonian is typically diagonalized through the Bogoliubov transformation [1], which is the general unitary basis change

$$\begin{pmatrix} c_{\mathbf{k}_s+\delta\mathbf{k},\uparrow} \\ c^\dagger_{\mathbf{k}_s-\delta\mathbf{k},\downarrow} \end{pmatrix} = \begin{pmatrix} u_{\delta\mathbf{k}} & v_{\delta\mathbf{k}} \\ v^*_{\delta\mathbf{k}} & -u^*_{\delta\mathbf{k}} \end{pmatrix} \begin{pmatrix} \chi_{\delta\mathbf{k},1} \\ \chi^\dagger_{-\delta\mathbf{k},2} \end{pmatrix}, \tag{3.22}$$

where the fermionic bogolon fields $\chi_{\delta\mathbf{k},j}$ with pseudo-spin index $j = 1, 2$ form the diagonal basis. We define the energies

$$E_s \stackrel{\text{def}}{=} \frac{k_s^2}{2m_s}, \tag{3.23}$$

$$\zeta_{\delta\mathbf{k}} \stackrel{\text{def}}{=} \sqrt{(\epsilon_{\delta\mathbf{k}} + E_s)^2 + |\Delta_0|^2}, \tag{3.24}$$

and assuming that we have $\Delta_0 = |\Delta_0|e^{i\phi_\Delta}$, we have the transformation matrix elements

$$u_{\delta\mathbf{k}} = \sqrt{\frac{1}{2}\left(1 + \frac{\epsilon_{\delta\mathbf{k}} + E_s}{\zeta_{\delta\mathbf{k}}}\right)}, \tag{3.25}$$

$$v_{\delta\mathbf{k}} = e^{i\phi_\Delta}\sqrt{\frac{1}{2}\left(1 - \frac{\epsilon_{\delta\mathbf{k}} + E_s}{\zeta_{\delta\mathbf{k}}}\right)}. \tag{3.26}$$

Note that we have here fixed the phases of $u_{\delta\mathbf{k}}$ and $v_{\delta\mathbf{k}}$, but any choice with $\arg(u_{\delta\mathbf{k}}) + \arg(v_{\delta\mathbf{k}}) = \phi_\Delta$ would apply. The diagonalisation can then be performed on matrix form in the basis used in Eq. (3.22),

$$
\begin{aligned}
H_{\text{SC, }\alpha=0} &= \frac{1}{2}\sum_{\delta\mathbf{k}} \begin{pmatrix} c^\dagger_{\mathbf{k}_s+\delta\mathbf{k},\uparrow} \\ c_{\mathbf{k}_s-\delta\mathbf{k},\downarrow} \end{pmatrix}^T \begin{pmatrix} \epsilon_{\mathbf{k}_s+\delta\mathbf{k}} & \Delta_0 \\ \Delta_0^* & -\epsilon_{\mathbf{k}_s-\delta\mathbf{k}} \end{pmatrix} \begin{pmatrix} c_{\mathbf{k}_s+\delta\mathbf{k},\uparrow} \\ c^\dagger_{\mathbf{k}_s-\delta\mathbf{k},\downarrow} \end{pmatrix} \\
&= \frac{1}{2}\sum_{\delta\mathbf{k}} \begin{pmatrix} \chi^\dagger_{\delta\mathbf{k},1} \\ \chi_{-\delta\mathbf{k},2} \end{pmatrix}^T \begin{pmatrix} \frac{\delta\mathbf{k}\cdot\mathbf{k}_s}{m_s} + \zeta_{\delta\mathbf{k}} & 0 \\ 0 & \frac{\delta\mathbf{k}\cdot\mathbf{k}_s}{m_s} - \zeta_{\delta\mathbf{k}} \end{pmatrix} \begin{pmatrix} \chi_{\delta\mathbf{k},1} \\ \chi^\dagger_{-\delta\mathbf{k},2} \end{pmatrix} \\
&= \sum_{\delta\mathbf{k},j=1,2} \left(\frac{\delta\mathbf{k}\cdot\mathbf{k}_s}{m_s} + \zeta_{\delta\mathbf{k}} \right) \chi^\dagger_{\delta\mathbf{k},j}\chi_{\delta\mathbf{k},j}, \tag{3.27}
\end{aligned}
$$

where we have used $\zeta_{\delta\mathbf{k}} = \zeta_{-\delta\mathbf{k}}$ for the last step. As expected, we recover the Doppler shifted dispersion as discussed in Section 2.5.2.

3.5.2 Degenerate perturbation theory

Having established the $\alpha = 0$ case, we can now add the SOC perturbatively by assuming a small, but non-zero α, such that the SOC term is the smallest term at all momenta. First we convert the SOC Hamiltonian to the bogolon basis using Eq. (3.22),

$$
\begin{aligned}
H_{\text{SOC}} &= \alpha\sum_{\delta\mathbf{k}}[\delta k_z + i(\delta k_x + k_s)]c^\dagger_{\mathbf{k}_s+\delta\mathbf{k},\uparrow}c_{\mathbf{k}_s+\delta\mathbf{k},\downarrow} + \text{h. c.} \\
&= i\alpha\sum_{\delta\mathbf{k}}\left[\left(k_s + (\delta k_x - i\delta k_z)\frac{\epsilon_{\delta\mathbf{k}} + E_s}{\zeta_{\delta\mathbf{k}}}\right)\chi^\dagger_{\delta\mathbf{k},1}\chi_{\delta\mathbf{k},2} \right. \\
&\qquad \left. - (\delta k_x + i\delta k_z)(v^*_{\delta\mathbf{k}}u_{\delta\mathbf{k}}\chi_{-\delta\mathbf{k},2}\chi_{\delta\mathbf{k},2} - u^*_{\delta\mathbf{k}}v_{\delta\mathbf{k}}\chi^\dagger_{\delta\mathbf{k},1}\chi^\dagger_{-\delta\mathbf{k},1}) + \text{h. c.} \right]. \tag{3.28}
\end{aligned}
$$

Since the unperturbed Hamiltonian in Eq. (3.27) is degenerate in the pseudo-spin index j, we use degenerate perturbation theory [50] to approximate the effect of a small SOC. To lowest order, the energy contribution will lift the degeneracy, and the correct $\alpha \to 0$ limit of the perturbed basis states will be the linear combination of unperturbed basis states which diagonalize the degenerate subspaces of the SOC term. Considering only

26

this subspace, we neglect all contributions other than those which mix χ_1 and χ_2. In other words, we neglect all but the first term of Eq. (3.28), which can then be written

$$\alpha \sum_{\delta\mathbf{k}} \begin{pmatrix} \chi^\dagger_{\delta\mathbf{k},1} \\ \chi^\dagger_{\delta\mathbf{k},2} \end{pmatrix}^T \begin{pmatrix} 0 & k_s + (\delta k_x - i\delta k_z)\frac{\epsilon_{\delta\mathbf{k}}+E_s}{\zeta_{\delta\mathbf{k}}} \\ k_s + (\delta k_x + i\delta k_z)\frac{\epsilon_{\delta\mathbf{k}}+E_s}{\zeta_{\delta\mathbf{k}}} & 0 \end{pmatrix} \begin{pmatrix} \chi_{\delta\mathbf{k},1} \\ \chi_{\delta\mathbf{k},2} \end{pmatrix} \quad (3.29)$$

By diagonalising this contribution we can identify the diagonal elements as the first order energy shifts,

$$\alpha \sum_{\delta\mathbf{k}} \begin{pmatrix} d^\dagger_{\delta\mathbf{k},+} \\ d^\dagger_{\delta\mathbf{k},-} \end{pmatrix}^T \begin{pmatrix} \left| k_s + (\delta k_x + i\delta k_z)\frac{\epsilon_{\delta\mathbf{k}}+E_s}{\zeta_{\delta\mathbf{k}}} \right| & 0 \\ 0 & -\left| k_s + (\delta k_x + i\delta k_z)\frac{\epsilon_{\delta\mathbf{k}}+E_s}{\zeta_{\delta\mathbf{k}}} \right| \end{pmatrix} \begin{pmatrix} d_{\delta\mathbf{k},+} \\ d_{\delta\mathbf{k},-} \end{pmatrix}, \quad (3.30)$$

and the eigenstates as the associated rotated basis,

$$\begin{pmatrix} \chi_{\delta\mathbf{k},1} \\ \chi_{\delta\mathbf{k},2} \end{pmatrix} = \frac{1}{\sqrt{2}} \begin{pmatrix} -ie^{-i\theta_{\delta\mathbf{k}}} & ie^{-i\theta_{\delta\mathbf{k}}} \\ e^{i\theta_{\delta\mathbf{k}}} & e^{i\theta_{\delta\mathbf{k}}} \end{pmatrix} \begin{pmatrix} d_{\delta\mathbf{k},+} \\ d_{\delta\mathbf{k},-} \end{pmatrix}, \quad (3.31)$$

with the angle

$$\theta_{\delta\mathbf{k}} = \frac{1}{2} \arg \left(k_s + (\delta k_x + i\delta k_z)\frac{\epsilon_{\delta\mathbf{k}}+E_s}{\zeta_{\delta\mathbf{k}}} \right). \quad (3.32)$$

Thus, to first order in α we find the diagonal SC surface Hamiltonian

$$H_{\text{SC}} = \sum_{\delta\mathbf{k},\, r=\pm} \left(\frac{\delta\mathbf{k} \cdot \mathbf{k}_s}{m_s} + \zeta_{\delta\mathbf{k}} + r\alpha \left| k_s + (\delta k_x + i\delta k_z)\frac{\epsilon_{\delta\mathbf{k}}+E_s}{\zeta_{\delta\mathbf{k}}} \right| \right) d^\dagger_{\delta\mathbf{k},r} d_{\delta\mathbf{k},r}, \quad (3.33)$$

whose effect on the QH edge we will now investigate.

3.6   Proximity effect

To arrive at an effective description of the induced superconductivity in the QH edge state we integrate out the superconductor fields. This requires formulating the Euclidian action corresponding to the Hamiltonian, plugging it into the corresponding partition function, solving the path integral over the SC fields, and extracting the Hamiltonian again. Integrating out degrees of freedom in this way is a standard approach with detailed treatments found in e.g. Ref. [62, sec. 4.2] and Ref. [63, chs. 23-25]. Here we summarize only the necessary elements to arrive at the results.

3.6.1   Integrating out the superconductor

We consider the system described by the Hamiltonian Eq. (3.17) derived in the previous chapter. For a more unified description of the total system, we will shift the QH edge momentum q by k_s like we have shifted the SC momentum, i.e. we change variables to

$$\delta q = q - k_s, \quad (3.34)$$

such that the QH edge Hamiltonian is

$$H_{\text{edge}} = \sum_{\delta q} E_{k_s+\delta q} \psi^\dagger_{k_s+\delta q} \psi_{k_s+\delta q}. \tag{3.35}$$

The quantum partition function corresponding to the system is

$$Z = \int D[d^\dagger d \psi^\dagger \psi] e^{-S[d^\dagger d \psi^\dagger \psi]}, \tag{3.36}$$

where d is the vector of Grassmann numbers corresponding to the SC fields, ψ is vector of Grassmann numbers corresponding to the QH fields and S is the Euclidean action of the system, which means it is expressed in terms of the discrete Matsubara frequencies ω_n.

The path integral has the measure

$$D[d^\dagger d \psi^\dagger \psi] = \prod_{\delta\mathbf{k},\delta q,\omega_n} d(d^\dagger_{\delta\mathbf{k},\omega_n}) d(d_{\delta\mathbf{k},\omega_n}) d\psi^\dagger_{\delta q,\omega_n} d\psi_{\delta q,\omega_n}. \tag{3.37}$$

We divide the action into terms only involving edge fields $S_0[\psi^\dagger \psi]$ and the remaining terms involving a mix of SC and edge fields $\delta S[d^\dagger d \psi^\dagger \psi]$. The notation of δS implies the view of SC and tunneling as small corrections to the edge state. The total action is then $S = S_0 + \delta S$, with

$$S_0[\psi^\dagger \psi] = \sum_{q,\omega_n} \psi^\dagger_{q,\omega_n} (-i\omega_n) \psi_{q,\omega_n} + H_{\text{edge}}[\psi^\dagger \psi] \tag{3.38}$$

$$\delta S[d^\dagger d \psi^\dagger \psi] = \sum_{\delta\mathbf{k},\omega_n} d^\dagger_{\delta\mathbf{k},\omega_n} (-i\omega_n) d_{\delta\mathbf{k},\omega_n} + H_{\text{SC}}[d^\dagger d] + H_{\text{tunn}}[d^\dagger d \psi^\dagger \psi]. \tag{3.39}$$

We have here assumed that the pairing amplitude Δ_0 is independent of ω, corresponding to the assumption that pairing occurs between fields with the same time coordinate. This instantaneous assumption neglects any contributions from finite time differences. Interestingly, including finite time differences can qualitatively change the problem since it will then involve odd-frequency pairing [64], but that case will not be treated in this thesis.

We can choose to perform the path integral in Eq. (3.36) over the superconductor fields $d^\dagger, d$ only, which will leave us with an effective Hamiltonian in terms of the edge fields $\psi^\dagger, \psi$. To do this, we recast the path integral in the form of a Gaussian vector integral by defining the vector fields

$$\eta_{\delta\mathbf{k},\omega_n} = \begin{pmatrix} d_{\delta\mathbf{k},1,\omega_n} \\ d^\dagger_{-\delta\mathbf{k},2,-\omega_n} \end{pmatrix} \tag{3.40}$$

$$\varphi^\dagger_{\boldsymbol{\kappa},\omega_n} = -\Gamma \begin{pmatrix} iu_{\boldsymbol{\kappa}} e^{-i\theta_{\boldsymbol{\kappa}}} \psi^\dagger_{k_s+\delta q,\omega_n} - v^*_{\boldsymbol{\kappa}} e^{i\theta_{\boldsymbol{\kappa}}} \psi_{k_s-\delta q,-\omega_n} \\ -iu^*_{\boldsymbol{\kappa}} e^{i\theta_{-\boldsymbol{\kappa}}} \psi_{k_s-\delta q,-\omega_n} + v_{\boldsymbol{\kappa}} e^{-i\theta_{-\boldsymbol{\kappa}}} \psi^\dagger_{k_s+\delta q,\omega_n} \end{pmatrix} \tag{3.41}$$

where $\boldsymbol{\kappa} = (\delta q, \delta k_y, \delta k_z)$, the phase $\theta_{\boldsymbol{\kappa}}$ is defined in Eq. (3.32), and Γ is the tunneling energy defined in Eq. (3.16). We note that the φ field has units of energy. We also define the diagonal matrix

$$\Lambda_{\delta\mathbf{k},\omega_n} = \begin{pmatrix} -i\omega_n + E_{\text{surf},\delta\mathbf{k},+} & 0 \\ 0 & -i\omega_n - E_{\text{surf},-\delta\mathbf{k},-} \end{pmatrix} \tag{3.42}$$

28

where

$$E_{\text{surf},\delta\mathbf{k},r} = \left(\frac{\delta\mathbf{k} \cdot \mathbf{k}_s}{m_s} + \zeta_{\delta\mathbf{k}} + r\alpha \left| k_s + (\delta k_x + i\delta k_z)\frac{\epsilon_{\delta\mathbf{k}} + E_s}{\zeta_{\delta\mathbf{k}}} \right| \right) \tag{3.43}$$

is the SC surface energy of Eq. (3.33). We can then write out δS in terms of vector fields

$$\delta S[\eta^\dagger\eta\varphi^\dagger\varphi] = \sum_{\delta\mathbf{k},\omega_n} \eta^\dagger_{\delta\mathbf{k},\omega_n} \Lambda_{\delta\mathbf{k},\omega_n} \eta_{\delta\mathbf{k},\omega_n} - \sum_{\boldsymbol{\kappa},\omega_n} \left(\varphi^\dagger_{\boldsymbol{\kappa},\omega_n} \eta_{\boldsymbol{\kappa},\omega_n} + \eta^\dagger_{\boldsymbol{\kappa},\omega_n} \varphi_{\boldsymbol{\kappa},\omega_n} \right). \tag{3.44}$$

Before we can write up the path integral, we must be careful in correctly treating the different momenta involved. Since the order of multiplication in the path integral measure is irrelevant, we can separate the product in the path integral measure into a product over those momenta involved in tunneling, i.e. $\delta\mathbf{k} = \boldsymbol{\kappa}$ with $\kappa_x = k_s$, and the remaining momenta $\delta\mathbf{k}'$ with $\delta k'_x \neq k_s$

$$\prod_{\delta\mathbf{k}} = \prod_{\boldsymbol{\kappa}} \prod_{\delta\mathbf{k}'} . \tag{3.45}$$

We will then apply the identities

$$e^{\sum_i a_i} = \prod_i e^{a_i} \tag{3.46}$$

$$\prod_{i=-N}^{N} b_i \prod_{j=-N}^{N} e^{a_j} = \prod_{i=-N}^{N} b_i e^{a_i}, \tag{3.47}$$

for general commuting numbers a_i, b_i and a general limit N. We note that though Grassmann numbers anti-commute like fermionic fields, pairs of Grassmann numbers commute, and since the action is bi-linear in all fields, the above identities apply. The path integral over the SC fields from Eq. (3.36) then becomes

$$\int D[\eta^\dagger\eta\varphi^\dagger\varphi] e^{-\delta S[\eta^\dagger\eta\varphi^\dagger\varphi]} = \prod_{\boldsymbol{\kappa},\omega_n} \left[\int d\eta^\dagger_{\boldsymbol{\kappa},\omega_n} d\eta_{\boldsymbol{\kappa},\omega_n} d\varphi^\dagger_{\boldsymbol{\kappa},\omega_n} d\varphi_{\boldsymbol{\kappa},\omega_n} e^{S'_{\boldsymbol{\kappa},\omega_n}[\eta^\dagger\eta\varphi^\dagger\varphi]} \right]$$
$$\times \prod_{\delta\mathbf{k}',\omega_n} \left[\int d\eta^\dagger_{\delta\mathbf{k}',\omega_n} d\eta_{\delta\mathbf{k}',\omega_n} e^{S''_{\delta\mathbf{k}',\omega_n}[\eta^\dagger\eta]} \right] \tag{3.48}$$

where we have divided the action into the fields that take part in the tunneling

$$S'_{\boldsymbol{\kappa},\omega_n}[\eta^\dagger\eta\varphi^\dagger\varphi] = -\eta^\dagger_{\boldsymbol{\kappa},\omega_n} \Lambda_{\boldsymbol{\kappa},\omega_n} \eta_{\boldsymbol{\kappa},\omega_n} + \varphi^\dagger_{\boldsymbol{\kappa},\omega_n} \eta_{\boldsymbol{\kappa},\omega_n} + \eta^\dagger_{\boldsymbol{\kappa},\omega_n} \varphi_{\boldsymbol{\kappa},\omega_n}, \tag{3.49}$$

and those which do not

$$S''_{\delta\mathbf{k}',\omega_n}[\eta^\dagger\eta] = -\eta^\dagger_{\delta\mathbf{k}',\omega_n} \Lambda_{\delta\mathbf{k}',\omega_n} \eta_{\delta\mathbf{k}',\omega_n}. \tag{3.50}$$

The integrals on the right hand side of Eq. (3.48) are well defined Gaussian integrals over Grassmann numbers [62], and we can resolve the path integral to

$$\int D[\eta^\dagger\eta] e^{-\delta S[\eta^\dagger\eta\varphi^\dagger\varphi]} = \exp\left(\sum_{\boldsymbol{\kappa},\omega_n} \left[\varphi^\dagger_{\boldsymbol{\kappa},\omega_n} \Lambda^{-1}_{\boldsymbol{\kappa},\omega_n} \varphi_{\boldsymbol{\kappa},\omega_n} + C \right] \right) \tag{3.51}$$

where we have defined the constant

$$C = \ln\left(\det(\Lambda_{\boldsymbol{\kappa},\omega_n})\right) + \ln\left(\det(\Lambda_{\delta \mathbf{k}',\omega_n})\right), \tag{3.52}$$

which constitutes a simple shift of the action and will be ignored.

Returning to the partition function Eq. (3.36), we can insert the result of Eq. (3.51) to find

$$Z = \int D[\psi^\dagger \psi] \exp\left(-S_0[\psi^\dagger \psi] - \sum_{\boldsymbol{\kappa},\omega_n} \varphi^\dagger_{\boldsymbol{\kappa},\omega_n} \Lambda^{-1}_{\boldsymbol{\kappa},\omega_n} \varphi_{\boldsymbol{\kappa},\omega_n}\right) = \int D[\psi^\dagger \psi] e^{-S_{\mathrm{eff}}[\psi^\dagger \psi]}, \tag{3.53}$$

where the argument of the exponent becomes the effective action S_{eff} describing the proximitized edge. Note that the only fields present are the ψ fields, with the φ vector fields simply being a compact way of writing up the involved combinations of ψ fields.

3.6.2 Effective Hamiltonian

Finally we need to convert the action into a Hamiltonian. To do that, we assume that the action $\delta S[\psi^\dagger \psi]$ only induces instantaneous effects in the QH edge, neglecting any other effects. As in the previous section, this implies that the induced parameters contained in $\Lambda^{-1}_{\boldsymbol{\kappa},\omega_n}$ are independent of ω_n. As the frequency enters as $1/(i\omega_n + E_{\mathrm{surf},\boldsymbol{\kappa},\pm})$, we will find the greatest magnitude of induced effects at $\omega_n = 0$. Going forward, we will fix the Matsubara frequency in $\Lambda_{\boldsymbol{\kappa},\omega_n}$ to zero and treat the resulting system.

Given a $\Lambda_{\boldsymbol{\kappa}}$ independent of ω_n, we can write up the effective action on the form

$$S_{\mathrm{eff}}[\psi^\dagger \psi] = \sum_{\omega_n, \delta\mathbf{k}} \psi^\dagger_{\omega_n, \delta\mathbf{k}}(-i\omega_n)\psi_{\omega_n, \delta\mathbf{k}} + H_{\mathrm{eff}}, \tag{3.54}$$

where we have the effective Hamiltonian of the system

$$H_{\mathrm{eff}} = H_{\mathrm{edge}} + \delta H. \tag{3.55}$$

Here H_{edge} is defined in Eq. (3.2) and

$$\delta H = \sum_{\boldsymbol{\kappa}} \varphi^\dagger_{\boldsymbol{\kappa}} \Lambda^{-1}_{\boldsymbol{\kappa}} \varphi_{\boldsymbol{\kappa}} \tag{3.56}$$

corresponding to the latter term of the effective action of Eq. (3.53) at $\omega_n = 0$. Since the effective Hamiltonian in terms of ψ is a key result of this thesis we will now resolve the above expression in detail. The matrix Λ is diagonal, and thus the inverse is trivial to evaluate

$$\Lambda^{-1}_{\boldsymbol{\kappa}} = \begin{pmatrix} E^{-1}_{\mathrm{surf},\boldsymbol{\kappa},+} & 0 \\ 0 & -E^{-1}_{\mathrm{surf},-\boldsymbol{\kappa},-} \end{pmatrix}. \tag{3.57}$$

The matrix elements diverge in the case of $E_{\mathrm{surf},\boldsymbol{\kappa},+} = 0$, corresponding to the critical Doppler shift as discussed in Section 2.5.2. However, since we have assume that we are below this critical shift, we avoid the singularity.

The lack of off-diagonal elements in Λ^{-1} means δH depends in a simple way on $\varphi^\dagger_{\boldsymbol{\kappa}} \varphi_{\boldsymbol{\kappa}}$. We find

$$\delta H = \sum_{\boldsymbol{\kappa}} \left(\frac{\varphi^\dagger_{\boldsymbol{\kappa},1} \varphi_{\boldsymbol{\kappa},1}}{E_{\mathrm{surf},\boldsymbol{\kappa},+}} - \frac{\varphi^\dagger_{\boldsymbol{\kappa},2} \varphi_{\boldsymbol{\kappa},2}}{E_{\mathrm{surf},-\boldsymbol{\kappa},-}} \right). \tag{3.58}$$

The sum over κ is symmetric, which lets us change the signs of κ in the second term,

$$\delta H = \sum_{\kappa} \left(\frac{\varphi_{\kappa,1}^{\dagger}\varphi_{\kappa,1}}{E_{\text{surf},\kappa,+}} - \frac{\varphi_{-\kappa,2}^{\dagger}\varphi_{-\kappa,2}}{E_{\text{surf},\kappa,-}} \right). \tag{3.59}$$

Recalling the definition of $E_{\text{surf},\kappa,\pm}$ in Eq. (3.43), we can split off the SOC contribution by defining the $\alpha = 0$ energy

$$E_{\alpha=0,\kappa} = \frac{\delta q k_s}{m_s} + \zeta_{\kappa}, \tag{3.60}$$

as well as the momentum

$$\kappa_{\alpha} = \left| k_s + (\delta q + i\delta k_z) \frac{\epsilon_{\kappa} + E_s}{\zeta_{\kappa}} \right|, \tag{3.61}$$

such that $E_{\text{surf},\kappa,r} = E_{\alpha=0,\kappa} + r\alpha\kappa_{\alpha}$. This lets us simplify δH by writing

$$\delta H = \sum_{\kappa} \left(\frac{\varphi_{\kappa,1}^{\dagger}\varphi_{\kappa,1}}{\alpha\kappa_{\alpha} + E_{\alpha=0,\kappa}} + \frac{\varphi_{-\kappa,2}^{\dagger}\varphi_{-\kappa,2}}{\alpha\kappa_{\alpha} - E_{\alpha=0,\kappa}} \right). \tag{3.62}$$

We can put the two terms on a common denominator and find

$$\begin{aligned}
\delta H &= \sum_{\kappa} \frac{(\alpha\kappa_{\alpha} - E_{\alpha=0,\kappa})\varphi_{\kappa,1}^{\dagger}\varphi_{\kappa,1} + (\alpha\kappa_{\alpha} + E_{\alpha=0,\kappa})\varphi_{-\kappa,2}^{\dagger}\varphi_{-\kappa,2}}{(\alpha\kappa_{\alpha})^2 - E_{\alpha=0,\kappa}^2} \\
&= \sum_{\kappa} \frac{E_{\alpha=0,\kappa}(\varphi_{-\kappa,2}^{\dagger}\varphi_{-\kappa,2} - \varphi_{\kappa,1}^{\dagger}\varphi_{\kappa,1}) + \alpha\kappa_{\alpha}(\varphi_{-\kappa,2}^{\dagger}\varphi_{-\kappa,2} + \varphi_{\kappa,1}^{\dagger}\varphi_{\kappa,1})}{(\alpha\kappa_{\alpha})^2 - E_{\alpha=0,\kappa}^2},
\end{aligned} \tag{3.63}$$

where the second step is a simple re-arrangement of terms. This expression contains all orders of α though, which is inconsistent with the perturbation expansion in Section 3.5.2. Taylor expanding the expression and discarding terms higher than first order corresponds to simply omitting the α^2 term in the denominator, such that the form of δH which is consistent with perturbation theory is

$$\delta H = -\sum_{\kappa} \frac{1}{E_{\alpha=0,\kappa}^2} \left[E_{\alpha=0,\kappa}(\varphi_{-\kappa,2}^{\dagger}\varphi_{-\kappa,2} - \varphi_{\kappa,1}^{\dagger}\varphi_{\kappa,1}) + \alpha\kappa_{\alpha}(\varphi_{-\kappa,2}^{\dagger}\varphi_{-\kappa,2} + \varphi_{\kappa,1}^{\dagger}\varphi_{\kappa,1}) \right], \tag{3.64}$$

Noting that u_{κ}, v_{κ} are symmetric in κ, we can write the components of φ as

$$\begin{aligned}
\frac{\varphi_{\kappa,1}^{\dagger}\varphi_{\kappa,1}}{\Gamma^2} &= \left(-iu_{\kappa}e^{-i\theta_{\kappa}}\psi_{k_s+\delta q}^{\dagger} + v_{\kappa}^{*}e^{i\theta_{\kappa}}\psi_{k_s-\delta q} \right)\left(iu_{\kappa}^{*}e^{i\theta_{\kappa}}\psi_{k_s+\delta q} + v_{\kappa}e^{-i\theta_{\kappa}}\psi_{k_s-\delta q}^{\dagger} \right) \\
&= |u_{\kappa}|^2 \psi_{k_s+\delta q}^{\dagger}\psi_{k_s+\delta q} + |v_{\kappa}|^2 \psi_{k_s-\delta q}\psi_{k_s-\delta q}^{\dagger} \\
&\quad - iu_{\kappa}v_{\kappa}e^{-2i\theta_{\kappa}}\psi_{k_s+\delta q}^{\dagger}\psi_{k_s-\delta q}^{\dagger} + iu_{\kappa}^{*}v_{\kappa}^{*}e^{2i\theta_{\kappa}}\psi_{k_s-\delta q}\psi_{k_s+\delta q}, \tag{3.65}
\end{aligned}$$

$$\begin{aligned}
\frac{\varphi_{-\kappa,2}^{\dagger}\varphi_{-\kappa,2}}{\Gamma^2} &= \left(iu_{\kappa}^{*}e^{i\theta_{\kappa}}\psi_{k_s+\delta q} - v_{\kappa}e^{-i\theta_{\kappa}}\psi_{k_s-\delta q}^{\dagger} \right)\left(-iu_{\kappa}e^{-i\theta_{\kappa}}\psi_{k_s+\delta q}^{\dagger} - v_{\kappa}^{*}e^{i\theta_{\kappa}}\psi_{k_s-\delta q} \right) \\
&= |u_{\kappa}|^2 \psi_{k_s+\delta q}\psi_{k_s+\delta q}^{\dagger} + |v_{\kappa}|^2 \psi_{k_s-\delta q}^{\dagger}\psi_{k_s-\delta q} \\
&\quad + iu_{\kappa}v_{\kappa}e^{-2i\theta_{\kappa}}\psi_{k_s-\delta q}^{\dagger}\psi_{k_s+\delta q}^{\dagger} - iu_{\kappa}^{*}v_{\kappa}^{*}e^{2i\theta_{\kappa}}\psi_{k_s+\delta q}\psi_{k_s-\delta q}. \tag{3.66}
\end{aligned}$$

By commuting the fermion fields of the last line, we find

$$\frac{\varphi^\dagger_{-\boldsymbol{\kappa},2}\varphi_{-\boldsymbol{\kappa},2}}{\Gamma^2} = -|u_{\boldsymbol{\kappa}}|^2 \psi^\dagger_{k_s+\delta q}\psi_{k_s+\delta q} - |v_{\boldsymbol{\kappa}}|^2 \psi_{k_s-\delta q}\psi^\dagger_{k_s-\delta q}$$
$$- iu_{\boldsymbol{\kappa}}v_{\boldsymbol{\kappa}}e^{-2i\theta_{\boldsymbol{\kappa}}}\psi^\dagger_{k_s+\delta q}\psi^\dagger_{k_s-\delta q} + iu^*_{\boldsymbol{\kappa}}v^*_{\boldsymbol{\kappa}}e^{2i\theta_{\boldsymbol{\kappa}}}\psi_{k_s-\delta q}\psi_{k_s+\delta q}. \qquad (3.67)$$

We see that the sum in Eq. (3.64) cancels the two first terms of each product, while the difference cancels the two last terms of each product,

$$\delta H = 2\Gamma^2 \sum_{\boldsymbol{\kappa}} \frac{1}{E^2_{\alpha=0,\boldsymbol{\kappa}}}\Big[E_{\alpha=0,\boldsymbol{\kappa}}(|u_{\boldsymbol{\kappa}}|^2\psi^\dagger_{k_s+\delta q}\psi_{k_s+\delta q} + |v_{\boldsymbol{\kappa}}|^2\psi_{k_s-\delta q}\psi^\dagger_{k_s-\delta q})$$
$$+ \alpha\kappa_\alpha(iu_{\boldsymbol{\kappa}}v_{\boldsymbol{\kappa}}e^{-2i\theta_{\boldsymbol{\kappa}}}\psi^\dagger_{k_s+\delta q}\psi^\dagger_{k_s-\delta q} + \mathrm{h.\,c.})\Big]. \qquad (3.68)$$

We can now identify two types of contribution from the SC in the effective Hamiltonian, namely a renormalization of the kinetic energy $\delta E_{\delta q}$ and a pairing amplitude $\Delta_{\delta q}$,

$$\boxed{H_{\text{eff}} = \sum_{\delta q}\left[(E_{k_s+\delta q} + \delta E_{\delta q})\psi^\dagger_{k_s+\delta q}\psi_{k_s+\delta q} + \left(\frac{\Delta_{\delta q}}{2}\psi^\dagger_{k_s+\delta q}\psi^\dagger_{k_s-\delta q} + \mathrm{h.\,c.}\right)\right].} \qquad (3.69)$$

We can identify the kinetic contribution from Eq. (3.68) by commuting the fermionic fields

$$\sum_{\boldsymbol{\kappa}}\left[\frac{|u_{\boldsymbol{\kappa}}|^2}{E_{\alpha=0,\boldsymbol{\kappa}}}\psi^\dagger_{k_s+\delta q}\psi_{k_s+\delta q} + \frac{|v_{\boldsymbol{\kappa}}|^2}{E_{\alpha=0,\boldsymbol{\kappa}}}\psi_{k_s-\delta q}\psi^\dagger_{k_s-\delta q}\right]$$
$$= \sum_{\boldsymbol{\kappa}}\left[\frac{|u_{\boldsymbol{\kappa}}|^2}{E_{\alpha=0,\boldsymbol{\kappa}}}\psi^\dagger_{k_s+\delta q}\psi_{k_s+\delta q} - \frac{|v_{\boldsymbol{\kappa}}|^2}{E_{\alpha=0,\boldsymbol{\kappa}}}\psi^\dagger_{k_s-\delta q}\psi_{k_s-\delta q}\right] + \text{const.}, \quad (3.70)$$

whereupon ignoring the constant and changing summation variables $\boldsymbol{\kappa} \to -\boldsymbol{\kappa}$, and thus $\delta q \to -\delta q$, in the second term leads to the contribution

$$\delta E_{\delta q} = 2\Gamma^2 \sum_{\delta k_y,\delta k_z}\left(\frac{|u_{\boldsymbol{\kappa}}|^2}{E_{\alpha=0,\boldsymbol{\kappa}}} - \frac{|v_{\boldsymbol{\kappa}}|^2}{E_{\alpha=0,-\boldsymbol{\kappa}}}\right). \qquad (3.71)$$

The induced pairing amplitude $\Delta_{\delta q}$, which must be odd in δq due to the fermionic nature of the fields, can be written as as $\Delta_{\delta q} = (\tilde{\Delta}_{\delta q} - \tilde{\Delta}_{-\delta q})/2$, where the pairing term in Eq. (3.68) leads to the definition

$$\tilde{\Delta}_{\delta q} = i\Gamma^2\alpha \sum_{\delta k_y,\delta k_z} \frac{\kappa_\alpha u_{\boldsymbol{\kappa}}v_{\boldsymbol{\kappa}}e^{-2i\theta_{\boldsymbol{\kappa}}}}{E^2_{\alpha=0,\boldsymbol{\kappa}}}. \qquad (3.72)$$

In the next sections we will write out these effective parameters $\delta E_{\delta q}$ and $\Delta_{\delta q}$ in terms of externally applied parameters.

3.6.3 Induced pairing

To simplify the pairing amplitude in Eq. (3.72) we first note that according to Eqs. (3.32) and (3.61), we have that κ_α is defined as the amplitude of a complex number, while $2\theta_{\boldsymbol{\kappa}}$ is the argument of the same complex number, yielding

$$\kappa_\alpha e^{-2i\theta_{\boldsymbol{\kappa}}} = k_s + (\delta q - i\delta k_z)\frac{\epsilon_{\boldsymbol{\kappa}} + E_s}{\zeta_{\boldsymbol{\kappa}}}. \qquad (3.73)$$

We then note that

$$u_{\boldsymbol{\kappa}} v_{\boldsymbol{\kappa}} = \frac{\Delta_0}{2\zeta_{\boldsymbol{\kappa}}}, \tag{3.74}$$

which gives us

$$\tilde{\Delta}_{\delta q} = \frac{i}{2}\Gamma^2 \alpha \Delta_0 \sum_{\delta k_y, \delta k_z} \frac{\zeta_{\boldsymbol{\kappa}} k_s + (\epsilon_{\boldsymbol{\kappa}} + E_s)(\delta q - i\delta k_z)}{\zeta_{\boldsymbol{\kappa}}^2 \left(\frac{q k_s}{m_s} + \zeta_{\boldsymbol{\kappa}}\right)^2}. \tag{3.75}$$

Once again, the divergence at $q k_s / m_s = -\zeta_{\boldsymbol{\kappa}}$, is avoided by assuming a sub-critical Doppler shift, see Section 2.5.2.

Finally, we see that the term with δk_z in the numerator will be anti-symmetric in δk_z and evaluate to zero over the symmetric summation range, while the remaining terms are symmetric in the summation variables and remain,

$$\tilde{\Delta}_{\delta q} = \frac{i}{2}\Gamma^2 \alpha \Delta_0 \sum_{\delta k_y, \delta k_z} \frac{\zeta_{\boldsymbol{\kappa}} k_s + (\epsilon_{\boldsymbol{\kappa}} + E_s)\delta q}{\zeta_{\boldsymbol{\kappa}}^2 \left(\frac{\delta q k_s}{m_s} + \zeta_{\boldsymbol{\kappa}}\right)^2}. \tag{3.76}$$

The momenta are discretized in steps of $d(\delta k_{y/z}) = 2\pi/L_{y/z}$, with $L_{y/z}$ the relevant length dimension of the SC, so for large L_y and L_z we can approximate the sum as an integral (i.e. take the continuum limit)

$$\sum_{\delta k_{y/z}=-\infty}^{\infty} = L_{y/z} \sum_{k=-\infty}^{\infty} \frac{d(\delta k_{y/z})}{2\pi} \simeq L_{y/z} \int_{-\infty}^{\infty} \frac{d(\delta k_{y/z})}{2\pi}. \tag{3.77}$$

By noting that δk_y and δk_z only appear inside $\zeta_{\boldsymbol{\kappa}}$ and $\epsilon_{\boldsymbol{\kappa}}$, both in the form $\delta k_y^2 + t k_z^2$, we can straightforwardly convert to polar coordinates with radius $\delta k = \sqrt{\delta k_y^2 + \delta k_z^2}$ and find

$$\begin{aligned}
\tilde{\Delta}_{\delta q} &= \frac{i}{2}\Gamma_L^2 \alpha \Delta_0 \int_0^{2\pi} d\phi \int_0^{\infty} \frac{d(\delta k)}{(2\pi)^2} \frac{\delta k[\zeta_{\boldsymbol{\kappa}} k_s + (\epsilon_{\boldsymbol{\kappa}} + E_s)\delta q]}{\zeta_{\boldsymbol{\kappa}}^2 \left(\frac{\delta q k_s}{m_s} + \zeta_{\boldsymbol{\kappa}}\right)^2} \\
&= \frac{i}{2}\Gamma_L^2 \alpha \Delta_0 d\phi \int_0^{\infty} \frac{d(\delta k)}{2\pi} \frac{\delta k[\zeta_{\boldsymbol{\kappa}} k_s + (\epsilon_{\boldsymbol{\kappa}} + E_s)\delta q]}{\zeta_{\boldsymbol{\kappa}}^2 \left(\frac{\delta q k_s}{m_s} + \zeta_{\boldsymbol{\kappa}}\right)^2},
\end{aligned} \tag{3.78}$$

where we have resolve the angular integral in the second step, and defined the tunneling amplitude $\Gamma_L = \Gamma\sqrt{L_y L_z}$ as modified by the conversion from sum to integral. This result will be investigated further in Section 3.7.

As we can clearly see, for $\alpha = 0$ the induced pairing vanishes as expected in the case without spin-flipping mechanisms. The role of the Meissner current is more subtle, and will be discussed further in the context of transport through the Andreev edge state.

3.6.4 Kinetic renormalization

We will now conduct a closer investigation of the kinetic renormalization in Eq. (3.71). We rewrite the expression into one fraction

$$\delta E_{\delta q} = 2\Gamma^2 \sum_{\delta k_y, \delta k_z} \frac{E_{\alpha=0,-\boldsymbol{\kappa}}|u_{\boldsymbol{\kappa}}|^2 - E_{\alpha=0,\boldsymbol{\kappa}}|v_{\boldsymbol{\kappa}}|^2}{E_{\alpha=0,\boldsymbol{\kappa}} E_{\alpha=0,-\boldsymbol{\kappa}}}, \tag{3.79}$$

which, using the fact that $|u_{\boldsymbol{\kappa}}|^2 + |v_{\boldsymbol{\kappa}}|^2 = 1$, can be re-arranged into

$$\delta E_{\delta q} = 2\Gamma^2 \sum_{\delta k_y, \delta k_z} \frac{\zeta_{\boldsymbol{\kappa}}(|u_{\boldsymbol{\kappa}}|^2 - |v_{\boldsymbol{\kappa}}|^2) - \delta q k_s/m_s}{\zeta_{\boldsymbol{\kappa}}^2 - (\delta q k_s/m_s)^2}. \tag{3.80}$$

We can resolve

$$|u_{\boldsymbol{\kappa}}|^2 - |v_{\boldsymbol{\kappa}}|^2 = \frac{\epsilon_{\boldsymbol{\kappa}} + E_s}{\zeta_{\boldsymbol{\kappa}}}, \tag{3.81}$$

to find

$$\delta E_{\delta q} = 2\Gamma^2 \sum_{\delta k_y, \delta k_z} \frac{\epsilon_{\boldsymbol{\kappa}} + E_s - \delta q k_s/m_s}{\zeta_{\boldsymbol{\kappa}}^2 - (\delta q k_s/m_s)^2}. \tag{3.82}$$

Finally, writing out $\zeta_{\boldsymbol{\kappa}}^2$ yields

$$\delta E_{\delta q} = 2\Gamma^2 \sum_{\delta k_y, \delta k_z} \frac{\epsilon_{\boldsymbol{\kappa}} + E_s - \delta q k_s/m_s}{(\epsilon_{\boldsymbol{\kappa}} + E_s)^2 - (\delta q k_s/m_s)^2 + |\Delta_0|^2}. \tag{3.83}$$

We again convert this sum to an integral,

$$\delta E_{\delta q} = 2\Gamma_L^2 \int_0^\infty \frac{d(\delta k)}{2\pi} \frac{\delta k(\epsilon_{\boldsymbol{\kappa}} + E_s - \delta q k_s/m_s)}{(\epsilon_{\boldsymbol{\kappa}} + E_s)^2 - (\delta q k_s/m_s)^2 + |\Delta_0|^2}. \tag{3.84}$$

This energy accounts for the effect of the SC on the QH edge state beyond pairing, with the interesting feature that it is independent of the SOC, i.e. persists for $\alpha = 0$. This reflects the fact that single electrons can tunnel without a spin-flip mechanism, but they will not carry any superconducting correlation with them until full Cooper pairs can tunnel.

3.7 Effective dispersion

Before we move on to transport calculations using the effective Hamiltonian, we will first diagonalize it and consider the limit of small δq to investigate the effective dispersion of the proximitized edge state, as well as investigating the behavior of $\delta E_{\delta q}$ and $\Delta_{\delta q}$. The effective Hamiltonian we have derived describes a BCS-like Hamiltonian with pairing between spinless fermions. Such a system is well understood, see for example the work by Read and Green [65].

It is straightforward to diagonalize the effective Hamiltonian Eq. (3.69) in much the same way we diagonalized the original BCS Hamiltonian, and arrive at the dispersion

$$E_{\delta q, \pm}^{\text{eff}} = \frac{1}{2}\left[\tilde{E}_{\delta q} - \tilde{E}_{-\delta q} \pm \sqrt{\left(\tilde{E}_{\delta q} + \tilde{E}_{-\delta q}\right)^2 + 4|\Delta_{\delta q}|^2} \right], \tag{3.85}$$

where

$$\tilde{E}_{\delta q} = E_{k_s + \delta q} + \delta E_{\delta q}. \tag{3.86}$$

The associated eigenvectors are

$$V_+ = \begin{pmatrix} \tilde{u}_{\delta q} \\ \tilde{v}_{\delta q}^* \end{pmatrix} \qquad V_- = \begin{pmatrix} \tilde{v}_{\delta q} \\ -\tilde{u}_{\delta q}^* \end{pmatrix} \tag{3.87}$$

where

$$\tilde{u}_{\delta q} = \sqrt{\frac{1}{2}\left(1 + \frac{\tilde{E}_{\delta q} + \tilde{E}_{-\delta q}}{\sqrt{(\tilde{E}_{\delta q} + \tilde{E}_{-\delta q})^2 + 4|\Delta_{I,\delta q}|^2}}\right)},$$

$$\tilde{v}_{\delta q} = ie^{-i\phi_\Delta}\sqrt{\frac{1}{2}\left(1 - \frac{\tilde{E}_{\delta q} + \tilde{E}_{-\delta q}}{\sqrt{(\tilde{E}_{\delta q} + \tilde{E}_{-\delta q})^2 + 4|\Delta_{I,\delta q}|^2}}\right)},$$

(3.88)

Note that we have here fixed the phases of $\tilde{u}_{\delta q}$ and $\tilde{v}_{\delta q}$, but any choice with $\arg(u_{\delta \mathbf{k}}) + \arg(v_{\delta \mathbf{k}}) = \phi_\Delta + \pi$ would apply. The angle results from the observation in Eq. (3.78) that $\arg(\Delta_{\delta q}) = \arg(i\Delta_0)$.

Experiments [24, 25] report the detection of particle/hole mixing as the primary indicator of induced SC, and as discussed in Section 2.4, this mixing is greatest at the avoided crossings between particle-like and hole-like bands, which for induced SC has magnitude $|\Delta_{\delta q}|$. In Eq. (3.85) we see that for $|\Delta_{\delta q}| = 0$ we find $E_{\delta q,\pm}^{\text{eff}} = \pm\tilde{E}_{k_s\pm\delta q}$. When both values equal zero for the same δq value, the pairing will cause an avoided crossing near the Fermi energy and we will see the greatest effect. For $q_F = k_s$, both energies $\pm\tilde{E}_{k_s+\delta q}$ cross zero at $\delta q = 0$, and thus the parameters $q_F \simeq k_s$ and $\delta q \simeq 0$ are the most relevant for transport experiments. We will now consider the small δq limit $\delta q \ll q_F$, and then interpret the condition $q_F = k_s$.

Since the pairing amplitude is odd in δq, its expansion around $\delta q = 0$ contains no constant terms, and we have the linear approximation

$$\Delta_{\delta q} \simeq ie^{i\phi_\Delta}\Delta_{\text{p}}\delta q \tag{3.89}$$

with the real p-wave pairing amplitude

$$\Delta_{\text{p}} = -i\partial_{\delta q}\Delta_{\delta q}\Big|_{\delta q=0}. \tag{3.90}$$

This can be evaluated by taking the derivative in Eq. (3.78), giving

$$\Delta_{\text{p}} = \frac{m_s\Gamma_L^2\alpha}{2\pi|\Delta_0|}\left(\frac{E_s(E_s - \mu_s) + |\Delta_0|^2/4}{(E_s - \mu_s)^2 + |\Delta_0|^2} + \frac{E_s}{|\Delta_0|}\left\{\arctan\left[\frac{E_s - \mu_s}{|\Delta_0|}\right] - \frac{\pi}{2}\right\}\right). \tag{3.91}$$

We can simplify this expression by assuming a metallic SC with $E_s, |\Delta_0| \ll \mu_s$, letting us approximate

$$\Delta_{\text{p}} \simeq -\Gamma_L^2\alpha\frac{m_sE_s}{2|\Delta_0|^2}. \tag{3.92}$$

This approximate expression is proportional to both SOC α and Meissner current E_s, though the full impact of the latter will not become clear until we perform transport calculations. It is interesting to note that the induced amplitude depends on the inverse square of the SC pairing amplitude $\Delta_{\text{p}} \propto |\Delta_0|^{-2}$, i.e. the linear part of the induced pairing increases with weaker pairing in the SC. However, as discussed in Section 3.4, the model is based on the assumption that neither SOC nor the magnetic field are strong enough to close the SC gap, meaning the limit $|\Delta_0| \to 0$ is not accurately described. In particular, the supercurrent bound in Eq. (3.18) corresponds to the energy bound

$$\frac{E_s}{|\Delta_0|^2} \ll \frac{1}{4\mu_s}, \tag{3.93}$$

35

which is small since $\mu_s \gg |\Delta_0|, E_s$. Moreover, a dependence on the inverse SC gap is expected in the context of p-wave pairing, where local pairing is suppressed by the Pauli principle, meaning the pairing has the SC coherence length $\xi \propto 1/|\Delta_0|$ as a characteristic length scale [47].

Next, the kinetic energy renormalization can be expanded as

$$\delta E_{\delta q} = \delta E_{\delta q=0} + \delta v \delta q, \tag{3.94}$$

where we have defined the velocity $\delta v = \partial_{\delta q}(\delta E_{\delta q})|_{\delta q=0}$. The constant term formally diverges in the infinite limit, but since realistically only states up to some finite bandwidth will contribute, we can freely replace the upper limit with a large, finite number. Assuming that the upper limit is some large δk_c, we find

$$\delta E_{\delta q=0} = \frac{m_s \Gamma_L^2}{2\pi} \ln \left(\frac{|\Delta_0|^2 + [\delta k_c^2/(2m_s) - \mu_s + E_s]^2}{|\Delta_0|^2 + (\mu_s - E_s)^2} \right). \tag{3.95}$$

This constitutes a renormalization of the constant U_0 in Eq. (3.8), but in an experimental setting this shift can be compensated by e.g. the application of a gate voltage, and going forward we will ignore it such that the Fermi energy E_F still measures the energy difference between the middle of the SC gap and the lowest Landau level. The velocity is

$$\delta v = -\frac{k_S \Gamma_L^2}{\pi |\Delta_0|} \left[\frac{\pi}{2} - \arctan \left(\frac{-\mu_s + E_s}{|\Delta_0|} \right) \right], \tag{3.96}$$

which we can again approximate for $\mu \gg E_s, |\Delta_0|$ as

$$\delta v \simeq -\frac{k_S \Gamma_L^2}{|\Delta_0|}. \tag{3.97}$$

Applying the approximations in Eqs. (3.92) and (3.97) to the effective dispersion in Eq. (3.85) we can plot the dispersion to second order in δq in Fig. 3.4 for different values of the Fermi energy. Note that since the induced parameters $\delta E_{\delta q}, \Delta_{\delta q}$ are odd in δq, they contribute only to first order in δq, while the original QH edge dispersion E_q is quadratic in δq and its contribution is unmodified.

3.8 Particle/hole mixing

As discussed in the previous section, the experimentally interesting effect is particle/hole mixing near the Fermi energy. This happens at $\delta q = 0$ when $q_F = k_s$, which corresponds to $E_F = E_{k_s} = \omega_c$. As shown in Fig. 3.4, $E_F = \omega_c$ is indeed the condition under which the bands touch, while for $E_F < \omega_c$ the bands are separate and for $E_F > \omega_c$ we see avoided crossings. To see better understand the particle/hole mixing at the avoided crossings, we write up the effective Hamiltonian on matrix form in the Nambu basis $(\psi_{k_s+\delta q}, \psi_{k_s-\delta q}^\dagger)$, such that

$$H_{\text{eff}} = \frac{1}{2} \sum_{\delta q} \begin{pmatrix} \psi_{k_s+\delta q}^\dagger \\ \psi_{k_s-\delta q} \end{pmatrix}^T \begin{pmatrix} \tilde{E}_{\delta q} & \Delta_{\delta q} \\ \Delta_{\delta q}^* & -\tilde{E}_{-\delta q} \end{pmatrix} \begin{pmatrix} \psi_{k_s+\delta q} \\ \psi_{k_s-\delta q}^\dagger \end{pmatrix}. \tag{3.98}$$
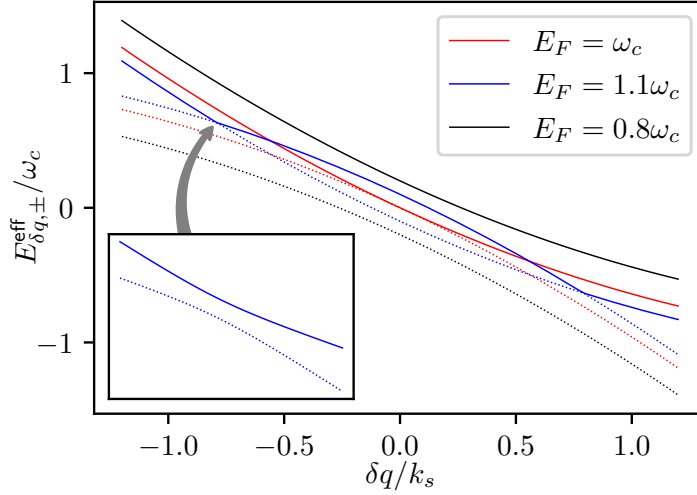
Figure 3.4: *The effective dispersion in Eq. (3.85) to second order in δq for different Fermi energies. Solid and dotted lines denote particle-like bands, $E_{\delta q,+}^{eff}$, and hole-like bands, $E_{\delta q,-}^{eff}$, respectively. The inset shows the avoided crossing for $E_F > \omega_c$. The dispersion has been calculated for effective parameters $m_s = 10m_e$, $\mu_s = 4 \cdot 10^3 \omega_c$, $|\Delta_0| = 40\omega_c$, $\lambda = 0.8\ell$, and $\Gamma_L = \alpha = \omega_c \ell$.*

Particles and holes are treated as separate particles in a scattering calculation. We therefore explicitly define the particle p and hole h operators

$$
\begin{aligned}
p_{\delta q}^\dagger &\stackrel{\text{def}}{=} \psi_{k_s+\delta q}^\dagger, \\
h_{\delta q}^\dagger &\stackrel{\text{def}}{=} \psi_{k_s-\delta q}.
\end{aligned}
\tag{3.99}
$$

With this definition we are counting an electron operator such as $\psi_{k_s+\delta q}$ twice, once as the particle operator $p_{\delta q}$ and once as the hole operator $h_{-\delta q}^\dagger$. This double counting is, however, already accounted for in Eq. (3.98) by the factor $1/2$ in front. Physically, it is not an issue, since describing an electron state as either a particle or hole state are equivalent. Then the Hamiltonian is

$$
H_{\text{eff}} = \frac{1}{2} \sum_{\delta q} \begin{pmatrix} p_{\delta q}^\dagger \\ h_{\delta q}^\dagger \end{pmatrix}^T \begin{pmatrix} \tilde{E}_{\delta q} & \Delta_{\delta q} \\ \Delta_{\delta q}^* & -\tilde{E}_{-\delta q} \end{pmatrix} \begin{pmatrix} p_{\delta q} \\ h_{\delta q} \end{pmatrix}
\tag{3.100}
$$

In the absence of pairing, i.e. for $\Delta_{\delta q} \to 0$, the holes are simply a doubling of the particle system, but with opposite energy and momentum. The hybridization of these two types of particles becomes clear upon diagonalization in the presence of pairing. Explicitly, $\tilde{u}$ and $\tilde{v}$ as defined in Eq. (3.88) determine the amplitudes of the particle and hole states,

$$
H_{\text{eff}} = \frac{1}{2} \sum_{\delta q} \begin{pmatrix} \tilde{u}_{\delta q} p_{\delta q}^\dagger + \tilde{v}_{\delta q}^* h_{\delta q}^\dagger \\ \tilde{v}_{\delta q} p_{\delta q}^\dagger - \tilde{u}_{\delta q}^* h_{\delta q}^\dagger \end{pmatrix}^T \begin{pmatrix} E_{\delta q,+}^{\text{eff}} & 0 \\ 0 & E_{\delta q,-}^{\text{eff}} \end{pmatrix} \begin{pmatrix} \tilde{u}_{\delta q}^* p_{\delta q} + \tilde{v}_{\delta q} h_{\delta q} \\ \tilde{v}_{\delta q}^* p_{\delta q} - \tilde{u}_{\delta q} h_{\delta q} \end{pmatrix}.
\tag{3.101}
$$

Recalling the definitions in Eq. (3.88),

$$\tilde{u}_{\delta q} = \sqrt{\frac{1}{2}\left(1 + \frac{\tilde{E}_{\delta q} + \tilde{E}_{-\delta q}}{\sqrt{(\tilde{E}_{\delta q} + \tilde{E}_{-\delta q})^2 + 4|\Delta_{I,\delta q}|^2}}\right)},$$

$$\tilde{v}_{\delta q} = ie^{-i\phi_\Delta}\sqrt{\frac{1}{2}\left(1 - \frac{\tilde{E}_{\delta q} + \tilde{E}_{-\delta q}}{\sqrt{(\tilde{E}_{\delta q} + \tilde{E}_{-\delta q})^2 + 4|\Delta_{I,\delta q}|^2}}\right)},$$

(3.102)

we see that an even mix $|\tilde{v}|^2 = |\tilde{u}|^2 = 1/2$ occurs at a point $\delta q = \delta q_{1/2}$ where $\tilde{E}_{\delta q_{1/2}} = -\tilde{E}_{-\delta q_{1/2}}$. This is the point which minimizes the distance between the bands, which becomes

$$|E^{\text{eff}}_{\delta q_{1/2},+} - E^{\text{eff}}_{\delta q_{1/2},-}| = |\Delta_{\delta q_{1/2}}|.$$

(3.103)

Since we are interested in the behavior near the Fermi energy, we found in the previous section that we should consider $q_F \simeq k_s$ where the QH edge Fermi momentum matches the Meissner current momentum at the SC surface. Recalling the definition in Eq. (3.9),

$$q_F(E_F) = \frac{2}{\ell}\left(1 + \frac{\lambda}{2\ell} - \sqrt{\frac{E_F}{\omega_c}}\right)$$

(3.104)

as well as the fact that we found $k_s = \lambda/\ell^2$ in Section 2.5.1, we see that the condition $q_F \simeq k_S$ corresponds to $E_F \simeq \omega_c$. Let us define a quantity Ω measuring the departure from this condition,

$$\Omega = \omega_c - E_F.$$

(3.105)

The full behavior of the amplitudes $|\tilde{u}_{\delta q}|$ and $|\tilde{v}_{\delta q}|$ under the condition $\Omega \simeq 0$ is shown in Fig. 3.5. We see that for $\Omega < 0$, a shift between particle-like and hole-like states occurs, while for $\Omega > 0$ there is only weak mixing. The evenly mixed states only occur at avoided crossings, and thus only for $\Omega \leq 0$. Transition across the resonance $\Omega = 0$ is discontinuous, with

$$\lim_{\Omega \to 0^+} |\tilde{u}_{\delta q=0}|^2 = 1,$$

(3.106)

$$\lim_{\Omega \to 0^-} |\tilde{u}_{\delta q=0}|^2 = 0,$$

(3.107)

where $0^\pm$ means zero approached from the positive (+) or the negative side (−). At $\Omega = 0$ exactly we have $\tilde{E}_{\delta q=0} = 0$, and we can apply L'Hôpital's rule to see that

$$\lim_{\delta q \to 0}\left(\left.\frac{\tilde{E}_{\delta q} + \tilde{E}_{-\delta q}}{\sqrt{(\tilde{E}_{\delta q} + \tilde{E}_{-\delta q})^2 + 4|\Delta_{I,\delta q}|^2}}\right|_{\Omega=0}\right) = 0$$

(3.108)

since $\tilde{E}_{\delta q}$ depends on the square of δq, while $|\Delta_{\delta q}|$ depends linearly on δq. In that case, $|\tilde{u}_{\delta q=0}| = |\tilde{v}_{\delta q=0}| = 1/2$. This description is analogous to that of complex p-wave pairing between spinless fermions by Read and Green [65], where the pairing depends on momentum as $\Delta_{\text{cP}} = \Delta_0(k_x - ik_y)$. In that context, we see that Ω is the order parameter
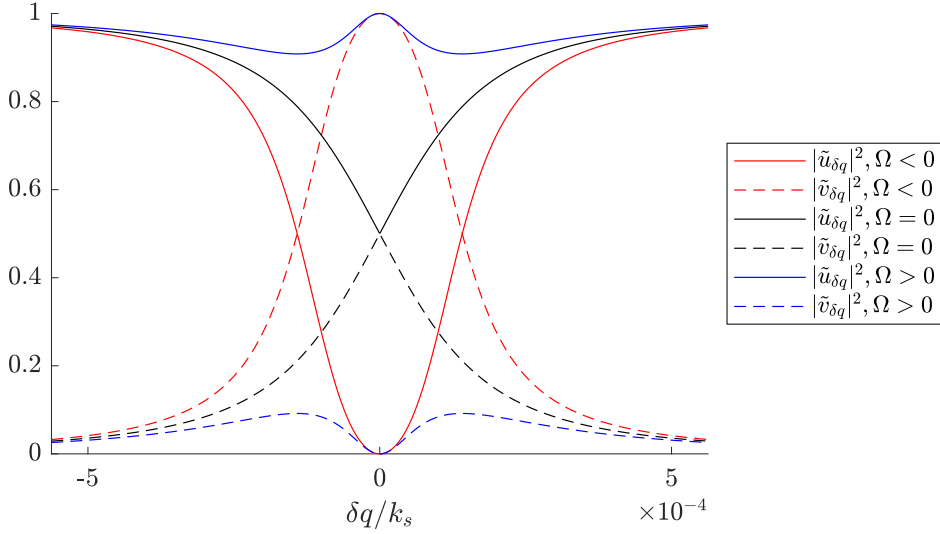
Figure 3.5: *The amplitudes of the particle-like state $|u_{\delta q}|^2$ (full lines) and the hole-like state $|v_{\delta q}|^2$ (dashed lines) for the case of avoided crossings $\Omega < 0$ (red), touching bands $\Omega = 0$ (black), and no avoided crossings $\Omega > 0$ (blue). For illustrative purposes, the deviations from the resonance conditions are chosen to be small, $\Omega = \pm 5 \cdot 10^{-9} \, \omega_c$, and we have the same effective parameters as in Fig. 3.4.*

of a topological phase transition. Then $\Omega > 0$ describes the strong-pairing phase where the position dependence of the pairing will fall off quickly, corresponding to tightly bound pairs, while $\Omega < 0$ describes the weak-pairing phase with the pairing amplitude decaying slowly in space. Furthermore, $\Omega = 0$ marks the topological phase transition where the gap between the upper and lower bands of the effective dispersion closes.

It is clear that for any non-zero amplitude of the induced pairing $|\Delta_{\mathrm{p}}| \neq 0$, the degree of particle-hole mixing is determined by the resonance condition, which in turn depends on the externally tunable parameters of E_F, which is controlled by e.g. a gate voltage, and ω_c which is controlled by the strength of the applied magnetic field. But while the pairing amplitude does not control the degree of mixing, it controls how fast the mixed states decays into non-mixed states as a function of δq. Thus for small Δ_{p}, the shift from particle-like state to hole-like state will happen across a narrow interval of δq. As we saw in Eq. (3.92), the width of the transition is thus increased for greater amplitudes of tunneling and SOC, as well as larger effective mass and larger London penetration depth since $E_s \propto \lambda^2$. Meanwhile it is decreased for larger SC pairing amplitude $|\Delta_0|$. None of these parameters depend simply on easily varied externally applied parameters. In the next chapter we will attach measurable quantities to the particle/hole transition, and in that context we will take consider more detailed behavior.

3.8.1 Finite tunneling barrier

The resonance condition corresponds to finding the Fermi energy at the second Landau level. This is problematic, since we have assumed that there is only one edge state, i.e. we are at filling factor $\nu = 1$. In the presence of more edge states, the situation changes qualitatively as interplay between the edge states is introduced, as has been shown using a phenomenological model [33, 58], and which will be explored further in Chapter 5.

The fact that crossing the resonance condition corresponds to crossing the second Landau level is a consequence of the assumption of a hard wall confining potential in
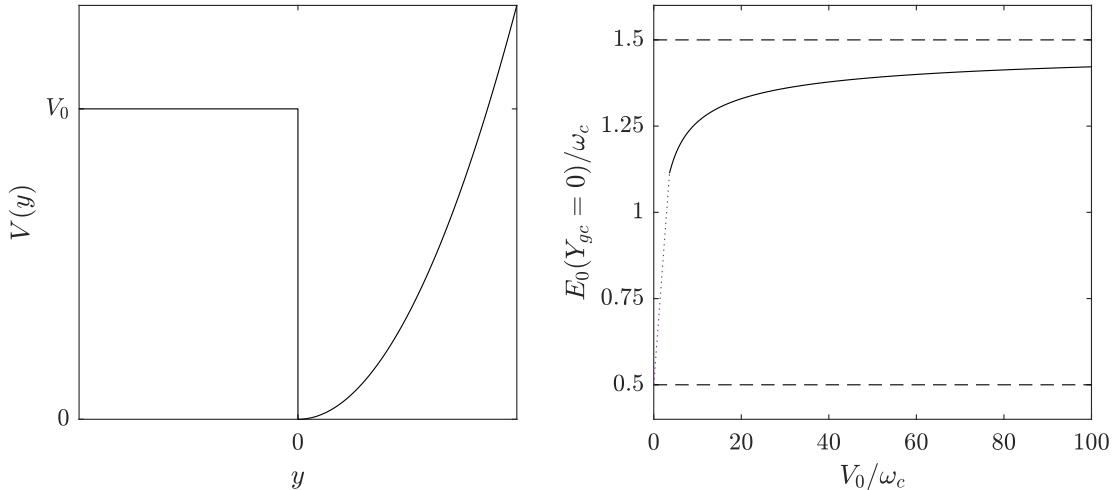
Figure 3.6: *Left: Sketch of a half harmonic oscillator with a step of size V_0 in the middle. Right: The lowest energy eigenvalue of the half harmonic oscillator (full line) with the zero and infinite barrier limits marked by dashed lines. The half harmonic oscillator ground state asymptotically approaches the infinite barrier result $E = 3\omega_c/2$ from below. This system corresponds to a QH edge state with guiding center coordinate $Y_{gc} = 0$ confined by a finite edge potential. The dotted line indicates a linear interpolation between the full harmonic oscillator ground state energy and the lowest potential barrier treated numerically.*

the derivation of the approximate QH edge dispersion in Section 2.2. The condition $q_F = k_s$ generally corresponds to fixing the Fermi energy with the condition $E_{\delta q=0} = 0$. Since $k_s = \lambda \ell^2$, the state corresponding to $\delta q = q - k_s = 0$ is the harmonic oscillator state with guiding center coordinate $Y_{gc} = 0$, i.e. with a barrier in the middle. The ground state energy of a harmonic oscillator with a barrier in the middle was solved in Ref. [40] in both the finite and infinite cases. For a one-dimensional system with the potential, see the left side of Fig. 3.6

$$\frac{V(y)}{\omega_c} = \begin{cases} V_0/\omega_c \text{ for } y \leq 0, \\ y^2/(2\ell^2) \text{ for } y > 0, \end{cases} \tag{3.109}$$

i.e. a half harmonic oscillator with a finite step in the middle, the lowest energy eigenvalue is given by a transcendental equation whose numerical solution is shown on the right side of Fig. 3.6. Note that in the $V_0 \to 0$ limit, Eq. (3.109) does not become a harmonic oscillator, and thus solutions with small V_0 are ignored in Fig. 3.6, with the full harmonic oscillator limit indicated by a dotted line. We see that for greater barrier strengths, the energy approaches the second Landau level at $E = 3\omega_c/2$ asymptotically from below. Thus, for large but finite barriers, we predict that the resonance condition is found at some Fermi energy near, but below, the second Landau level, $E_F < \omega_c$.

3.9 Summary

We present an approximate QH edge dispersion with a Fermi energy E_F measuring the energy difference from the lowest Landau level to the Fermi level, and find that a constant vector potential at the SC surface is a good approximation for experimentally relevant materials. We then assume Rashba SOC at the SC surface to allow for the critical spin-flip needed for Andreev reflection, and model the tunneling coupling between the

systems. We then find that the total model predicts lower critical SC fields than found in experiment, which underlines the qualitative nature of the model.

We assume that the SOC is small compared to the SC gap, and consider it perturbatively to first order. The resulting diagonal SC Hamiltonian is then integrated out, resulting in an effective model of the proximitized QH edge with induced pairing and contributions to the kinetic energy,

$$H_{\text{eff}} = \sum_{\delta q} \left[(E_{k_s + \delta q} + \delta E_{\delta q}) \psi^{\dagger}_{k_s + \delta q} \psi_{k_s + \delta q} + \left(\frac{\Delta_{\delta q}}{2} \psi^{\dagger}_{k_s + \delta q} \psi^{\dagger}_{k_s - \delta q} + \text{h. c.} \right) \right]. \quad (3.110)$$

The full expressions for $\delta E_{\delta q}$ and $\Delta_{\delta q}$ are derived, with the pairing amplitude being

$$\Delta_{\delta q} = -i e^{i \phi_{\Delta}} \Gamma_L^2 \alpha \frac{m_s E_s}{2 |\Delta_0|^2} \delta q, \quad (3.111)$$

in the lowest order in δq. The effective dispersion of the system sees avoided crossings between particle and hole bands, which indicates particle-hole mixing. This mixing occurs even for weakly induced pairing, and we derive the resonance condition

$$\Omega = \omega_c - E_F, \quad (3.112)$$

which is the energy for which the system undergoes a topological phase transition between weak and strong pairing. This condition corresponds to the condition $q_F = k_s$, and is thus fundamentally linked to the Meissner effect at the SC surface. We predict that for finite barrier strengths at the interface, the transition occurs at Fermi energies below ω_c.

Having derived the effective Hamiltonian, we proceed to predict the experimental signatures associated with the system it describes.

Transport through the proximitized edge

We now wish to investigate transport through the proximitized edge states, also known as Andreev edge states. In particular, we will draw inspiration from experiments [24, 25] and consider the setup sketched in Fig. 4.1. Here four leads with chemical potentials $\mu_{1,...,4}$ are connected to a two-dimensional electron gas (2DEG) in the quantum Hall (QH) phase. A current I is passed through the system, carried by the chiral edge states which propagate in a clockwise direction. As the current passes through the Andreev edge states characterized by induced superconductivity, the particle and hole states
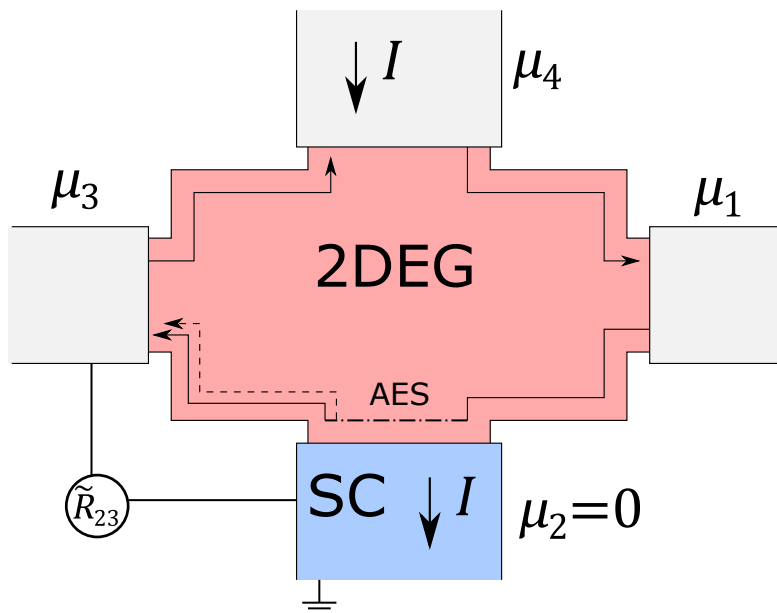
Figure 4.1: *A sketch of a transport experiment measuring the downstream resistance $\tilde{R}_{23} = dV_3/dI$, where $V_3 = \mu_3/e$. A 2DEG in a strong magnetic field is connected to three normal leads and one grounded SC lead (lead 2). A current I is injected through lead 4 and leaves through lead 2, while leads 1 and 3 are voltage leads measuring μ_1 and μ_3. Due to the proximity effect, the edge channel passing lead 2 consists of Andreev edge states (AES) which are mixtures of particle and hole states.*

mix. Since the particle and hole states have opposite charge, the mixing can be detected in the charge transport. In particular, we will consider the effect of the mixing on the differential resistance as measured downstream of the SC-QH interface, i.e. between terminals 2 and 3

$$\tilde{R}_{23} = \frac{dV_3}{dI} \tag{4.1}$$

where $V_3 = \mu_3/e$ is the voltage corresponding to the chemical potential μ_3 with e being the elementary charge. We assume that the SC is grounded such that the chemical potential of the other terminals are measured in relation to μ_2, and fix it to the middle of the SC gap, $\mu_2 = 0$. This further means that the SC can absorb an arbitrary amount of charge. We note that the chemical potential μ_2 corresponding to the voltage of terminal 2, and the SC chemical potential μ_s which enters into the BCS Hamiltonian are different quantities, since μ_s represents what the chemical potential of the metallic SC would be in the absence of superconductivity.

For the integer QH case, transport can be modeled by a scattering calculation in the Landauer-Büttiker formalism. We will present this formalism in a particle-hole context, and use it to predict the effect of the induced superconductivity on $\tilde{R}_{23}$. For further reading see Ref. [42]. Going forward we will work in units where $|e| = 1$ such that charge current and probability current are the same.

4.1 Scattering in the particle-hole basis

As discussed in Section 2.2, the chiral edge state conduction in QH systems is one-dimensional and ballistic, i.e. insensitive to backscattering. This insensitivity is qualitatively different from superconductivity, where electron scattering involves breaking apart a Cooper pair and thus exciting electrons above the SC gap of magnitude $|\Delta_0|$. Instead, due to the chirality of the edge states, backscattering in a QH edge would involve scattering to the opposite edge of the 2DEG, and is thus strongly suppressed by the macroscopic distance involved. What type of transport do we then expect in the proximitized edge, superconducting or ballistic? As shown in Section 3.7, the proximity effect does not induce a gap into the QH edge, and also does not affect the chirality of the edge state by introducing any backscattering channels. Thus the transport will remain ballistic.

One-dimensional charge transport through ballistic channels is well understood in the Landauer-Büttiker formalism [42], which relates transport quantities such as current to the microscopic details of the ballistic system. This formalism can be extended to the superconducting case [13,14,24] by explicitly taking particle-hole mixing into account as for example done in the seminal paper by Blonder, Tinkham and Klapwijk [48]. In this section we use these formalisms to carefully derive the current of a superconducting, ballistic edge channel in terms of the scattering amplitudes between particle and hole states.

4.1.1 Particles and holes

We will first derive the current of a general 1D system of particles and holes, and then apply it to the specific case shown in Fig. 4.1. The discussion of particles and holes will be similar to that of Section 3.8, but it is necessary to repeat in clear detail to ensure consistent definitions for transport calculations.

Consider the electron operator c_k which annihilates a one-dimensional electron with momentum k and kinetic energy $\epsilon_k = k^2/(2m) - E_F$, where m is the electron mass and $E_F = k_F^2/(2m)$ is the Fermi energy with associated Fermi momentum k_F. We define the operator as annihilating a particle for momenta above a fixed momentum k_0, and define it as creating a hole for momenta below k_0

$$c_k = \begin{cases} p_{k-k_0} \text{ for } k > k_0, \\ h_{k_0-k}^\dagger \text{ for } k \leq k_0, \end{cases} \tag{4.2}$$

where we have made the arbitrary choice of having a hole operator at $k = k_0$. Typically we have $k_0 = k_F$, but in light of the role of the supercurrent momentum in the previous chapter, we will keep k_0 general, and show that the choice has no effect on the current. The particle and hole definitions correspond to

$$p_k = c_{k_0+k} \text{ for } k > 0,$$
$$h_k = c_{k_0-k}^\dagger \text{ for } k \geq 0 \tag{4.3}$$

The free electron Hamiltonian is then

$$\begin{aligned} H_1 &= \sum_{k>k_0} \epsilon_k c_k^\dagger c_k + \sum_{k\leq k_0} \epsilon_k c_k^\dagger c_k \\ &= \sum_{k>k_0} \epsilon_k p_{k-k_0}^\dagger p_{k-k_0} + \sum_{k\leq k_0} \epsilon_k h_{k_0-k} h_{k_0-k}^\dagger \\ &= \sum_{k>0} \epsilon_{k+k_0} p_k^\dagger p_k + \sum_{k\geq 0} \epsilon_{k_0-k} h_k h_k^\dagger, \end{aligned} \tag{4.4}$$

where the last term involved shifting the momentum variable. For energies near the Fermi energy, we can linearize the spectrum around the Fermi momentum $k_F = \sqrt{2mE_F}$ as $\epsilon_k = v_F(k - k_F)$ and thus define

$$\begin{aligned} \epsilon_{p,k} &= \epsilon_{k+k_0} = v_F(k + k_0 - k_F), \\ \epsilon_{h,k} &= -\epsilon_{k_0-k} = v_F(k - k_0 + k_F), \end{aligned} \tag{4.5}$$

where we have used that $\epsilon_{k_F} = 0$. An important detail that we will apply later is that particles and holes only differ by the sign of the (shifted) Fermi momentum $k_0 - k_F$. In other words, the two particles share the same group velocity v_F, but their bands are separated by an energy $2v_F(k_0 - k_F)$. For $k_0 = k_F$, the two bands are the same. The Hamiltonian becomes

$$H_1 = \sum_{k>0} \epsilon_{p,k} p_k^\dagger p_k + \sum_{k\geq 0} \epsilon_{h,k} h_k^\dagger h_k + \text{const.}, \tag{4.6}$$

where the constant is added due to the fermionic nature of the fields $\{h_k, h_k^\dagger\} = 1$ and will be ignored. We note that the linearization implies infinite bands, which means it introduces an implicit momentum cutoff beyond which the linear model fails.

4.1.2 Current

The probability current density J passing through the one-dimensional system is given by the continuity equation under conservation of charge

$$\partial_t \rho + \partial_x J = 0, \tag{4.7}$$

where $\rho(x)$ is the local density operator whose time evolution is given by

$$\partial_t \rho = i[H_1, \rho],$$ (4.8)

with the Hamiltonian H_1 defined in Eq. (4.6). For the linearized system of free electrons in one dimension, the result is well known [42], and the average probability current density can be expressed in terms of momentum states

$$\langle J \rangle = \frac{v_F}{L} \sum_k \langle c_k^\dagger c_k \rangle.$$ (4.9)

In other words, the probability density is the summed product of electron density $1/L$ and velocity v_F for each occupied state. In particular, assuming all states are occupied below k_F, and none above, we have

$$\langle J \rangle = \frac{v_F}{L} \sum_{k \leq k_F} 1,$$ (4.10)

which formally diverges due to the assumption of an infinite band. In one dimension, the current density J is the same as the current I [42], and so we can write the average current in terms of particles and holes as

$$
\begin{aligned}
\langle I \rangle &= \frac{v_F}{L} \left(\sum_{k > k_0} \langle c_k^\dagger c_k \rangle + \sum_{k \leq k_0} \langle c_k^\dagger c_k \rangle \right) \\
&= \frac{v_F}{L} \left(\sum_{k > k_0} \langle p_{k-k_0}^\dagger p_{k-k_0} \rangle + \sum_{k \leq k_0} \langle h_{k_0-k} h_{k_0-k}^\dagger \rangle \right) \\
&= \frac{v_F}{L} \left(\sum_{k > 0} \langle p_k^\dagger p_k \rangle - \sum_{k \geq 0} \langle h_k^\dagger h_k \rangle + \sum_{k \leq k_0} 1 \right).
\end{aligned}
$$ (4.11)

Despite particles and holes having the same group velocity, see Eq. (4.5), and thus moving in the same direction, particles contribute positively to the current, while holes contribute negatively to the current.

We now consider a system where electrons are allowed to move in two directions with velocities $\pm v_F$, labeling those moving in the positive direction as incoming with associated operator i_k, and those moving in the negative direction as outgoing with associated operator o_k. Ultimately this will used to model the currents in and out of the terminals in Fig. 4.1. Since we now simply have two free electron systems in one dimension, we can repeat the above analysis to write the current of the system as

$$\langle I \rangle = \frac{v_F}{L} \left(\sum_k \langle i_k^\dagger i_k \rangle - \sum_k \langle o_k^\dagger o_k \rangle \right).$$ (4.12)

As we did in Eq. (4.3), we can then define in- and outgoing particle operators as $p_{i/o,k}$, as well as the equivalent hole operators $h_{i/o,k}$, with i indicating incoming and o indicating

outgoing. The current in terms of particles and holes then becomes

$$\langle I \rangle = \frac{v_F}{L} \left(\sum_{k>k_0} \langle p^\dagger_{i,k-k_0} p_{i,k-k_0} \rangle - \sum_{k \leq k_0} \langle h^\dagger_{i,k_0-k} h_{i,k_0-k} \rangle + \sum_{k \leq k_0} 1 \right)$$

$$- \frac{v_F}{L} \left(\sum_{k>k_0} \langle p^\dagger_{o,k-k_0} p_{o,k-k_0} \rangle - \sum_{k \leq k_0} \langle h^\dagger_{o,k_0-k} h_{o,k_0-k} \rangle + \sum_{k \leq k_0} 1 \right). \quad (4.13)$$

We resolve the parentheses and find that the constant contributions cancel since they correspond to opposite electron currents,

$$\langle I \rangle = \frac{v_F}{L} \left(\sum_{k>k_0} \left[\langle p^\dagger_{i,k-k_0} p_{i,k-k_0} \rangle - \langle p^\dagger_{o,k-k_0} p_{o,k-k_0} \rangle \right] \right.$$

$$\left. - \sum_{k \leq k_0} \left[\langle h^\dagger_{i,k_0-k} h_{i,k_0-k} \rangle - \langle h^\dagger_{o,k_0-k} h_{o,k_0-k} \rangle \right] \right)$$

$$= \frac{v_F}{L} \left(\sum_{k>0} \left[\langle p^\dagger_{i,k} p_{i,k} \rangle - \langle p^\dagger_{o,k} p_{o,k} \rangle \right] + \sum_{k \geq 0} \left[-\langle h^\dagger_{i,k} h_{i,k} \rangle + \langle h^\dagger_{o,k} h_{o,k} \rangle \right] \right), \quad (4.14)$$

where we have shifted the momentum variable in the second step. We find that ingoing particles and outgoing holes contribute positively to the current, while outgoing particles and ingoing holes contribute negatively, which is what we would expect. All the currents discussed are independent of the choice of k_0, as they should be.

4.1.3 Scattering

We will now modify Eq. (4.14) to account for the scattering of incoming particle into outgoing particles at the terminals. In the continuum limit $\sum_k \to L \int dk/2\pi$ we have

$$\langle I \rangle = v_F \int_0^\infty \frac{dk}{2\pi} \left(\langle p^\dagger_{i,k} p_{i,k} \rangle + \langle h^\dagger_{o,k} h_{o,k} \rangle - \langle p^\dagger_{o,k} p_{o,k} \rangle - \langle h^\dagger_{i,k} h_{i,k} \rangle \right). \quad (4.15)$$

For the scattering context will relabel the fields $p_{i,k} \to i_{p,k}$ etc., which will make future notation more readable. In this labeling we have

$$\langle I \rangle = v_F \int_0^\infty \frac{dk}{2\pi} \left(\langle i^\dagger_{p,k} i_{p,k} \rangle + \langle o^\dagger_{h,k} o_{h,k} \rangle - \langle o^\dagger_{p,k} o_{p,k} \rangle - \langle i^\dagger_{h,k} i_{h,k} \rangle \right). \quad (4.16)$$

Furthermore, in preparation for treating the NS junction between normal edge state and proximitized edge state, we note that for a system without translational invariance momentum is not conserved, but energy is. We relabel the states in terms of energy instead of momentum as i_E, o_E by performing the substitution $k = E/v_F$,

$$\langle I \rangle = \frac{1}{2\pi} \int dE \left(\langle i^\dagger_{p,E} i_{p,E} \rangle + \langle o^\dagger_{h,E} o_{h,E} \rangle - \langle o^\dagger_{p,E} o_{p,E} \rangle - \langle i^\dagger_{h,E} i_{h,E} \rangle \right). \quad (4.17)$$

In a multi-terminal system with ballistic conduction, the in- and outgoing modes of each terminal are related through the scattering matrix [42] as

$$o_{m,j,E} = \sum_{\substack{n \\ l=p,h}} t^*_{m,n,j,l}(E) i_{n,l,E}, \quad (4.18)$$

47

where the indices $j, l \in \{p, h\}$ describe whether we are dealing with particles or hole, while the indices $m, n = 1, 2, 3, \ldots$ label the terminals. In the four-terminal case, the scattering matrix has dimensions 8×8 to account for both particles and holes, with the matrix elements $t_{m,n,j,l}(E)$ being the amplitude a particle of type l from terminal n being transmitted to terminal m as a particle of type j, all at energy E. Due to the ballistic nature of the conduction, the energy does not change in the transmission process. Applying this relation between in- and outgoing particles to the current in Eq. (4.17) while keeping the order of terms, we have the current through terminal m

$$\langle I_m \rangle = \frac{1}{2\pi} \int dE \Bigg(\langle i_{m,p,E}^\dagger i_{m,p,E} \rangle + \sum_{\substack{n \\ l=p,h}} |t_{m,n,h,l}(E)|^2 \langle i_{n,l,E}^\dagger i_{n,l,E} \rangle$$
$$- \sum_{\substack{n \\ l=p,h}} |t_{m,n,p,l}(E)|^2 \langle i_{n,l,E}^\dagger i_{n,l,E} \rangle - \langle i_{m,h,E}^\dagger i_{m,h,E} \rangle \Bigg). \quad (4.19)$$

Since the expectation values involved are for number operators at a certain energy, we can resolve them by assigning a chemical potential μ_m and assuming Fermi distributions $n_F(E - \mu_m)$ in each lead. For the particle operators, this leads to

$$\langle i_{m,p,E}^\dagger i_{n,p,E'} \rangle = \delta(E - E')\delta_{m,n} n_F(E - \mu_m). \quad (4.20)$$

Since we know from Eq. (4.5) that the only difference between particle Hamiltonian and hole Hamiltonian is the sign of the chemical potential, we also have

$$\langle i_{m,h,E}^\dagger i_{n,h,E'} \rangle = \delta(E - E')\delta_{m,n} n_F(E + \mu_m). \quad (4.21)$$

We can then write out the particle and hole terms of the current, which after re-arranging the terms becomes

$$\langle I_m \rangle = \frac{1}{2\pi} \int dE \Bigg(\langle i_{m,p,E}^\dagger i_{m,p,E} \rangle - \langle i_{m,h,E}^\dagger i_{m,h,E} \rangle$$
$$+ \sum_n \Bigg[\left(|t_{m,n,h,p}(E)|^2 - |t_{m,n,p,p}(E)|^2 \right) \langle i_{n,p,E}^\dagger i_{n,p,E} \rangle$$
$$+ \left(|t_{m,n,h,h}(E)|^2 - |t_{m,n,p,h}(E)|^2 \right) \langle i_{n,h,E}^\dagger i_{n,h,E} \rangle \Bigg] \Bigg), \quad (4.22)$$

where evaluating the expectation values yields

$$\langle I_m \rangle = \frac{1}{2\pi} \sum_n \int dE \Bigg(n_F(E - \mu_m) + \left(|t_{m,n,h,p}(E)|^2 - |t_{m,n,p,p}(E)|^2 \right) n_F(E - \mu_n)$$
$$+ \left(|t_{m,n,h,h}(E)|^2 - |t_{m,n,p,h}(E)|^2 \right) n_F(E + \mu_n) - n_F(E + \mu_m) \Bigg). \quad (4.23)$$

To calculate the current through the system we then need to derive expressions for the transmission amplitudes t. We will do this by solving the first quantization Schrödinger equation corresponding to the system and finding the solutions for an NS junction.
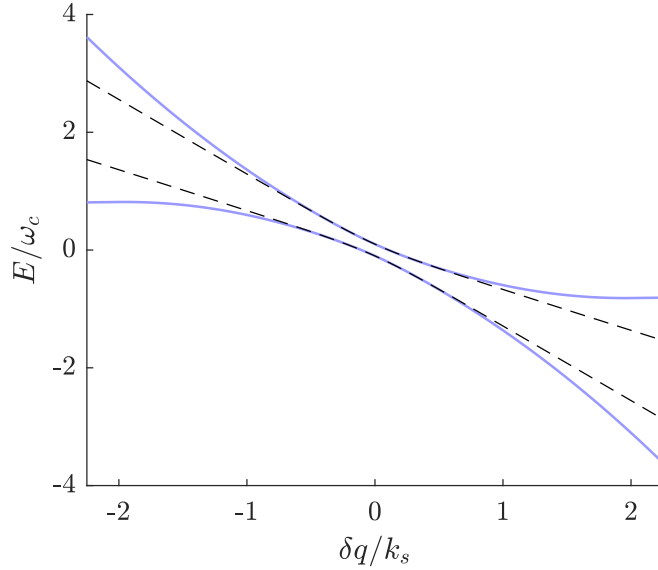
Figure 4.2: *The spectrum in Eq. (4.26) (black dashed line) of the linear effective QH edge Hamiltonian compared to the full effective spectrum in Eq. (3.85) (blue full line). It is plotted for $\Omega = \omega_c/10$ with an exaggerated $\Delta_p = v_F/\sqrt{10}$ for illustrative purposes. While the spectrum is a good approximation for $\Omega \geq 0$, it is symmetric across $\Omega = 0$ and thus fails to take into account the avoided crossings at $\Omega < 0$.*

4.2 Position-dependent parameters

To model electron scattering through a proximitized region of the QH edge, we will consider what is effectively a one dimensional chiral system with a proximitized region surrounded by two normal regions, i.e. an NSN junction. This will be modeled by introducing position dependence into the parameters of the Hamiltonian as follows.

We consider the linear approximations around $\delta q = 0$ of Eqs. (3.89) and (3.94), as well as the linear approximation of the non-proximitized QH edge dispersion

$$E_{k_S+\delta q} \simeq \Omega - \omega_c \ell \delta q \tag{4.24}$$

with Ω defined as $\omega_c - E_F$ in Eq. (3.105). Under these approximations, the effective Hamiltonian of the proximitized QH edge in Eq. (3.100) becomes

$$H_{\text{eff,lin}} = \frac{1}{2} \sum_{\delta q} \begin{pmatrix} p_{\delta q}^\dagger \\ h_{\delta q}^\dagger \end{pmatrix}^T \begin{pmatrix} \Omega + v_F \delta q & i\Delta_{\text{p}} \delta q \\ -i\Delta_{\text{p}} \delta q & -\Omega + v_F \delta q \end{pmatrix} \begin{pmatrix} p_{\delta q} \\ h_{\delta q} \end{pmatrix}, \tag{4.25}$$

where we have $v_F = -\omega_c \ell + \delta v$. By linearizing $E_{k_S+\delta q}$, the following transport calculations are far more tractable, but at the cost of treating a slightly different model than that derived in the previous chapter. To illustrate the difference, we can diagonalize Eq. (4.25) to find the spectrum

$$E_{\text{eff,lin},\delta q,\pm} = \frac{1}{2}\left(v_F \delta q \pm \sqrt{\Omega^2 + (\Delta_{\text{p}} \delta q)^2}\right). \tag{4.26}$$

This spectrum is shown in Fig. 4.2 for $\Omega = \omega_c/10$, and with an exaggerated pairing amplitude $\Delta_{\text{p}} = v_F/\sqrt{10}$ for illustrative purposes. Since $E_{\text{eff,lin},\delta q}$ is symmetric across $\Omega = 0$, it fails to take into account the introduction of avoided crossings, but at $\Omega \geq 0$

and small momenta, which will be the focus of the analysis, the physics are unchanged by the approximation.

To allow for a spatially inhomogeneous system we Fourier transform to position space

$$p_{\delta q} = \frac{1}{\sqrt{L_0}} \int dx e^{-i\delta q x} p(x),$$

$$h_{\delta q} = \frac{1}{\sqrt{L_0}} \int dx e^{-i\delta q x} h(x),\tag{4.27}$$

where L_0 is the total length of the system, distinct from the length of the SC segment L. Then, we find

$$H_{\text{eff,lin}} = \frac{1}{2} \int dx \begin{pmatrix} p^\dagger(x) \\ h^\dagger(x) \end{pmatrix}^T \begin{pmatrix} \Omega - iv_F\partial_x & \Delta_\mathrm{p}\partial_x \\ -\Delta_\mathrm{p}\partial_x & -\Omega - iv_F\partial_x \end{pmatrix} \begin{pmatrix} p(x) \\ h(x) \end{pmatrix}.\tag{4.28}$$

Using this convention, the $p(x)$ and $h(x)$ modes propagate in the same direction, i.e. both towards the left for $v_F < 0$. We now introduce the NSN junction by assuming that the edge is only superconducting in a region $-L/2 < x < L/2$. We assume the transition between N and S regions to be steep on the length scale of the wave function, and model it as a step function, such that the Hamiltonian has the parameters

$$\Delta_\mathrm{p}(x) = \Delta_\mathrm{p}\, \theta(x + L/2)\theta(x - L/2),$$

$$v_F(x) = \omega_c\ell + \delta v\, \theta(x + L/2)\theta(x - L/2).\tag{4.29}$$

Note that since we ignored the constant shift in the linearization of $\delta E_{\delta q}$, see Eq. (3.94), we are technically missing a spatial dependence on Ω as well. Such a shift would constitute a potential barrier between the normal and proximitized regions, which cannot affect a chiral system with no backscattering, where perfect transmission is enforced by the conservation of probability current. In a physical scenario, a non-negligible potential barrier would force the edge state inwards into the 2DEG, in a similar situation to experiments where a superconducting finger protrudes into the 2DEG [22]. In the absence of crossed Andreev reflection, we do not expect any qualitative effects of this push beyond the weakening of the induced superconductivity as the edge state is pushed further away from the SC. This does not appear to be a concern in comparable experiments [24, 25], and we will assume no such potential barrier exists.

When introducing position dependence into the parameters in the Hamiltonian, they no longer commute with ∂_x, and care must be taken to ensure Hermiticity of the Hamiltonian. Since there are multiple Hermitian Hamiltonians which correspond to Eq. (4.28) in the limit of position independence, this is not a unique choice. This problem is well-known in the context of position dependent mass in semiconductor heterostructures [66], and the choice is not expected to have any effect within the accuracy of the presented model. We follow Ref. [15] and replace the product with an anti-commutator,

$$\Delta_\mathrm{p}\, i\partial_x \to \frac{1}{2}\{\Delta_\mathrm{p}(x), i\partial_x\},\tag{4.30}$$

and similarly for v_F. This has the correct limit for position-independent parameters and the Hamiltonian remains Hermitian. This can be seen if we define the matrix

$$M(x) = \begin{pmatrix} v_F(x) & i\Delta_\mathrm{p}(x) \\ -i\Delta_\mathrm{p}(x) & v_F(x) \end{pmatrix},\tag{4.31}$$

50

and write the NSN Hamiltonian

$$H_{\text{NSN}} = H_{\text{NSN},0} + H_{\text{NSN},M} \tag{4.32}$$

in terms of $M(x)$ and the spinor $\psi(x) = (p(x), h(x))^T$

$$H_{\text{NSN},0} = -\frac{i}{4} \int dx \psi^\dagger(x) \Omega \sigma_z \psi(x), \tag{4.33}$$

$$H_{\text{NSN},M} = -\frac{i}{4} \int dx \psi^\dagger(x) \{M(x), \partial_x\} \psi(x), \tag{4.34}$$

where σ_z is the Pauli matrix. Since $H_{\text{NSN},0}$ is trivially Hermitian, we can the check Hermiticity of $H_{\text{NSN},M}$ by writing out the anti-commutator

$$H_{\text{NSN},M} = -\frac{i}{4} \int dx \left(\psi^\dagger(x) M(x) [\partial_x \psi(x)] + \psi^\dagger(x) [\partial_x M(x) \psi(x)] \right). \tag{4.35}$$

Since $M(x)$ is unitary, we can replace it with $M^\dagger(x)$ integrate by parts in the second term

$$H_{\text{NSN},M} = -\frac{i}{4} \int dx \left(\psi^\dagger(x) M(x) [\partial_x \psi(x)] - [\partial_x \psi^\dagger(x)] M^\dagger(x) \psi(x) \right). \tag{4.36}$$

Since we have $[-i\partial_x \psi(x)]^\dagger = -i\partial_x \psi^\dagger(x)$ (i.e. the momentum operator is Hermitian), the Hamiltonian is Hermitian

$$H_{\text{NSN},M} = -\frac{1}{4} \int dx \left(i\psi^\dagger(x) M(x) [\partial_x \psi(x)] + \text{h. c.} \right). \tag{4.37}$$

We note that going forward, the most practical form to use is that in Eq. (4.35), written out as

$$\begin{aligned}
H_{\text{NSN},M} &= -\frac{i}{4} \int dx \left(\psi^\dagger(x) M(x) [\partial_x \psi(x)] + \psi^\dagger(x) [\partial_x M(x) \psi(x)] \right) \\
&= -\frac{i}{4} \int dx \left(\psi^\dagger(x) M(x) [\partial_x \psi(x)] + \psi^\dagger(x) [\partial_x M(x)] \psi(x) + \psi^\dagger(x) M(x) [\partial_x \psi(x)] \right) \\
&= -\frac{i}{2} \int dx \psi^\dagger(x) M(x) [\partial_x \psi(x)] - \frac{i}{4} \int dx \psi^\dagger(x) [\partial_x M(x)] \psi(x) \tag{4.38}
\end{aligned}$$

Given this NSN Hamiltonian, we are ready to discuss transport across the junction.

4.3   Boundary conditions

To calculate scattering across the NSN junction, we must ensure that we apply the correct boundary conditions at each NS junction. These are obtained by imposing continuity of the current through the interfaces. We thus need to first derive the correct form of the current operators associated with the Hamiltonian in Eq. (4.32).

4.3.1 Current

To find the current operator, we will use the one dimensional continuity equation

$$\partial_t \rho(x) + \partial_x J(x) = 0. \tag{4.39}$$

We define the local density as

$$\rho(x) = \psi^\dagger(x)\psi(x) \tag{4.40}$$

with the time evolution

$$\partial_t \rho(x) = i[H_{\text{NSN}}, \rho(x)]. \tag{4.41}$$

We can write out the Hamiltonian as a sum of particle and hole components with $\psi_1(x) = p(x)$ and $\psi_2(x) = h(x)$, such that

$$H_{\text{NSN}} = -\frac{i}{2} \sum_{r,s} \int dx\, \psi_r^\dagger (N_{rs} + M_{rs}\partial_x)\psi_s \tag{4.42}$$

with the matrix

$$N(x) = i\Omega\sigma_z + \frac{1}{2}\partial_x M(x). \tag{4.43}$$

The commutator describing the time evolution of the density is then

$$i[H_{\text{NSN}}, \rho(y)] = \frac{1}{2} \sum_{r,s,m} \int dx \left[\psi_r^\dagger(x)\Big(N_{rs}(x) + M_{rs}(x)\partial_x\Big)\psi_s(x), \psi_m^\dagger(y)\psi_m(y) \right]. \tag{4.44}$$

Defining the differential operator $D_{rs}(x) = N_{rs}(x) + M_{rs}(x)\partial_x$, we have

$$\partial_t \rho(y) = \frac{1}{2} \sum_{r,s,m} \int dx \left[\psi_r^\dagger(x)D_{rs}(x)\psi_s(x), \psi_m^\dagger(y)\psi_m(y) \right]. \tag{4.45}$$

We can then apply the commutator Eq. (B.16) from Appendix B to see

$$\partial_t \rho(y) = \frac{1}{2} \sum_{r,s,m} \int dx\, \psi_r^\dagger(x)\psi_m(y)\delta_{m,s}D_{rs}(x)\delta(x-y) - \psi_m^\dagger(y)\delta_{r,m}\delta(x-y)D_{rs}(x)\psi_s(x). \tag{4.46}$$

We write out $D(x)$ and integrate by parts in the first term

$$\begin{aligned}
\partial_t \rho(y) &= \frac{1}{2} \sum_{r,s,m} \int dx \Bigg\{ \Big[N_{rs}(x)\psi_r^\dagger(x) + M_{rs}(x)\psi_r^\dagger(x)\partial_x \Big]\delta_{m,s}\psi_m(y)\delta(x-y) \\
&\quad - \psi_m^\dagger(y)\delta_{r,m}\delta(x-y)\Big[N_{rs}(x) + M_{rs}(x)\partial_x \Big]\psi_s(x) \Bigg\} \\
&= \frac{1}{2} \sum_{r,s,m} \int dx \Bigg\{ \Big[N_{rs}(x)\psi_r^\dagger(x) - \partial_x[M_{rs}(x)\psi_r^\dagger(x)] \Big]\delta_{m,s}\psi_m(y)\delta(x-y) \\
&\quad - \psi_m^\dagger(y)\delta_{r,m}\delta(x-y)\Big[N_{rs}(x) + M_{rs}(x)\partial_x \Big]\psi_s(x) \Bigg\}, \tag{4.47}
\end{aligned}$$

after which we can evaluate the m sum and the x integral,

$$\partial_t \rho(y)$$

$$= \frac{1}{2} \sum_{r,s} \left\{ \left[N_{rs}(y)\psi_r^\dagger(y) - \partial_y[M_{rs}(y)\psi_r^\dagger(y)] \right] \psi_s(y) - \psi_r^\dagger(y) \left[N_{rs}(y) + M_{rs}(y)\partial_y \right] \psi_s(y) \right\}.$$

(4.48)

We note that the N terms cancel, and we are left with

$$\partial_t \rho(y) = -\frac{1}{2} \sum_{r,s} \left\{ \partial_y[M_{rs}(y)\psi_r^\dagger(y)]\psi_s(y) + \psi_r^\dagger(y)M_{rs}(y)\partial_y\psi_s(y) \right\}$$

$$= -\frac{1}{2} \sum_{r,s} \partial_y \left[\psi_r^\dagger(y)M_{rs}(y)\psi_s(y) \right]$$

(4.49)

where the contents of the parenthesis is a matrix product. Comparing to Eq. (4.39), we see that the current is

$$J(x) = \frac{1}{2}\psi^\dagger(x)M(x)\psi(x).$$

(4.50)

Note that this is technically only determined up to a constant, but since we only need the current operator to ensure continuity of current, this constant has no effect and can be ignored.

4.3.2 Continuity of the wave function

Since the system in consideration consists of non-interacting electrons, we can make a first quantization description of the scattering. By solving the Schrödinger equation to find the wave functions of each region, we can match these wave functions according to the boundary conditions. This will result in the scattering matrix elements needed to find the current from the Landauer-Büttiker formula in Eq. (4.23).

The boundary conditions of the problem are based on current conservation and will be derived in detail. We will follow the strategy laid out in Ref. [67] and start by assuming $|\Delta_p(x)| < |v_F(x)|$ for all x, corresponding to weak induced pairing. The eigenvalues of $M(x)$ are $v_F(x) \pm \Delta_p(x)$, and since these are positive and $M(x)$ is Hermitian, $M(x)$ is positive definite. This implies the existence of a positive, Hermitian matrix $A(x) = A^\dagger(x)$ such that

$$M(x) = \begin{pmatrix} v_F(x) & i\Delta_p(x) \\ -i\Delta_p(x) & v_F(x) \end{pmatrix} = UD(x)U^\dagger = U\sqrt{D(x)}U^\dagger U\sqrt{D(x)}U^\dagger = A(x)A(x).$$

(4.51)

Here we have defined the unitary matrix U and the diagonal matrix $D(x)$

$$U = \frac{1}{\sqrt{2}} \begin{pmatrix} -i & i \\ 1 & 1 \end{pmatrix},$$

(4.52)

$$D(x) = \begin{pmatrix} v_F(x) - \Delta_p(x) & 0 \\ 0 & v_F(x) + \Delta_p(x) \end{pmatrix},$$

(4.53)

such that $A(x) = U\sqrt{D(x)}U^\dagger$. We can then recast the derivative of $M(x)$,

$$\partial_x M(x) = U\left(\partial_x \sqrt{D(x)}\right)U^\dagger U\sqrt{D(x)}U^\dagger + U\sqrt{D(x)}U^\dagger U\left(\partial_x \sqrt{D(x)}\right)U^\dagger. \tag{4.54}$$

Since $U^\dagger U = I$ and diagonal matrices commute, we have

$$\partial_x M(x) = 2U\sqrt{D(x)}\left(\partial_x \sqrt{D(x)}\right)U^\dagger = 2A(x)\partial_x A(x), \tag{4.55}$$

which lets us write the Hamiltonian in Eq. (4.34) as

$$H_{\text{NSN},M} = -\frac{i}{2}\int dx\, \psi^\dagger(x) A(x)[\partial_x A(x)]\psi(x). \tag{4.56}$$

The Schrödinger equation in first quantization corresponding to the Hamiltonian is then

$$\mathcal{H}(x)\phi(x) = -\frac{i}{2}A(x)\partial_x[A(x)\phi(x)] + \frac{1}{2}\Omega\sigma_z\phi(x) = E\phi(x) \tag{4.57}$$

where $\phi(x) = (\phi_1(x), \phi_2(x))^T$ has two components for particle and hole, respectively. We can recast the equation in terms of the rotated spinor wave function

$$\tilde{\phi}(x) = A(x)\phi(x), \tag{4.58}$$

so that it becomes

$$-\frac{i}{2}A(x)\partial_x\tilde{\phi}(x) + \frac{1}{2}\Omega\sigma_z A^{-1}(x)\tilde{\phi}(x) = EA^{-1}(x)\tilde{\phi}(x). \tag{4.59}$$

Multiplying by $A^{-1}(x)$ from the left we have

$$-\frac{i}{2}\partial_x\tilde{\phi}(x) + \frac{1}{2}\Omega A^{-1}(x)\sigma_z A^{-1}(x)\tilde{\phi}(x) = E\left[A^{-1}(x)\right]^2\tilde{\phi}(x), \tag{4.60}$$

which can be re-arranged into the form

$$\partial_x\tilde{\phi}(x) = Q(x)\tilde{\phi}(x), \tag{4.61}$$

where we can use $M^{-1} = [A^{-1}(x)]^2$ to define

$$\begin{aligned}
Q(x) &= 2iEM^{-1}(x) - i\Omega A^{-1}(x)\sigma_z A^{-1}(x)\\
&= \frac{2i}{\tilde{v}_F^2(x)}\begin{pmatrix} v_F(x)E - \Omega\tilde{v}_F(x)/2 & i\Delta_{\text{p}}(x)E \\ -i\Delta_{\text{p}}(x)E & v_F(x)E + \Omega\tilde{v}_F(x)/2 \end{pmatrix},
\end{aligned} \tag{4.62}$$

with the renormalized velocity

$$\tilde{v}_F(x) = \sqrt{v_F^2(x) - \Delta_{\text{p}}^2(x)}. \tag{4.63}$$

In the context of a single NS boundary, we can consider this boundary to be found at $x = 0$ and integrate Eq. (4.61) over a narrow interval of width 2ϵ around the boundary. Since the matrices on the right hand side are all bounded for $|v_F| > |\Delta_1|$, if we assume that $\tilde{\phi}(x)$ is bounded as well, we see that the right hand side vanishes and the boundary condition becomes

$$\tilde{\phi}(\epsilon) - \tilde{\phi}(-\epsilon) = 0. \tag{4.64}$$

This, in turn, means that the wave function $\phi(x)$ obeys the boundary condition

$$A(x)\phi(x)|_{x=\epsilon} = A(x)\phi(x)|_{x=-\epsilon} \tag{4.65}$$

Hence, the simplest model of spatial dependence taking the form of a step function implies a discontinuous wave function. As pointed out in Ref. [67], this is an artifact of the model, which stems from the discontinuous form of the Hamiltonian parameters as described in Eq. (4.29). When we consider the physical current Eq. (4.66) in the first quantization picture, we see that for a state given by $\phi(x)$, the current

$$J(x) = \frac{1}{2}\phi^\dagger(x)M(x)\phi(x) = \frac{1}{2}\tilde{\phi}^\dagger(x)\tilde{\phi}(x) \tag{4.66}$$

remains continuous.

4.4 Transfer matrix

We will now solve Eq. (4.61) for $\tilde{\phi}(x)$ in the N and S regions, and connect the solutions through the boundary condition in Eq. (4.65). This will let us derive the scattering matrix elements needed to calculate the current in Eq. (4.23).

Considering again a single NS junction at $x = 0$, we solve Eq. (4.61) separately for $x \gtrless 0$ and then impose continuity of $\tilde{\phi}(x)$ at $x = 0$. We will assume that on each side, the parameters are constant, such that $M^{-1}(x)$ is a piecewise constant function M^{-1}. This allows us to solve the equation on either side of the boundary, after which we will connect the solutions.

To make the calculations more tractable, we define the velocity and length

$$\tilde{v}_F = \sqrt{v_F^2 - \Delta_{\mathrm{p}}^2},$$
$$\tilde{L} = \frac{\tilde{v}_F^2}{\sqrt{4\Delta_{\mathrm{p}}^2 E^2 + \tilde{v}_F^2 \Omega^2}}, \tag{4.67}$$

as well as the three parameters

$$a = 2v_F/\tilde{v}_F^2,$$
$$b = 2\Delta_{\mathrm{p}}/\tilde{v}_F^2, \tag{4.68}$$
$$c = \Omega/\tilde{v}_F.$$

4.4.1 Wave function

On a given side, we then have to solve the two coupled equations,

$$-i\partial_x \tilde{\phi}_1(x) = aE\tilde{\phi}_1(x) - ibE\tilde{\phi}_2(x) - c\tilde{\phi}_1(x), \tag{4.69}$$
$$-i\partial_x \tilde{\phi}_2(x) = ibE\tilde{\phi}_1(x) + aE\tilde{\phi}_2(x) + c\tilde{\phi}_2(x), \tag{4.70}$$

The general solution of this coupled system is given by

$$\tilde{\phi}_1(x) = C_1 e^{iaEx}\cos(x/\tilde{L}) + \tilde{L}(bEC_2 - icC_1)e^{iaEx}\sin(x/\tilde{L}),$$
$$\tilde{\phi}_2(x) = C_2 e^{iaEx}\cos(x/\tilde{L}) - \tilde{L}(bEC_1 - icC_2)e^{iaEx}\sin(x/\tilde{L}). \tag{4.71}$$

We have two integration constants $C_{1,2}$. At $x = 0$, we have $\tilde{\phi}_{1,2}(0) = C_{1,2}$. Therefore, continuity of $\tilde{\phi}(x)$ means that the constants $C_{1,2}$ are identical on both sides. Hence, the most general continuous solution, valid for all x, reads

$$\tilde{\phi}_1(x) = C_1 e^{ia_\pm Ex} \cos(x/\tilde{L}_\pm) + \tilde{L}_\pm (b_\pm E C_2 - ic_\pm C_1)\tilde{L}_\pm e^{ia_\pm Ex} \sin(x/\tilde{L}_\pm),$$
$$\tilde{\phi}_2(x) = C_2 e^{ia_\pm Ex} \cos(x/\tilde{L}_\pm) - \tilde{L}_\pm (b_\pm E C_1 - ic_\pm C_2) e^{ia_\pm Ex} \sin(x/\tilde{L}_\pm), \quad (4.72)$$

where $a_\pm = a(x \gtrless 0)$ and similarly for $b_\pm$, $c_\pm$ and $\tilde{L}_\pm$. Written as a spinor, this means

$$\tilde{\phi}(x \gtrless 0) =$$
$$e^{ia_\pm Ex} \left[\cos(x/\tilde{L}_\pm)\mathbb{1}_2 + \tilde{L}_\pm b_\pm E \sin(x/\tilde{L}_\pm) \begin{pmatrix} 0 & 1 \\ -1 & 0 \end{pmatrix} - ic_\pm \tilde{L}_\pm \sin(x/\tilde{L}_\pm) \begin{pmatrix} 1 & 0 \\ 0 & -1 \end{pmatrix} \right] C,$$
$$(4.73)$$

where $C = (C_1, C_2)^T$. Next, we translate this to the wave function $\phi(x)$ by using $\phi(x) = A^{-1}(x)\tilde{\phi}(x)$. For this we need the inverse of the matrix $A(x)$. Using Eq. (4.51), we find that this is given by

$$A^{-1}(x) = U[\sqrt{D(x)}]^{-1}U^\dagger, \quad (4.74)$$

where we have used the fact that the matrix $\sqrt{D}$ is (trivially) invertible because it is diagonal and positive-definite. Therefore, we have

$$\phi(x \gtrless 0) = A^{-1}(x)\tilde{\phi}(x)$$
$$= e^{ia_\pm Ex} \left[\cos(x/\tilde{L}_\pm)U[\sqrt{D(x)}]^{-1}U^\dagger + \tilde{L}_\pm b_\pm E \sin(x/\tilde{L}_\pm)U[\sqrt{D(x)}]^{-1}U^\dagger \begin{pmatrix} 0 & 1 \\ -1 & 0 \end{pmatrix} \right.$$
$$\left. - i\tilde{L}_\pm c_\pm \sin(x/\tilde{L}_\pm)U[\sqrt{D(x)}]^{-1}U^\dagger \begin{pmatrix} 1 & 0 \\ 0 & -1 \end{pmatrix} \right] C \quad (4.75)$$

This solves the discontinuous wave function $\phi(x)$ up to the constant vector C, which will be fixed in the next section.

4.4.2 Interface transfer matrix

We are now ready to derive the transfer matrix T, which relates modes at $x > 0$ to modes at $x < 0$,

$$\phi(0_-) = T\phi(0_+). \quad (4.76)$$

To find T we do not need to determine C, because taking the limit $x \to 0$ on both sides of the boundary yields

$$\phi(0_\pm) = U[\sqrt{D(0_\pm)}]^{-1}U^\dagger C \quad (4.77)$$

We can use the first of these equations to express C in terms of $\phi(0_+)$,

$$C = U[\sqrt{D(0_+)}]U^\dagger \phi(0_+), \quad (4.78)$$

which immediately yields the transfer matrix

$$\phi(0_-) = U[\sqrt{D(0_-)}]^{-1}[\sqrt{D(0_+)}]U^\dagger \phi(0_+). \quad (4.79)$$

56

If we assume that we have an N region on the right ($x > 0$) and an S region on the left ($x < 0$) , we can write down the N to S transfer matrix explicitly as

$$T_{\text{SN}} = \frac{\sqrt{v_0}}{2} \begin{pmatrix} i & -i \\ 1 & 1 \end{pmatrix} \begin{pmatrix} \sqrt{v_F - \Delta_{\text{p}}} & 0 \\ 0 & \sqrt{v_F + \Delta_{\text{p}}} \end{pmatrix}^{-1} \begin{pmatrix} -i & 1 \\ i & 1 \end{pmatrix} \tag{4.80}$$

Interestingly, this transfer matrix is not unitary. However, we recall that the unitarity of scattering matrices is implied by conservation of current [50], and as we saw in Eq. (4.66), current conservation holds for $\tilde{\phi}$ rather than ϕ. We can rewrite Eq. (4.76) as

$$\tilde{\phi}(0_-) = A_- T A_+^{-1} \tilde{\phi}(0_+), \tag{4.81}$$

and since $T_{\text{SN}} = A_-^{-1} A_+$, we have

$$\tilde{\phi}(0_-) = \tilde{\phi}(0_+), \tag{4.82}$$

as also implied by continuity of $\tilde{\phi}$. Since the only available channel across the boundary is transmission, $\tilde{\phi}$ must be perfectly transmitted, which in turn implies non-unitary T_{SN}. Even in the case $\Delta_{\text{p}} = 0$, we can see from Eq. (4.80) that T is non-unitary due to the different velocities in the two regions. To find the transfer matrix from S to N we repeat the above process to find

$$T_{\text{SN}} = \frac{1}{2\sqrt{v_0}} \begin{pmatrix} i & -i \\ 1 & 1 \end{pmatrix} \begin{pmatrix} \sqrt{v_F - \Delta_{\text{p}}} & 0 \\ 0 & \sqrt{v_F + \Delta_{\text{p}}} \end{pmatrix} \begin{pmatrix} -i & 1 \\ i & 1 \end{pmatrix}. \tag{4.83}$$

4.4.3 NSN junction

To evaluate the scattering amplitudes between the terminals sketched out in Fig. 4.1, we need to combine the above results to describe a full NSN junction. We assume that we have normal conducting regions at $x < -L/2$ and $x > L/2$, and a superconductor region at $|x| < L/2$. We will assume that L is great enough only plane wave states contribute to coupling across the junction.

Based on this assumption, we can directly apply the transfer matrices we have derived so far. In analogy to Eq. (4.76), we can relate the N and S region solutions by

$$\begin{aligned} \phi(-L/2 - \epsilon) &= T_{NS}\phi(-L/2 + \epsilon), \\ \phi(L/2 - \epsilon) &= T_{SN}\phi(L/2 + \epsilon), \end{aligned} \tag{4.84}$$

where ϵ is an infinitesimal distance. To fully account for the transport across the junction, we also need to describe the transport within the S region by relating $\phi(-L/2 + \epsilon)$ to $\phi(L/2 - \epsilon)$. Looking at Eq. (4.73), we recall that $\tilde{\phi}(0) = C$, and thus we see that $\tilde{\phi}(x)$ is related to $\tilde{\phi}(0)$ through

$$\tilde{\phi}(x) = e^{iaEx}T_0(x)\tilde{\phi}(0), \tag{4.85}$$

where we have defined the matrix

$$T_0(x) = \begin{pmatrix} \cos(x/\tilde{L}) - ic\tilde{L}\sin(x/\tilde{L}) & bE\tilde{L}\sin(x/\tilde{L}) \\ -bE\tilde{L}\sin(x/\tilde{L}) & \cos(x/\tilde{L}) + ic\tilde{L}\sin(x/\tilde{L}) \end{pmatrix}. \tag{4.86}$$

This matrix is unitary, as can be checked by applying the fact that $\tilde{L} = 1/\sqrt{b^2 E^2 + c^2}$. All quantities are implicitly of their S region form. We find the relation

$$\tilde{\phi}(-x) = e^{-iaEx} T_0(-x) \tilde{\phi}(0) = e^{-iaEx} T_0(-x) \left(e^{-iaEx} T_0^{-1}(x) \tilde{\phi}(x) \right). \tag{4.87}$$

We transform back to ϕ to get the relation

$$\phi(-x) = e^{-2iaEx} A^{-1}(-x) T_0(-x) T_0^{-1}(x) A(x) \phi(x), \tag{4.88}$$

Settings $x = L/2$ allows us to define the transfer matrix across the S region

$$T_S = e^{-2iaEL/2} A^{-1}(-L/2) T_0(-L/2) T_0^{-1}(L/2) A(L/2). \tag{4.89}$$

The total transfer matrix for the NSN junction T_{NSN} is defined by

$$\phi(-L/2 - \epsilon) = T_{\mathrm{NSN}} \phi(L/2 + \epsilon), \tag{4.90}$$

meaning that it must be

$$T_{\mathrm{NSN}} = T_{\mathrm{NS}} T_S T_{\mathrm{SN}}. \tag{4.91}$$

Noting that $A T_{\mathrm{SN}} = \mathbb{1}\sqrt{v_F}$ and $T_{\mathrm{NS}} A^{-1} = \mathbb{1}(\sqrt{v_F})^{-1}$, we find that remarkably the NS and SN junction transfer matrices cancel out when inserting the definition of T_S. The matrix T_0 is unitary and obeys $T_0(-x) = T_0^\dagger(x)$, therefore

$$T_{\mathrm{NSN}} = e^{iaEL} T_0(-L/2) T_0^{-1}(L/2) = \left(T_0^\dagger(L/2) \right)^2. \tag{4.92}$$

Writing out the product and applying the double angle formulae

$$\sin(2x) = 2 \sin(x) \cos(x), \tag{4.93}$$
$$\cos(2x) = \cos^2(x) - \sin^2(x), \tag{4.94}$$

leads to the expression

$$T_{\mathrm{NSN}} = e^{2iaEL} \begin{pmatrix} \cos(L/\tilde{L}) + ic\tilde{L} \sin(L/\tilde{L}) & -bE\tilde{L} \sin(L/\tilde{L}) \\ bE\tilde{L} \sin(L/\tilde{L}) & \cos(L/\tilde{L}) - ic\tilde{L} \sin(L/\tilde{L}) \end{pmatrix}. \tag{4.95}$$

The physical meaning of this result is that applying the transfer matrix $T_0(x)$ twice to a state corresponds to translating that state by a distance $2x$, i.e. $T_0^2(x) = T_0(2x)$. It is worth dwelling on the fact that this matrix only depends on the parameters of the S region. We can understand this by considering the nature of transport through QH edge states. This transport is chiral and ballistic, meaning that everything must be either perfectly transmitted or tunnel into the superconductor. This tunneling is not affected by the parameters of the N regions, and thus any divergence from the well known ballistic transport of the QH edge should only depend on the nature of the superconductor and the length of the S region.
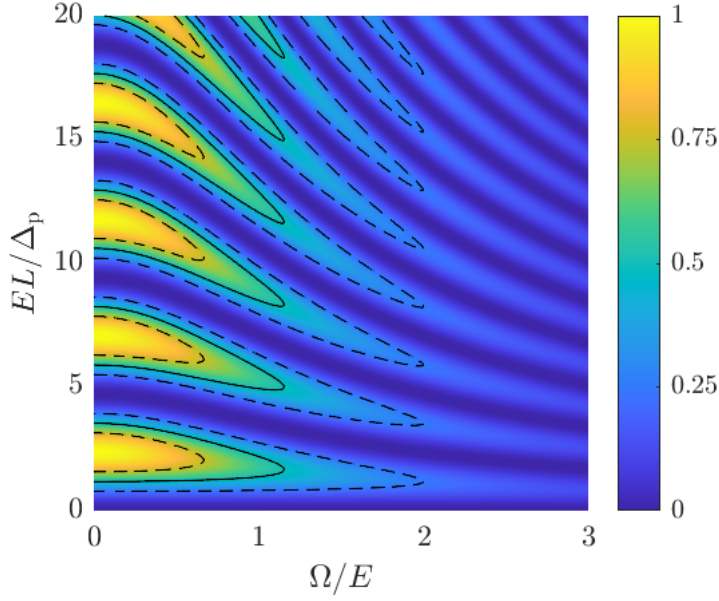
Figure 4.3: *The hole transmission probability P_h with $v_F/DeltaP = 2$ as a function of the system length L (in units of Δ_p/E) and the detuning from resonance Ω/E. The contour lines indicate $P_h = (0.25, 0.5, 0.75)$. We will later show that $P_h > 0.5$ corresponds to negative downstream resistance.*

4.5 Hole conversion probability

We are now ready to express a main result of this chapter, which is the the hole conversion probability $P_h(E)$ expressing the probability that an incoming particle is transmitted through the NSN junction as a hole. As we will see in the next section, this probability determines the behavior of the downstream resistance $\tilde{R}_{23}$. Since T_{NSN} is unitary, we can safely interpret it as a scattering matrix in the basis of particles and holes $(p, h)^T$, with the matrix elements

$$T_{\text{NSN}} = \begin{pmatrix} t_{pp} & t_{ph} \\ t_{hp} & t_{hh} \end{pmatrix}, \tag{4.96}$$

where t_{hp} is the amplitude of converting a particle into a hole. We thus find the hole conversion probability $P_h = |t_{hp}|^2$, which after inserting the definitions Eqs. (4.67) and (4.68) becomes

$$P_h(E) = \frac{1}{1 + \frac{1}{4}(\Omega/E)^2[(v_F/\Delta_p)^2 - 1]} \sin^2\left(\frac{\sqrt{4 + (\Omega/E)^2[(v_F/\Delta_p)^2 - 1]}}{(v_F/\Delta_p)^2 - 1} \frac{EL}{\Delta_p}\right). \tag{4.97}$$

This expression is plotted in Fig. 4.3. We see that the probability oscillates with an amplitude described by a Lorentzian curve centered around $\Omega/E = 0$ with a width determined by v_F/Δ_p. In particular we find the half-width-half maximum

$$\frac{\Omega_{\text{HWHM}}}{\mu_1} = \frac{2}{\sqrt{(v_F/\Delta_p)^2 - 1}}. \tag{4.98}$$

beyond which we always have $P_h < 1/2$. Thus, Δ_{p} determines the width of the Lorentzian, with $\Delta_{\mathrm{p}} \to 0$ leading to an infinitely narrow function. For finite Δ_{p}, the Lorentzian reaches unity at the resonance point $\Omega = 0$, corresponding to $k_s = \delta q_F$ as also discussed in Section 3.8. In other words, at resonance we can find perfect hole conversion, while far away from resonance the Andreev reflection is suppressed.

We also see that the hole conversion probability oscillates with the length L of the S region. The expression is symmetric around $\Omega = 0$, which is a consequence of the linearization of the effective Hamiltonian in Eq. (4.25). This oscillatory behavior has also been found in numerical treatments of the system [24, 25], where it is expressed as $P_h \propto \sin^2(q_{\mathrm{ph}}L/2)$, with $q_{\mathrm{ph}}/2$ interpreted as being the momentum difference between the particle-like and hole-like SC eigenstates. We can confirm this interpretation by considering the linearized spectrum in Eq. (4.26), namely

$$E_{\mathrm{eff,lin},\delta q,\pm} = \frac{1}{2}\left(v_F \delta q \pm \sqrt{\Omega^2 + (\Delta_{\mathrm{p}}\delta q)^2}\right). \tag{4.99}$$

If we consider a fixed energy E_0, then a state propagating through the proximitized edge segment will in general be a linear combination of the two energy eigenstates with energies $E_{\mathrm{eff,lin},\delta q_0,\pm} = E_0$. The momenta solving this equality is

$$\delta q_{0,\pm} = \frac{2(v_F/\Delta_{\mathrm{p}}) \pm \sqrt{4 + (\Omega/E_0)^2[(v_F/\Delta_{\mathrm{p}})^2 - 1]}}{(v_F/\Delta_{\mathrm{p}})^2 - 1}\frac{E_0}{\Delta_{\mathrm{p}}}, \tag{4.100}$$

meaning the momentum difference between the eigenstates is

$$q_{\mathrm{ph}} \stackrel{\mathrm{def}}{=} \delta q_{0,+} - \delta q_{0,-} = 2\frac{\sqrt{4 + (\Omega/E_0)^2[(v_F/\Delta_{\mathrm{p}})^2 - 1]}}{(v_F/\Delta_{\mathrm{p}})^2 - 1}\frac{E_0}{\Delta_{\mathrm{p}}}. \tag{4.101}$$

This corresponds to the result in Eq. (4.97). The oscillation of P_h reflects the fact that as a state propagates through the S region, it oscillates between a particle-like and a hole-like nature due to the momentum difference between these states. The S region length L determining when this oscillation is "interrupted" and the state stops oscillating as it passes into the N region.

The oscillation peaks at

$$\frac{\mu_1 L}{\Delta_{\mathrm{p}}} = \frac{\pi(2n+1)[(v_F/\Delta_{\mathrm{p}})^2 - 1]}{2\sqrt{4 + (\Omega/\mu_1)^2[(v_F/\Delta_{\mathrm{p}})^2 - 1]}}, \qquad n = 0, 1, 2 \ldots \tag{4.102}$$

For $\Omega = 0$, at these peaks we find perfect hole conversion $P_h = 1$. This is a quite striking result: despite the low transparency across the SC and QH interface implicitly assumed in a tunneling model, it is still possible to find perfect hole conversion. Even for very weak induced pairing it is technically possible, though as shown in Eq. (4.98), the strength of the induced pairing as represented by Δ_{p} controls how finely tuned the system has to be for perfect hole conversion to take place.

To understand the dependence of the downstream resistance $\tilde{R}_{23}$ on $P_h(E)$, and to find a physical interpretation of the energy argument, we will now insert the transmission amplitudes of Eq. (4.95) into the Landauer-Büttiker formula in Eq. (4.23).
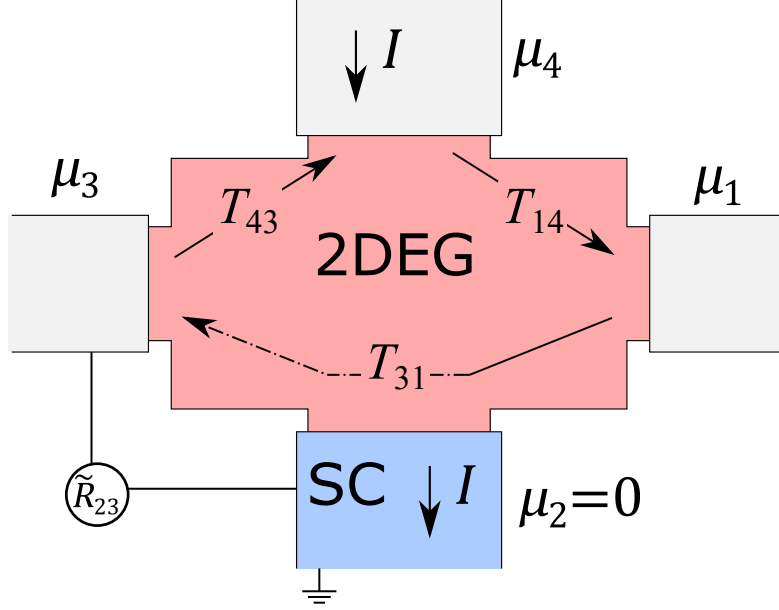
Figure 4.4: *A sketch of the treated transport experiment with transmission amplitude T_{ij} between the terminals.*

4.6 Downstream resistance

We recall the experimental setup from the start of the chapter, as shown in Fig. 4.4, where current is being transported through a 2DEG in a strong magnetic field through ballistic edge channels. Terminal 2 is grounded and superconducting, and the electrons passing between terminals 1 and 3 are converted into holes with probability $P_h(E)$ as given in Eq. (4.97). The current passing through each of the four leads is given by the expression derived in Eq. (4.23)

$$\langle I_m \rangle = \frac{1}{2\pi} \sum_n \int dE \Bigg(n_F(E - \mu_m) + \left(|t_{m,n,h,p}(E)|^2 - |t_{m,n,p,p}(E)|^2 \right) n_F(E - \mu_n)$$

$$+ \left(|t_{m,n,h,h}(E)|^2 - |t_{m,n,p,h}(E)|^2 \right) n_F(E + \mu_n) - n_F(E + \mu_m) \Bigg), \quad (4.103)$$

where $t_{m,n,p,h}$ is the scattering matrix element indicating the transmission amplitude of a hole at terminal n is transmitted as a particle to terminal m, etc. We recall that we are working in units of $|e| = 1$. Electron scattering in and out of terminal 2 is energetically forbidden, and the effect of the SC on the QH edge was shown in Chapter 3 to be effectively modeled by a QH edge state with induced superconductivity. Therefore in the transport calculation we will not explicitly account for terminal 2, instead effectively accounting for it through the induced NSN junction between terminals 1 and 3.

We are interested in investigating the effect of the NSN junction on the resistance $\tilde{R}_{23}$ downstream of the junction. To ensure an accurate description, we will first construct the scattering matrix for all four leads. Transport between the leads is restricted to the chiral edge states, meaning that scattering only occurs between sequential terminals, and only in one direction, $1 \rightarrow 3 \rightarrow 4 \rightarrow 1$. The outgoing electron mode from terminal m, denoted o_m, is related to the ingoing modes of the system i_n through the scattering

matrix,

$$\begin{pmatrix} i_{1,E} \\ i_{3,E} \\ i_{4,E} \end{pmatrix} = \begin{pmatrix} 0 & 0 & T_{14}(E) \\ T_{31}(E) & 0 & 0 \\ 0 & T_{43}(E) & 0 \end{pmatrix} \begin{pmatrix} o_{1,E} \\ o_{3,E} \\ o_{4,E} \end{pmatrix} \tag{4.104}$$

where $T_{ij}(E)$ denotes a 2×2 scattering matrix in the Nambu basis which describes scattering of particles and holes from lead j to lead i, see Fig. 4.4. For example, the first row of the matrix is interpreted as the incoming electrons in terminal 1 being the outgoing electrons of terminal 4 modified by the amplitude matrix T_{14}. We allow particle-hole conversion between leads 1 and 3, while the remaining scattering must take the form of ballistic transport scattering particles to particles and holes to holes

$$T_{31}(E) = T_{\mathrm{NSN}}(E) = \begin{pmatrix} t_{pp}(E) & t_{ph}(E) \\ t_{hp}(E) & t_{hh}(E) \end{pmatrix},$$

$$T_{14} = T_{43} = \begin{pmatrix} 1 & 0 \\ 0 & 1 \end{pmatrix}, \tag{4.105}$$

with T_{NSN} given by Eq. (4.95). The resulting 6×6 matrix T is unitary because,

$$T^\dagger T = \begin{pmatrix} 0 & T_{31}^\dagger(E) & 0 \\ 0 & 0 & T_{43}^\dagger \\ T_{14}^\dagger & 0 & 0 \end{pmatrix} \begin{pmatrix} 0 & 0 & T_{14} \\ T_{31}(E) & 0 & 0 \\ 0 & T_{43} & 0 \end{pmatrix}$$

$$= \begin{pmatrix} T_{31}^\dagger(E)T_{31}(E) & 0 & 0 \\ 0 & T_{43}^\dagger T_{43} & 0 \\ 0 & 0 & T_{14}^\dagger T_{14} \end{pmatrix} = \mathbb{1}, \quad (4.106)$$

where we used that T_{NSN} is unitary. Next, we calculate the currents using the generalized Landauer-Büttiker formula of Eq. (4.23). For the current at lead 3, we find,

$$\langle I_3 \rangle = \frac{1}{2\pi} \int_0^\infty dE \Big(n_F(E - \mu_3) - \big(|T_{31,pp}(E)|^2 - |T_{31,hp}(E)|^2 \big) n_F(E - \mu_1)$$

$$- \big(|T_{31,ph}(E)|^2 - |T_{31,hh}(E)|^2 \big) n_F(E + \mu_1) - n_F(E + \mu_3) \Big). \tag{4.107}$$

Note that despite this expression only involving the scattering matrix elements of incoming modes, it accounts for both incoming and outgoing modes as discussed in Section 4.1.2. We insert the scattering matrix elements from Eq. (4.96) and obtain

$$\langle I_3 \rangle = \frac{1}{2\pi} \int_0^\infty dE \Big(n_F(E - \mu_3) - \big(|t_{pp}(E)|^2 - |t_{hp}(E)|^2 \big) n_F(E - \mu_1)$$

$$- \big(|t_{ph}(E)|^2 - |t_{hh}(E)|^2 \big) n_F(E + \mu_1) - n_F(E + \mu_3) \Big). \tag{4.108}$$

We then use the definition $P_h(E) = |t_{hp}(E)|^2$, and apply unitarity $|t_{pp}(E)|^2 = 1 - |t_{hp}(E)|^2 = 1 - P_h(E)$ to find

$$\langle I_3 \rangle =$$

$$\frac{1}{2\pi} \int_0^\infty dE \Big(n_F(E - \mu_3) - n_F(E + \mu_3) - \big(1 - 2P_h(E)\big) \big(n_F(E - \mu_1) - n_F(E + \mu_1) \big) \Big).$$

$$\tag{4.109}$$

Similarly, we have the normal currents,

$$\langle I_4 \rangle = \frac{1}{2\pi} \int_0^\infty dE \Big(n_F(E - \mu_4) - n_F(E - \mu_3) + n_F(E + \mu_3) - n_F(E + \mu_4) \Big), \quad (4.110)$$

$$\langle I_1 \rangle = \frac{1}{2\pi} \int_0^\infty dE \Big(n_F(E - \mu_1) - n_F(E - \mu_4) + n_F(E + \mu_4) - n_F(E + \mu_1) \Big). \quad (4.111)$$

In the simplest case we take the zero-temperature limit so that the Fermi distribution is just a step function $n_F(E - \mu) = \theta(\mu - E)$. For the combinations of θ functions we have, we can use the following relation for a general function $f(E)$

$$\int_0^\infty dE f(E) \left[\theta(\mu - E) - \theta(-\mu - E) \right] = \begin{cases} \int_0^\mu dE f(E) & \text{for } \mu > 0 \\ -\int_0^{-\mu} dE f(E) & \text{for } \mu < 0 \end{cases}$$

$$= \operatorname{sgn}(\mu) \int_0^{|\mu|} dE f(E). \quad (4.112)$$

We see that $f(E)$ need only be defined for $E > 0$ in the integrand. However, if we assume that $f(E)$ is even around $E = 0$ (as $P_h(E)$ is), we can write this as

$$\int_0^\infty dE f(E) \left[\theta(\mu - E) - \theta(-\mu - E) \right] = \int_0^\mu dE f(E), \quad (4.113)$$

for any sign of μ. In the special case $f(E) = 1$, which is relevant for $\langle I_4 \rangle$ and $\langle I_1 \rangle$ this implies,

$$\int_0^\infty dE \left[\theta(\mu - E) - \theta(-\mu - E) \right] = \mu. \quad (4.114)$$

This means that at zero temperature

$$\langle I_4 \rangle = \frac{1}{2\pi} \left(\mu_4 - \mu_3 \right),$$
$$\langle I_1 \rangle = \frac{1}{2\pi} \left(\mu_1 - \mu_4 \right),$$
$$\langle I_3 \rangle = \frac{1}{2\pi} \left\{ \mu_3 - \int_0^{\mu_1} dE[1 - 2P_h(E)] \right\}. \quad (4.115)$$

In the experiment considered, a current is injected into lead 4, i.e., $\langle I_4 \rangle = I$, whereas the two other leads are voltage probes such that $\langle I_1 \rangle = \langle I_3 \rangle = 0$. From $\langle I_1 \rangle = 0$, we find $\mu_4 = \mu_1$. From the first equation, we can then determine μ_3 in terms of I and μ_1,

$$\mu_3 = \mu_1 - 2\pi I. \quad (4.116)$$

Inserting this in the third equation, we obtain an equation which allows us to determine $\mu_1(I)$ implicitly as a function of I,

$$\mu_1 = 2\pi I + \int_0^{\mu_1} dE[1 - 2P_h(E)], \quad (4.117)$$

where resolving part of the integral leads to the result

$$\int_0^{\mu_1} dE P_h(E) = \pi I. \quad (4.118)$$

63

The differential resistance which contains information about the hole conversion is then

$$\tilde{R}_{23} = \frac{dV_3}{dI}. \tag{4.119}$$

Restoring Planck's constant h and the elementary charge e such that

$$\mu_3 = \mu_1 - \frac{h}{e}I \tag{4.120}$$

we have

$$\tilde{R}_{23} = \frac{1}{e}\frac{d\mu_3}{dI} = \frac{1}{e}\frac{d\mu_1}{dI} - \frac{h}{e^2} \tag{4.121}$$

To calculate the remaining derivative, we face the fact that while $\mu_1(I)$ is difficult to differentiate, $I(\mu_1)$ is simple. We use the fact that for full derivatives the following holds for inverse functions

$$\frac{d\mu_1}{dI} = \left(\frac{dI}{d\mu_1}\right)^{-1}. \tag{4.122}$$

Since we have the identity

$$\frac{d}{d\mu_1}\int_0^{\mu_1} dE P_h(E) = P_h(\mu_1), \tag{4.123}$$

we find

$$\frac{d\mu_1}{dI} = \left(\frac{2e}{h}P_h(\mu_1)\right)^{-1} = \frac{h}{e}\frac{1}{2P_h(\mu_1)}. \tag{4.124}$$

Therefore, we have the result

$$\boxed{\tilde{R}_{23} = \frac{h}{e^2}\frac{1 - 2P_h(\mu_1)}{2P_h(\mu_1)},} \tag{4.125}$$

where $\mu_1 \overset{\text{def}}{=} \mu_1(I)$. This resistance is plotted on the left in Fig. 4.5 for $0 < P_h < 1$. Comparing this result to the zero resistance result of the QH effect without superconductivity has some subtle elements. We see that for zero induced pairing, $\Delta_{\rm p} \to 0$, we have no hole conversion $P_h(\mu_1) \to 0$ and thus infinite resistance $\tilde{R}_{23} \to \infty$. This is a consequence of the current passing through the SC terminal: zero hole conversion means suppressed Andreev reflection, and since that is the only process for electrons to cross the SC-QH interface, no current can pass through the system. This in turn implies infinite resistance.

To better compare with the case of no induced pairing, we instead consider the relationship between the chemical potentials of the terminals and $P_h(\mu_1)$. In the normal QH effect, longitudinal resistance is zero, meaning that there is no voltage difference between terminals on the same side of the system. Specifically, when the superconducting terminal 2 is grounded, the downstream terminal 3 must have $\mu_3 = 0$. If any electrons at $\mu_1 \neq 0$ are passed from terminal 2 to terminal 3, it would change μ_3 away from zero. This is clearest for $\mu_1 > 0$ where μ_3 would be raised to positive values, but since $P_h(\mu_1)$ is symmetric in μ_1, the same effect would hold for $\mu_1 < 0$.

From this perspective, it is clear that the zero resistance case must correspond to a neutralization of the charge transport between terminals 2 and 3, i.e. $P_h(\mu_1) = 1/2$. In
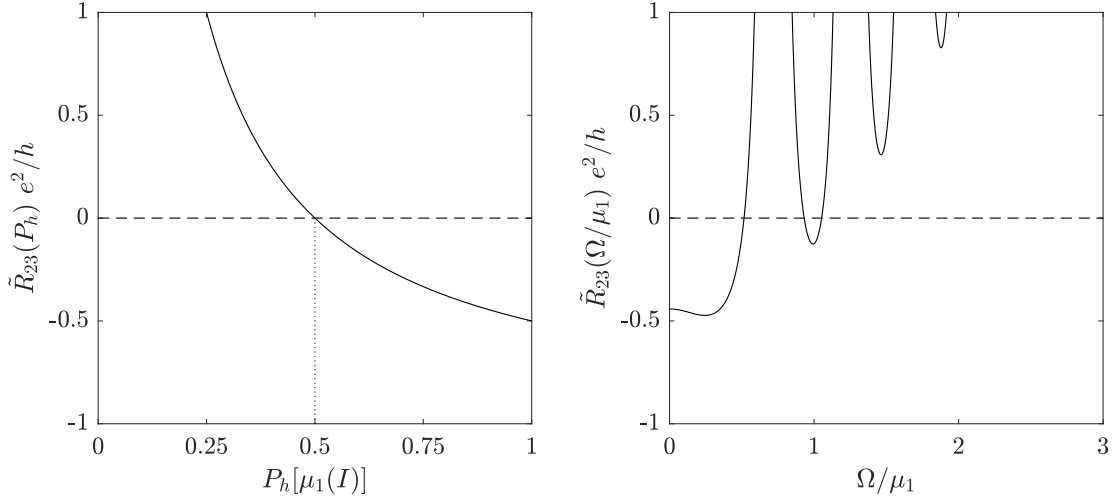
Figure 4.5: *Left: The downstream resistance $\tilde{R}_{23}$ (full line) as a function of the probability $P_h[\mu_1(I)]$ that electrons at chemical potential $\mu_1(I)$ are transmitted through the NSN junction as holes. The normal QH effect result $\tilde{R}_{23} = 0$ is marked with a dashed line, which crosses the full curve at $P_h = 1/2$. Right: The downstream resistance at $\mu_1 L/\Delta_p = 16$ oscillates above and below zero as a function of the resonance parameter Ω. This plot corresponds to a vertical slice of Fig. 4.3. The resistance unit in both plots is $h/e^2 \simeq 25.81$ kΩ.*

other words, the electrons being passed to terminal 3 have their charge canceled out by a corresponding amount of holes. Now, just like how a majority of electrons being passed to terminal 3 will change μ_3 towards μ_1, if a majority of holes are passed to terminal 3, μ_3 will change in the opposite direction. This means that for $P_h(\mu_1) > 1/2$ we will see negative resistance since μ_3 changes sign. The holes passing from terminals 2 to 3 can be interpreted as a current running the other way, meaning the negative resistance implies that we are measuring the "wrong direction". It is, however, important to point out that due to the chirality of the system, no physical current is flowing from terminals 3 to 2.

In recent experimental works on the system described, the condition $\tilde{R}_{23} < 0$ was considered the main indicator of the Andreev edge state [24, 25]. It should be noted that the Andreev edge state can exist without measuring negative resistance. Combining Eq. (4.97) and Eq. (4.125), we see that the energy argument to consider is μ_1,

$$P_h(\mu_1) = \frac{1}{1 + \frac{1}{4}(\Omega/\mu_1)^2[(v_F/\Delta_p)^2 - 1]} \sin^2\left(\frac{\sqrt{4 + (\Omega/\mu_1)^2[(v_F/\Delta_p)^2 - 1]}}{(v_F/\Delta_p)^2 - 1} \frac{\mu_1 L}{\Delta_p}\right),$$

(4.126)

and we want to investigate when $P_h(\mu_1) > 1/2$ as that is the region where Eq. (4.125) predicts negative resistance. Considering the example where the length is fixed at $\mu_1 L/\Delta_p = 16$, we plot a vertical slice of Fig. 4.3 to the right in Fig. 4.5. Near $\Omega = 0$, we see almost perfect hole conversion with $\tilde{R}_{23} \simeq -0.5e^2/h$, with oscillations around zero resistance as we increase Ω. An important result of this chapter is the fact that the interplay between momentum conservation and Meissner current represented by Ω plays a key role in predicting the conditions for negative resistance.

65

4.6.1 Expansion for small bias current

To determine the differential resistance for a given applied current, we still need to solve the equation

$$\int_0^{\mu_1(I)} dE\, P_h(E) = \pi I \tag{4.127}$$

for $\mu_1(I)$. Since there is no clear way of finding the antiderivative of P_h, which would let us solve the equation generally, we will solve it approximately for small I. For $I = 0$, the only solution of this equation is $\mu_1 = 0$ since $P_h(E) \geq 0$ by definition. Therefore, for small I, we will still have $\mu_1 \approx 0$, so we can Taylor expand the integrand around $E = 0$,

$$\int_0^{\mu_1(I)} dE\, P_h(E) = \int_0^{\mu_1(I)} dE\, \left[P_h(0) + E P_h'(0) + \frac{E^2}{2} P_h''(0) + O(E^3) \right]. \tag{4.128}$$

From Eq. (4.97), we see that $P_h(0) = 0$. We also have $P_h'(0) = 0$ since $P_h(E)$ is a symmetric function of E. Therefore, the leading order will be

$$\int_0^{\mu_1(I)} dE\, P_h(E) = \int_0^{\mu_1(I)} dE\, \left[\frac{E^2}{2} P_h''(0) + O(E^3) \right] = \frac{1}{6} P_h''(0) \mu_1^3 + O(\mu_1^4). \tag{4.129}$$

Since this integral equals πI we find the approximation,

$$\mu_1(I) \simeq \left(\frac{6\pi I}{P_h''(0)} \right)^{1/3},$$

$$P_h''(0) = \frac{8\Delta_{\mathrm{P}}^2}{\Omega^2(v_F^2 - \Delta_{\mathrm{P}}^2)} \sin^2 \left(\frac{2\Omega L}{\sqrt{v_F^2 - \Delta_{\mathrm{P}}^2}} \right). \tag{4.130}$$

For $\tilde{R}_{23}$, we can also Taylor expand for small μ_1 and thus find

$$\tilde{R}_{23} = \frac{h}{e^2} \frac{1 - 2P_h(\mu_1)}{2P_h(\mu_1)} \approx \frac{h}{e^2} \frac{1 - P_h''(0)\mu_1^2}{P_h''(0)\mu_1^2}. \tag{4.131}$$

Since we have assumed $P_h''(0)\mu_1^2 \ll 1$, we can further approximate

$$\tilde{R}_{23} \approx \frac{h}{e^2} \frac{1}{P_h''(0)\mu_1^2} = \frac{h}{e^2} [P_h''(0)]^{-1/3} (6\pi I)^{-2/3}. \tag{4.132}$$

In other words we predict that the relation

$$\tilde{R}_{23} \propto I^{-2/3} \tag{4.133}$$

provides an experimental indicator of the existence of the Andreev edge state

4.7 Experimental perspectives

The experiments on induced superconductivity in the quantum Hall edge involve three main geometries as outlined in Fig. 4.6. The first is the edge setup [19,24,25,68], which is the geometry treated in this thesis. The second is the finger setup [22,27] where a narrow
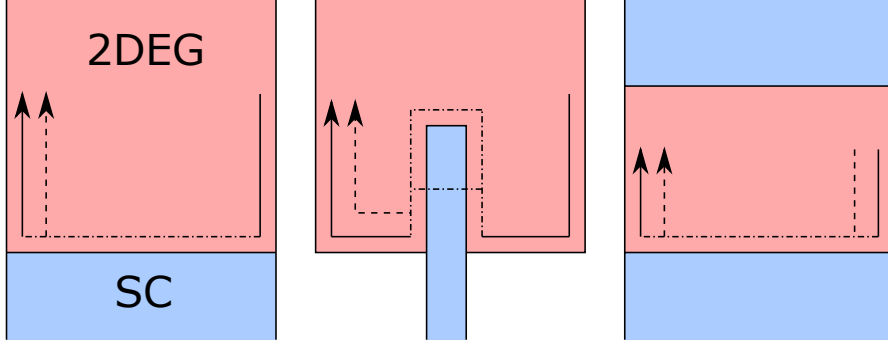
Figure 4.6: *Sketches of three common experimental setup, which we will call the edge setup (left), the finger setup (middle), and the SNS setup (right).*

superconductor protrudes into the 2DEG, allowing for crossed Andreev reflection across the SC. The third geometry involves a 2DEG between two SC's [20, 26], effectively forming an SNS junction. The presented model can only be expected describe the edge geometry, though there are still interesting elements from the other geometries we will comment on. We note that typical experimental parameters which are varied include the applied magnetic field B_0 and the Fermi energy E_F of the 2DEG in terms of an applied gate voltage.

As discussed in Section 3.4, care should be taken in comparing the results of this chapter directly with experiments, since the approximations and limits assumed do not necessarily apply to a general experimental situation. Indeed, some effects which have been neglected in this thesis have been the focus of work done by other groups in parallel to this thesis, e.g. the effect of vortices in the SC [29, 31], the effect of disorder in the SC [32] and the interplay between Meissner current and the angle of the SC wedge in a finger geometry [30]. In addition, while considering the model in the tunneling limit makes analytical derivations tractable, it may well be difficult to compare with experiments which generally strive for high barrier transparency.

In addition, the presented work seeks to derive analytical descriptions of the qualitative effects seen in experiment to allow for straightforward physical interpretation of the roles the parameters of the underlying models play in these effects. Thus, the purpose is not to account quantitatively for any particular experimental result, where other approaches including phenomenological models with fitted parameters [24, 25], numerical tight-binding simulations [28] and numerical solutions of transcendental equations [14] have already been applied. With these things in mind, we can proceed to comment on the experimental perspectives of the presented results.

- The first result we note is the prediction of how SOC in the SC comes into play in the induced superconductivity. It was speculated in Refs. [22, 27] that the induced superconductivity detected in a spin-polarized QH edge without SOC was made possible by inherent SOC in the Nb-based SC [69], and our results show that Rashba SOC in the SC with amplitude $\alpha \neq 0$ allows induced superconductivity with an amplitude $\Delta_\mathrm{p} \propto \alpha$ to first order in α, see Eq. (3.92).

- A strong, quantitative prediction of the presented model is the Pauli blockade at zero bias, $\mu_1 = 0$, or correspondingly zero current $I = 0$, as well as the scaling at small bias current $\tilde{R}_{23} \propto I^{-2/3}$. There are, however, to our knowledge no experiments currently available in the literature which report measurements of the
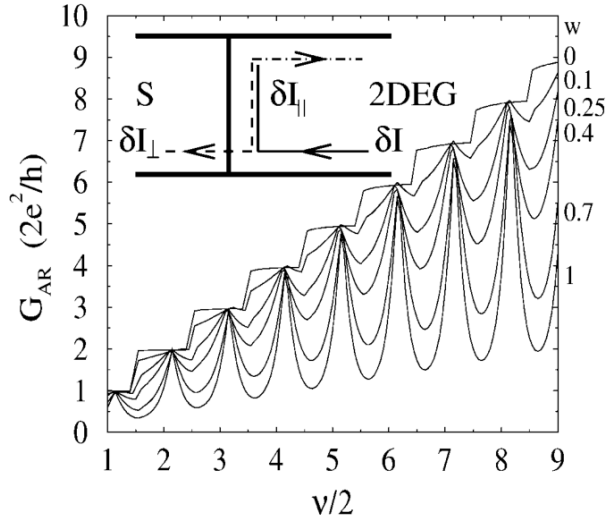
Figure 4.7: *In Ref. [13], the contribution from Andreev reflection to the conductance G_{AR} is calculated by numerically solving a transcendental equation resulting from wave-matching across the SC-QH interface. For a transparent interface $w = 0$, the Andreev reflection contribution increases in steps with increasing $\nu = 2E_F/\omega_c$. For a non-transparent interface $w > 0$, Andreev reflection is suppressed except for one point per step. Figure reproduced from Ref. [13].*

relevant parameters at filling factor $\nu = 1$, and at higher filling factor we expect the Pauli blockade to be circumvented [58].

- The critical role of the Meissner current in the suppression of Andreev reflection away from the resonance condition $q_F = k_s$ is of particular interest since it is tied to the tunneling coupling of the two systems. For a highly transparent interface, where a description in terms of evanescent electron excitations in the SC applies, the Meissner current plays no such critical role, and can be neglected without losing induced superconductivity. For such a system, it has been reported [13, 14] that at low transparency, Andreev reflection is suppressed for all 2DEG Fermi energies except one point between each Landau level, see Fig. 4.7.

  In the context of the tunneling model presented, a simple extension to account for higher filling factors while neglecting tunneling into different edge states would see the resonance condition fulfilled once per Landau level. Thus, a possible physical interpretation of this phenomenon is that at high interface transparency, the resonance condition plays no significant role, while in the tunneling limit, it determines when the induced superconductivity is entirely suppressed. To confirm this connection would require further work. Experimentally, it has been reported for an SNS setup experiment [20] that indicators of induced superconductivity only occurred at a single narrow energy range between each Landau level, while for other edge setup experiments [24, 25] signatures of induced superconductivity were found at a broad range of energies between the Landau level transitions.

- The edge setup experiments of Refs [24, 25] are of particular interest due to their geometry corresponding to the presented model. Ref. [24] has a 600nm long MoRe SC interface with graphene and sees strongly oscillating downstream resistance within each Landau level, while Ref. [25] has a $150\mu m$ NbTiN SC long interface coupled with a InAs 2DEG, and sees a downstream resistance which is essentially
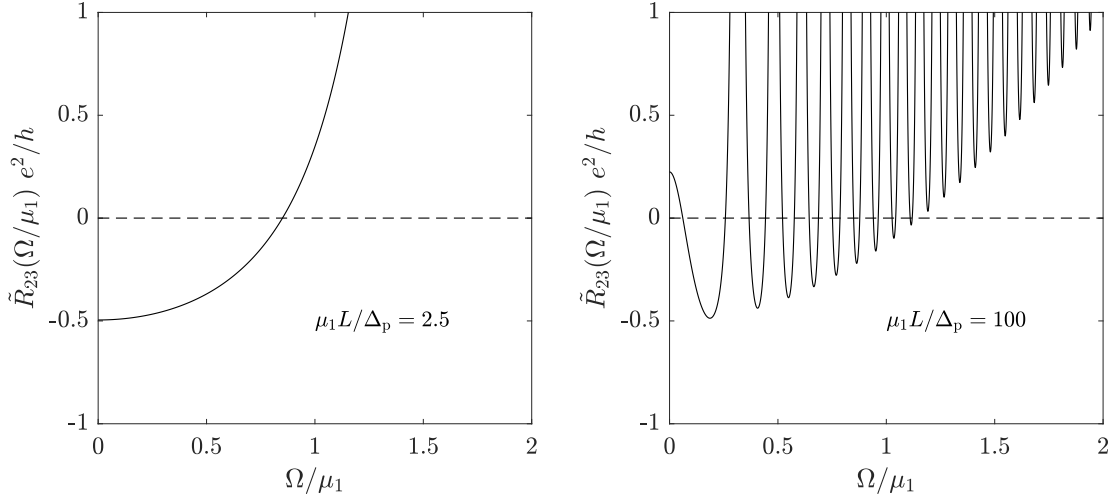
68

Figure 4.8: *For a fixed $v_F/\Delta_p = 2$, we predict increased resistance oscillations with increased $\mu_1 L/\Delta_p$, here shown with two examples of $\tilde{R}_{23}(\Omega/\mu_1)$ at fixed values of $\mu_1 L/\Delta_p$.*

independent of 2DEG Fermi energy within each Landau level. In addition to the effects of disorder and graphene-specific considerations as described in Ref. [28], both experiments argue that the oscillatory behavior should be in part understood through the content of the sine function in Eq. (4.126).

As we demonstrated in Eq. (4.101), inside an S-region of length L, a propagating state oscillates as $\sin^2(q_{ph}L/2)$ between particle-like and hole-like due to the momentum difference

$$q_{ph} = \frac{\sqrt{4 + (\Omega/\mu_1)^2[(v_F/\Delta_p)^2 - 1]}}{(v_F/\Delta_p)^2 - 1}\frac{\mu_1}{\Delta_p}, \tag{4.134}$$

between these two states, where we recall that $\mu_1(I)$ corresponds to the voltage difference resulting from the applied current I. For two experiments with equal q_{ph}, we would expect greater L to lead to more oscillations as Ω changes, see Fig. 4.8. However, the experiment with no oscillations has an interface length which is about 250 times longer than the experiment with strong oscillations. In the context of the presented model, this indicates a large difference in q_{ph} between experiments. If we define the momenta and lengths of the experiments to be $q_{ph,1}, L_1$ and $q_{ph,2}, L_2$, with $L_2 = 250 L_1$, then in order for the long experiment with L_2 to correspond to the left of Fig. 4.8, while the short experiment with L_1 correspond to the right, we would require $q_{ph,1}/q_{ph,2} \simeq 5 \cdot 10^3$. Assuming a fixed v_F/Δ_p, one way to achieve this would be to have this difference contained in μ_1/Δ_p, where we recall from Eq. (3.92) that the pairing amplitude depends on a number of material parameters

$$\Delta_p \simeq -\Gamma_L^2 \alpha \frac{m_s E_s}{2|\Delta_0|^2}, \tag{4.135}$$

from which a difference of several orders of magnitude between experiments might accumulate.

Furthermore, while previous work [22,24] reports measurements of small negative downstream resistance $-|\tilde{R}_{23}|$ with $|\tilde{R}_{23}| \ll h/e^2$, Ref. [25] reports negative downstream resistance with $|\tilde{R}_{23}| \sim h/e^2$. As shown in Fig. 4.5, this indicates significant hole conversion, with perfect hole conversion in a single edge state corresponding to a negative downstream resistance of $|\tilde{R}_{23}| = h/(2e^2)$. As our results suggest, perfect hole conversion is in principle possible even for weak induced pairing, as long as we can assume that all electrons tunneling across the interface Andreev reflect, i.e. that none are lost as quasiparticle excitations above the SC gap.

- Finally, it was recently reported [27] that induced superconductivity had successfully been detected in a 2DEG exhibiting fractional QH effect interfaced with a SC in the finger setup. A major benefit of the presented approach to modeling the QH-SC interface is much of the derivation does not depend on the explicit form of the QH edge Hamiltonian, and as we shall see in the next chapter, our results can be extended to the fractional QH case.

4.8 Summary

We consider a typical experimental transport measurement setup, in which the resistance $\tilde{R}_{23}$ downstream of the SC terminal is considered to be an indicator of a proximitized edge state due to the modified charge transport in a mixed particle-hole state. We derive the Landauer-Büttiker formalism for transport involving particles and holes, and see that despite having the same group velocity, particles add to the current and holes subtract.

We introduce position dependence in the parameters of the effective Hamiltonian to model an NSN junction, and approximate everything to linear order in δq, which is a good approximation for $\Omega \geq 0$, and less so otherwise. To ensure that we are applying the correct boundary conditions at the NS junctions, we derive the current operator for the proximitized system and require its continuity at the junctions, which turn out to imply discontinuity of the wave function. We then derive the scattering matrix of the system assuming $|v_F| > |\Delta_\mathrm{p}|$ to arrive at the amplitude of a particle being transmitted across the NSN junction as a hole,

$$P_h(E) = \frac{1}{1 + \frac{1}{4}(\Omega/E)^2[(v_F/\Delta_\mathrm{p})^2 - 1]} \sin^2\left(\frac{\sqrt{4 + (\Omega/E)^2[(v_F/\Delta_\mathrm{p})^2 - 1]}}{(v_F/\Delta_\mathrm{p})^2 - 1}\frac{EL}{\Delta_\mathrm{p}}\right),$$
(4.136)

which does not depend on the nature of the normal regions due to the lack of backscattering in a chiral edge. We see that hole transmission is strongest near the resonance $\Omega = 0$ and vanishes on the scale of Δ_p/v_F away from this point, that it vanishes at $E = 0$ due to a Pauli blockade, and that it oscillates as $\sin^2(q_\mathrm{ph}L)$ where q_ph is the momentum difference between the particle-like and hole-like modes in the proximitized region.

We then apply the derived Landauer-Büttiker formalism to predict the downstream resistance to be

$$\tilde{R}_{23} = \frac{h}{e^2}\frac{1 - 2P_h(\mu_1)}{2P_h(\mu_1)},$$
(4.137)

where the Planck constant is re-introduced for clarity. We find that the negative resistance, which happens for $P_h > 1/2$ and which experimentally indicates Andreev reflection, can

occur even for weak pairing. We further find that it depends strongly on the resonance condition $\Omega = 0$, which in turn is a consequence of the Meissner effect. We compare our predictions with relevant experiments, and find that our model supports the hypothesis about Andreev reflection being enabled by SOC in the SC, and predict how a difference in Δ_p for fixed v_F/Δ_p may account for why one experiment sees a strongly oscillating resistance as a function of Ω, while another does not.

CHAPTER 5

Induced superconductivity in the fractional quantum Hall state

As discussed in Chapter 1, a proximitized integer quantum Hall (QH) edge is useful in the search for Majorana fermions, but to find parafermions with more generalized anyonic exchange statistics, we must turn to the fractional QH edge [17]. We can extend our model to this case by introducing strong interaction between the electrons in the QH edge state Hamiltonian and replacing it with a chiral Luttinger liquid Hamiltonian, which is known to be an effective low-energy model of a fractional quantum Hall edge state.

5.1 The effective Hamiltonian

As in Chapters 3 and 4, we will treat a system consisting of QH edge state along the x-axis proximitized by an s-wave SC, see Fig. 5.1, described by the Hamiltonian

$$H = H_{\text{edge}} + H_{\text{sc}} + H_{\text{tunn}}, \tag{5.1}$$

where once again the second term describes the SC surface, and the third term describes tunneling between them, but this time the first term describes the *fractional* QH edge. In particular, the SC surface Hamiltonian is

$$H_{\text{sc}} = \sum_{\delta\mathbf{k},\sigma} \left[\epsilon_{\mathbf{k}_s+\delta\mathbf{k}} c^\dagger_{\mathbf{k}_s+\delta\mathbf{k},\sigma} c_{\mathbf{k}_s+\delta\mathbf{k},\sigma} + \left(\Delta_0 c^\dagger_{\mathbf{k}_s+\delta\mathbf{k},\uparrow} c^\dagger_{\mathbf{k}_s-\delta\mathbf{k},\downarrow} + \text{h. c.} \right) \right.$$
$$\left. + \left(\alpha[\delta k_z + i(\delta k_x + k_s)] c^\dagger_{\mathbf{k}_s+\delta\mathbf{k},\uparrow} c_{\mathbf{k}_s+\delta\mathbf{k},\downarrow} + \text{h. c.} \right) \right], \tag{5.2}$$
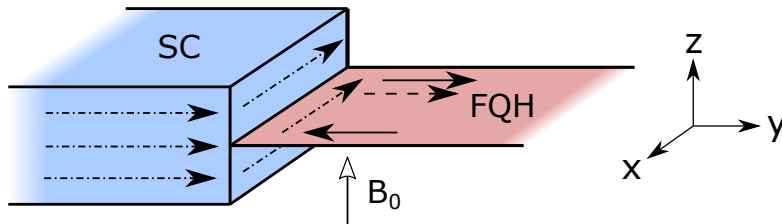

Figure 5.1: *An illustration of a fractional QH system interfaced with a SC.*

where $c_{\delta\mathbf{k},\sigma}$ annihilates a SC electron with momentum $\delta\mathbf{k}$ and spin σ. As in Chapter 3, momentum is measured relative to the supercurrent momentum $\mathbf{k}_s$, namely $\delta\mathbf{k} = \mathbf{k} - \mathbf{k}_s$. The first term describes the kinetic energy of the SC electrons $\epsilon_{\delta\mathbf{k}}$, the second term describes the s-wave pairing with complex pairing amplitude Δ_0, and the third term describes spin-orbit coupling with real amplitude α.

We assume as in Chapter 3 that the systems are coupled through local and spin-preserving electron tunneling and thus have the tunneling Hamiltonian

$$H_{\text{tunn}} = \gamma\sqrt{w_z w_y}\int_{-L/2}^{L/2} dx\, [\psi^\dagger(x)c_\uparrow(x,0,0) + \text{h. c.}]$$
$$= \Gamma\sum_{q,\mathbf{k}}\delta_{q,k_x}\left(\psi_q^\dagger c_{\mathbf{k},\uparrow} + \text{h. c.}\right), \tag{5.3}$$

where γ is the tunneling amplitude, w_z and w_y are the effective widths of the tunneling interface in the y, z dimensions, while L_y and L_z are lengths of the SC in the same dimensions. In the second line we have Fourier transformed into momentum space and introduced the modified amplitude

$$\Gamma = \gamma\sqrt{\frac{w_z w_y}{L_z L_y}}. \tag{5.4}$$

In Chapter 3 it was shown that integrating out the SC fields in Eq. (5.1) yields the effective QH edge state Hamiltonian

$$H_{\text{eff}} = H_{\text{edge}} + \sum_{\delta q}\left[\delta E_{\delta q}\psi_{k_s+\delta q}^\dagger\psi_{k_s+\delta q} + \left(\frac{\Delta_{\delta q}}{2}\psi_{k_s+\delta q}^\dagger\psi_{k_s-\delta q}^\dagger + \text{h. c.}\right)\right], \tag{5.5}$$

where $\delta E_{\delta q}$ is the SC contribution to the kinetic energy of the QH edge state, and $\Delta_{\delta q}$ is the induced pairing amplitude.

The effective Hamiltonian was derived without reference to the edge state Hamiltonian other than the assumptions that the edge state is one-dimensional and that the systems are coupled through electron tunneling. Thus, under the assumption of those two conditions, the effective Hamiltonian applies directly to the fractional QH case.

5.2   Chiral Tomonaga-Luttinger liquid theory

For a QH system at integer filling factors, the edge states can be modeled as one-dimensional channels of non-interacting electrons, see Chapter 2. To describe a QH edge state at fractional filling factors, we must however take electron-electron interactions explicitly into account. This can be done through the approximate wave function proposed by Laughlin [45], or the composite fermion approach [38], but the field theoretical approach by Wen [70] fits better into the framework we have developed so far, and strikes a good balance between accurate predictions and tractable calculations. The approach involves developing a field theoretical description of the 2DEG in the fractional QH phase and inserting the correct boundary conditions by hand. The resulting field theory shows that the low-energy physics of simple FQH states can accurately be described by a one-dimensional field theory on the same form as a chiral Tomonaga-Luttinger liquid [2, 71]. This effective theory of chiral, one-dimensional conductors describes the strongly interacting electron system in terms of free boson fields representing the

collective excitations of the electrons. In particular, the electron system can be accurately described through a Hamiltonian consisting of quadratic terms of bosonic fields with interactions encoded into a velocity v and an interaction parameter K. While the theory does not predict the value of these parameters beyond the non-interacting limit where $v = v_F$ and $K = 1$, it predicts the scaling of experimentally available quantities such as temperature in terms of exponents given by these parameters.

The connections between this theory and the system of a fractional QH edge can be hinted at by considering the following result: calculating the Hall resistance through a QH system by imposing a voltage difference between two spatially separated chiral fields yields the result [71]

$$R_H = \frac{2\pi}{Ke^2}, \tag{5.6}$$

which is exactly the expected Hall resistance if $K = \nu$. It turns out that a chiral Tomonaga-Luttinger theory with $K = \nu$ is indeed a good description at many filling factors, in particular the integer filling factors and the Laughlin sequence with $\nu = 1/(2n + 1)$ for an integer n. This remarkable connection between the filling factor ν and the interaction parameter K can be theoretically derived from the Chern Simons theory devised by Wen [2,70,72]. The rest of this section introduces the theoretical framework we will need to describe the proximitized fractional QH edge.

We will be following Refs. [2,70] to introduce the chiral boson theory. We assume that at low energies, the dispersion of the system is approximately linear up to a momentum cutoff q_0, corresponding to a short-distance cutoff $a = 1/q_0$. In a true one-dimensional conductor, such as a nanowire, this is related to the bandwidth of the system, while in the case of a QH edge state, the linearity approximation, and thus the cutoff, is rather related to the separation between Landau levels. The expressions involving the cutoff are only strictly mathematically exact in the limit $q_0 \to \infty$, but physically it is useful to keep q_0 finite. We take the edge state electrons to be moving to the left (negative direction). At low energies we have an effective description in terms of bosons,

$$\psi(x) = \frac{F}{\sqrt{2\pi/q_0}} e^{-iq_F x} e^{-i\Phi(x)/\sqrt{\nu}}, \tag{5.7}$$

where q_F is the Fermi momentum, $\Phi(x)$ is the bosonic field, ν is the filling factor of the fractional QH edge, and the operator F is the Klein factor [71]. This operator connects the bosonic description to the fermionic description by ensuring the correct raising and lowering of the fermion number, as well as ensuring the correct fermionic commutation relations. The exact form of the operator will not have any profound impact on our results, and we refer to Ref. [71] for more details. The boson field is defined as

$$\Phi(x) = i\sqrt{\frac{2\pi}{L}} \sum_{q>0} \frac{e^{-q/(2q_0)}}{\sqrt{q}} \left(e^{-iqx} b_q - e^{iqx} b_q^\dagger \right), \tag{5.8}$$

where L is the length of the edge and b_q is the boson annihilation operator for momentum q. This field obeys the commutation relation [2]

$$[\Phi(x), \Phi(y)] = \ln \left\{ \frac{1 - \exp\left[\frac{2\pi i}{L}(x - y + i/q_0)\right]}{1 - \exp\left[\frac{2\pi i}{L}(y - x + i/q_0)\right]} \right\}. \tag{5.9}$$

We will generally consider a macroscopically large interface corresponding to the thermodynamic limit $L \to \infty$, where

$$\lim_{L \to \infty} [\Phi(x), \Phi(y)] = -2i \arctan(q_0[x-y]). \tag{5.10}$$

In the limit $q_0 \to \infty$, we find the strict relation

$$[\Phi(x), \Phi(y)] = -i\pi \operatorname{sgn}(x-y), \tag{5.11}$$

which means

$$e^{-i\Phi(x)/\sqrt{\nu}} e^{-i\Phi(y)/\sqrt{\nu}} = e^{-i\Phi(y)/\sqrt{\nu}} e^{-i\Phi(x)/\sqrt{\nu}} \exp\left(-\frac{i\pi}{\nu} \operatorname{sgn}(x-y)\right). \tag{5.12}$$

Interestingly, for the Laughlin sequence $\nu = 1/(2n+1)$ with integer n, exchanging the exponentiated fields in space leads to a fermionic exchange phase, while other filling factors have a more general behavior. Ultimately, the correct commutation of electrons is ensured by the Klein factor.

Within this theory, it can be shown that the linearized interacting electron Hamiltonian can be approximated at low energies by the chiral Tomonaga-Luttinger liquid Hamiltonian

$$H_{1D} = \frac{v}{4\pi\nu} \int dx \left[\partial_x \Phi(x)\right]^2, \tag{5.13}$$

where v is the velocity of the bosonic excitations, which is the Fermi velocity $v = v_F$ in the non-interacting case.

At this point it is worth returning to the assumption that the fractional QH edge and the SC surface are coupled through electron tunneling. Since both systems have bosonic ground states, one might expect tunneling of bosonic quasiparticles between the systems. However, while quasiparticle tunneling is allowed between the edge states of a fractional QH system, electron tunneling is the only allowed coupling to a SC which does not host fractional quasiparticles [73].

5.3   Pairing Hamiltonian

We will now express the effective Hamiltonian in Eq. (5.5) in terms of the bosonic field $\Phi(x)$. By applying the results of the previous section, at $\nu = 1$ we can describe the non-superconducting case $\Delta_p = 0$ as

$$H_{1D} = \frac{v_F}{4\pi} \int dx \left[\partial_x \Phi(x)\right]^2, \tag{5.14}$$

where v_F contains all information about contributions to the kinetic energy from the proximity effect. Adding interaction and going to $\nu \neq 1$, we substitute $v_F \to v/\nu$. We can then add pairing by considering the $\Delta_p \neq 0$ case as expressed through the boson fields Φ. We can do this through the relation Eq. (5.7), but first we must transform the pairing Hamiltonian to position space using the Fourier transform

$$\psi_{k_s + \delta q} = \frac{1}{\sqrt{L}} \int_{-L/2}^{L/2} dx \, \psi(x) e^{i(k_s + \delta q)x}. \tag{5.15}$$

When applied to the induced pairing term

$$H_p = \frac{1}{2} \sum_{\delta q} \Delta_{\delta q} \psi^{\dagger}_{k_s - \delta q} \psi^{\dagger}_{k_s + \delta q} + \text{h. c.}, \tag{5.16}$$

we find

$$H_p = \frac{1}{2L} \int_{-L/2}^{L/2} dx_1 dx_2 \, \Delta_I(x_1 - x_2) e^{-ik_s(x_1 + x_2)} \psi^{\dagger}(x_1) \psi^{\dagger}(x_2) + \text{h. c.} \tag{5.17}$$

where we have introduced the spatial pairing amplitude

$$\Delta_I(x_1 - x_2) = \sum_{\delta q} \Delta_{\delta q} e^{-i\delta q(x_1 - x_2)}. \tag{5.18}$$

Note that since $\Delta_{\delta q}$ is odd around $\delta q = 0$, we could replace the complex exponential with a sine, but we will keep the exponentials for now. Applying the definition of electron fields in terms of Φ, Eq. (5.7), we find

$$H_p = \frac{q_0 F^2}{4\pi L} \int_{-L/2}^{L/2} dx_1 dx_2 \, \Delta_I(x_1 - x_2) e^{-i(k_s - q_F)(x_1 + x_2)} e^{i\Phi(x_1)/\sqrt{\nu}} e^{i\Phi(x_2)/\sqrt{\nu}} + \text{h. c.}, \tag{5.19}$$

which is the position space pairing Hamiltonian for filling factor ν in terms of the chiral bosonic field Φ.

5.3.1 Linear approximation

We can simplify the pairing Hamiltonian further by simplifying $\Delta_I(x_1 - x_2)$. We recall that in Chapter 3 we defined the antisymmetrized expression

$$\Delta_{\delta q} = \frac{1}{2} \left(\Delta'_{I,\delta q} - \Delta'_{I,-\delta q} \right), \tag{5.20}$$

which implies that at at sufficiently small δq, the pairing amplitude is accurately described by a linear approximation whose validity is evaluated below. Furthermore, as discussed in Chapter 4, we expect small δq contributions to dominate the low energy transport qualities of the system, and is thus the domain we are interested in. The explicit expression is

$$\Delta'_{I,\delta q} = i|\Delta_0|\Gamma^2 \alpha \sum_{k_y, k_z} \frac{k_s \zeta_{\boldsymbol{\kappa}} + (\epsilon_{\boldsymbol{\kappa}} + E_s)\delta q}{\zeta_{\boldsymbol{\kappa}}^2 (\delta q k_s / m_s + \zeta_{\boldsymbol{\kappa}})^2}. \tag{5.21}$$

Here we have the momentum $\boldsymbol{\kappa} = (\delta q, k_y, k_z)$, the superconductor electron mass m_s and the supercurrent energy $E_s = k_s/2m_s$, as well as the energy

$$\zeta_{\boldsymbol{\kappa}} = \sqrt{(\epsilon_{\boldsymbol{\kappa}} + E_s)^2 + |\Delta_0|^2} = \sqrt{\left(\frac{\delta q^2 + k_y^2 + k_z^2}{2m_s} - \mu_s + E_s \right)^2 + |\Delta_0|^2}. \tag{5.22}$$

As discussed in Chapter 3, the amplitude $\Delta'_{I,\delta q}$ becomes singular for $-\delta q k_s / m_s = \zeta_{\boldsymbol{\kappa}}$, corresponding to a critical current at the SC surface. Thus, the singularity imposes a

cutoff on our theory, corresponding to assuming that we are well within the superconducting regime of the SC surface. Since $\zeta_{\boldsymbol{\kappa}} \geq |\Delta_0|$ for all $\boldsymbol{\kappa}$, the singularity is always avoided when $|\delta q| < \delta q_\Delta$, where

$$\delta q_\Delta = \frac{|\Delta_0| m_s}{k_s}. \tag{5.23}$$

This imposes a bound on the large momentum cutoff of our theory, namely that $q_0 < \delta q_\Delta$. Assuming an unspecified cutoff within this constraint, we can approximate the pairing amplitude as

$$\Delta_{\delta q} \simeq i e^{i\phi_\Delta} \Delta_{\mathrm{p}} \delta q e^{-|\delta q|/q_0}, \tag{5.24}$$

where Δ_{p} is the real constant

$$\Delta_{\mathrm{p}} \simeq -m_s \alpha \Gamma^2 L_z L_y \frac{E_s}{|\Delta_0|^2}. \tag{5.25}$$

Going forward we will assume the induced SC phase to be $\phi_\Delta = 0$ without loss of generality. The linear approximation is adjusted with the soft cutoff $e^{-|\delta q|/q_0}$ suppressing contributions from higher momenta. This allows us to keep the full momentum summation range while capturing the small δq physics without any artifacts from a hard cutoff. The approximate expression in Eq. (5.24) allows us to partially evaluate the spatial integral in the pairing Hamiltonian, resulting in a form better suited for future calculations.

In particular, we can resolve the sum in Eq. (5.18). We first convert the sum to an integral by applying the large L limit,

$$\frac{1}{L}\Delta_I(x_1 - x_2) = \frac{1}{L}\sum_{\delta q} \Delta_{\delta q} e^{-i\delta q(x_1 - x_2)} \simeq i\Delta_{\mathrm{p}} \int_{-\infty}^{\infty} \frac{d(\delta q)}{2\pi} \delta q e^{-i\delta q(x_1 - x_2)} e^{-|\delta q|/q_0}. \tag{5.26}$$

We split up the integral into positive and negative momenta,

$$
\begin{aligned}
\frac{1}{L}\Delta_I(x_1 - x_2) \\
= i\Delta_{\mathrm{p}} \left[\int_{-\infty}^{0} \frac{d(\delta q)}{2\pi} \delta q e^{-i\delta q(x_1 - x_2)} e^{\delta q/q_0} + \int_{0}^{\infty} \frac{d(\delta q)}{2\pi} \delta q e^{-i\delta q(x_1 - x_2)} e^{-\delta q/q_0} \right],
\end{aligned} \tag{5.27}
$$

and apply the general integral identities

$$\int_{0}^{\infty} dq \, q e^{-iqx} e^{-q/q_0} = \left(\frac{1}{q_0} + ix \right)^{-2}, \tag{5.28}$$

$$\int_{-\infty}^{0} dq \, q e^{-iqx} e^{q/q_0} = -\left(\frac{1}{q_0} - ix \right)^{-2}, \tag{5.29}$$

to find the approximation

$$
\begin{aligned}
\frac{1}{L}\Delta_I(x_1 - x_2) &= \frac{i\Delta_{\mathrm{p}}}{2\pi} \left[\left(\frac{1}{q_0} + i(x_1 - x_2) \right)^{-2} - \left(\frac{1}{q_0} - i(x_1 - x_2) \right)^{-2} \right] \\
&= \frac{\Delta_{\mathrm{p}}}{\pi} \frac{2(x_1 - x_2)}{q_0(q_0^{-2} + (x_1 - x_2)^2)^2},
\end{aligned} \tag{5.30}
$$

We find the behavior shown in Fig. 5.2, noting in particular that $\Delta_I(x_1 - x_2)$ is odd around $x_1 - x_2 = 0$, and vanishes beyond a distance given by the length scale $1/q_0$.
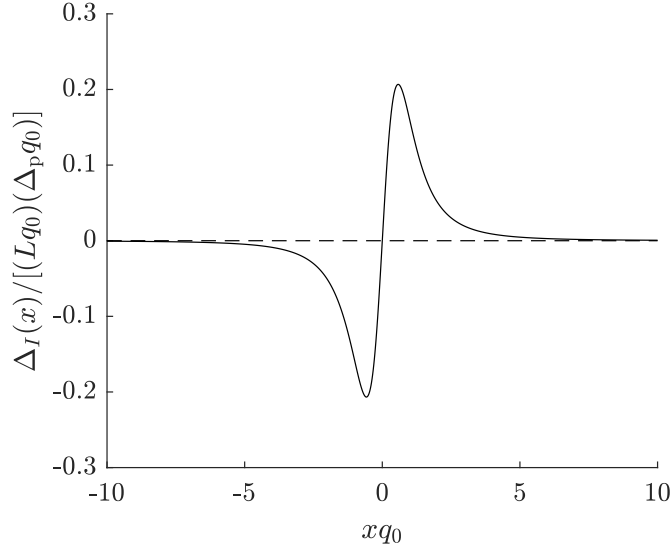
Figure 5.2: *The approximate spatial pairing in Eq.* (5.30) *is odd around the distance $x = 0$.*

5.3.2 Short distance approximation

As Fig. 5.2 shows, the spatial pairing is odd around zero distance and vanishes at large distances. The cutoff marks the momentum beyond which our model breaks down, which is approximately on the order of the separation of Landau levels. From our model dispersion of the QH edge presented in Chapter 3, we can approximate this to correspond to $q_0 \simeq 1/\ell$, corresponding to a cut-off length $1/q_0 \simeq \ell$, which under the assumptions of that chapter is around one nanometer. Assuming that the relevant physics involves momenta much smaller than q_0, we consider that in the limit $q_0 \to \infty$ the pairing is dominated by its $x_1 - x_2 \to 0$ behavior. Then the pairing amplitude approaches the form of the derivative of the Dirac delta function,

$$\Delta(x_1 - x_2) \sim \delta'(x_1 - x_2), \tag{5.31}$$

for which we have the identity for a general function $f(x)$

$$\int_{-\infty}^{\infty} dx \delta'(x) f(x) = - \int_{-\infty}^{\infty} dx \delta(x) f'(x). \tag{5.32}$$

To ensure the correct scaling, we will first define the the antiderivative $D_I(x)$ of the pairing amplitude

$$D_I'(x) \stackrel{\text{def}}{=} \Delta_I(x), \tag{5.33}$$

which we find to have the form

$$D_I(x) = - \frac{L\Delta_{\mathrm{p}}}{\pi q_0 \left(q_0^{-2} + x^2\right)}, \tag{5.34}$$

such that we recover the result from Eq. (5.30) using the chain rule,

$$D_I'(x) = - \frac{d}{du} \left(\frac{2L\Delta_{\mathrm{p}}}{q_0 u} \right) \frac{d}{dx} \left(\frac{1}{q_0^2} + x^2 \right) = \frac{2L\Delta_{\mathrm{p}} x}{\pi q_0 \left(q_0^{-2} + x^2\right)^2}, \tag{5.35}$$

If we then assume that $\Delta_I(x) = \mathcal{A}\delta'(x)$, the scaling factor $\mathcal{A}$ can be found as

$$\int dx D_I(x) = \mathcal{A} \int dx \delta(x) = \mathcal{A}. \tag{5.36}$$

Resolving this integral yields

$$\mathcal{A} = -L\Delta_{\mathrm{p}}, \tag{5.37}$$

and thus we have the correctly scaled approximation

$$\Delta_I(x) = -L\Delta_{\mathrm{p}}\delta'(x). \tag{5.38}$$

Physically, this approximation corresponds to only considering pairing between particles whose relative distance is very small but still non-zero, with zero-distance pairing being suppressed by the Pauli principle. We will now apply this short-distance approximation to the pairing Hamiltonian.

5.3.3 Simplifying the pairing term

Looking again at Eq. (5.19), we can exploit the fact that the pairing amplitude only depends on the distance $x_1 - x_2$. We formulate it in terms of relative and center-of-mass coordinates

$$r = x_1 - x_2, \qquad X = \frac{x_1 + x_2}{2}. \tag{5.39}$$

This change of coordinates has a unit Jacobian determinant and thus the integral becomes

$$H_p = \frac{q_0 F^2}{4\pi L} \int_{-L/2}^{L/2} dX \, e^{2i(k_s - q_F)X} \int_{-L}^{L} dr \, \Delta_I^*(r) e^{-i\Phi(X+r/2)/\sqrt{\nu}} e^{-i\Phi(X-r/2)/\sqrt{\nu}} + \mathrm{h.\,c.}, \tag{5.40}$$

where we have explicitly written out the term associated with $\Delta_{\delta q}^*$ instead of $\Delta_{\delta q}$. In anticipation of the application of the $\delta'(x)$ approximation, we see in Eq. (5.32) that only the slope around $r = 0$ will affect the result of the integral. We will therefore expand the exponent around $r = 0$ to linear order. To do this, we note that taking the derivative $\partial_r \Phi$ can be replaced with taking the derivative $\partial_X \Phi$ as follows. Using the definition of Φ from Eq. (5.8), we have

$$\partial_r \Phi(X \pm r/2)\Big|_{r=0}$$

$$= \mp \left[i\sqrt{\frac{2\pi}{L}} \sum_{q>0} \frac{e^{-q/(2q_0)}}{\sqrt{q}} \frac{iq}{2} \left(e^{-iq(X\pm r/2)} b_q + e^{iq(X\pm r/2)} b_q^\dagger \right) \right]_{r=0}. \tag{5.41}$$

We evaluate this expression at $r = 0$,

$$\partial_r \Phi(X \pm r/2)\Big|_{r=0} = \mp \frac{1}{2} i\sqrt{\frac{2\pi}{L}} \sum_{q>0} \frac{e^{-q/(2q_0)}}{\sqrt{q}} iq \left(e^{-iqX} b_q + e^{iqX} b_q^\dagger \right), \tag{5.42}$$

and note that the right hand side corresponds to taking the derivative of X instead of r, namely

$$\partial_r \Phi \left(X \pm \frac{r}{2} \right) \Big|_{r=0} = \pm \frac{1}{2} \partial_X \Phi(X). \tag{5.43}$$

Applying this result to exponential expanded to linear order around $r = 0$

$$\exp \left[-\frac{i}{\sqrt{\nu}} \Phi \left(X \pm \frac{r}{2} \right) \right] = \exp \left[-\frac{i}{\sqrt{\nu}} \left(\Phi(X) + \partial_r \Phi \left(X \pm \frac{r}{2} \right) \Big|_{r=0} r \right) \right]. \tag{5.44}$$

then yields

$$\exp \left[-\frac{i}{\sqrt{\nu}} \Phi \left(X \pm \frac{r}{2} \right) \right] = \exp \left[-\frac{i}{\sqrt{\nu}} \left(\Phi(X) \pm \partial_X \Phi \left(X \right) \frac{r}{2} \right) \right]. \tag{5.45}$$

We then factor the exponential into a product of exponentials. According to the Baker-Hausdorff lemma we have the following identities for operators A, B with $[A, B] \in \mathbb{C}$:

$$[A, e^B] = [A, B] e^B, \tag{5.46a}$$

$$e^{A+B} = e^A e^B e^{-[A,B]/2}, \tag{5.46b}$$

$$e^B e^A = e^A e^B e^{-[A,B]}. \tag{5.46c}$$

The first identity lets us evaluate the following useful commutator

$$\left[\partial_{x_2} \Phi(x_2), e^{-i\Phi(x_1)/\sqrt{\nu}} \right] = -\frac{i}{\sqrt{\nu}} \left[\partial_{x_2} \Phi(x_2), \Phi(x_1) \right] e^{-i\Phi(x_1)/\sqrt{\nu}}. \tag{5.47}$$

From the commutator in Eq. (5.9) it can be derived that [74]

$$[\Phi(x_1), \partial_{x_2} \Phi(x_2)]$$
$$= -\frac{2\pi i}{L} \left(\frac{1}{1 - \exp\left[-\frac{2\pi i}{L}(x_1 - x_2 - i/q_0) \right]} + \frac{1}{1 - \exp\left[\frac{2\pi i}{L}(x_1 - x_2 - i/q_0) \right]} \right). \tag{5.48}$$

In the thermodynamic limit $L \to \infty$ we can expand the exponentials and find

$$[\Phi(x_1), \partial_{x_2} \Phi(x_2)] \simeq \frac{2i}{q_0 \left[(x_1 - x_2)^2 + q_0^{-2} \right]}. \tag{5.49}$$

From here on we will assume that the commutator is evaluated in this limit. With this result we are ready to simplify the expanded product of exponentials

$$e^{-\frac{i}{\sqrt{\nu}} \Phi(X+r/2)} e^{-\frac{i}{\sqrt{\nu}} \Phi(X-r/2)} = e^{-\frac{i}{\sqrt{\nu}} \left[\Phi(X) + \frac{r}{2} \partial_X \Phi(X) \right]} e^{-\frac{i}{\sqrt{\nu}} \left[\Phi(X) - \frac{r}{2} \partial_X \Phi(X) \right]}. \tag{5.50}$$

Looking again at Eq. (5.46) we generally have

$$e^{A+B} e^{A-B} = e^A e^B e^{-[A,B]/2} e^A e^{-B} e^{[A,B]/2}$$
$$= e^A e^B e^A e^{-B}$$
$$= e^{2A} e^{-[A,B]} \tag{5.51}$$

This means the two exponentials become

$$e^{-\frac{i}{\sqrt{\nu}}\Phi(X+r/2)}e^{-\frac{i}{\sqrt{\nu}}\Phi(X-r/2)} = e^{-\frac{2i}{\sqrt{\nu}}\Phi(X)}e^{-[-i\Phi(X)/\sqrt{\nu},-i\partial_X\Phi(X)r/(2\sqrt{\nu})]}$$

$$= e^{-\frac{2i}{\sqrt{\nu}}\Phi(X)}e^{r/(2\nu)[\Phi(X),\partial_X\Phi(X)]}$$

$$= e^{-\frac{2i}{\sqrt{\nu}}\Phi(X)}e^{iq_0 r/\nu}, \tag{5.52}$$

where in the final step we have used that at zero distance, Eq. (5.49) becomes

$$\lim_{x_2\to x_1}\left[\Phi(x_1),\partial_{x_2}\Phi(x_2)\right] = 2iq_0. \tag{5.53}$$

We can then separate out the center-of-mass integral to obtain the pairing Hamiltonian

$$H_p = \frac{q_0 F^2}{4\pi L}\int_{-L/2}^{L/2} dX\ e^{2i(k_s-q_F)X}e^{-\frac{2i}{\sqrt{\nu}}\Phi(X)}\int_{-L}^{L} dr\ \Delta_I^*(r)e^{\frac{i}{\nu}rq_0} + \text{h.\,c.} \tag{5.54}$$

We apply the $\Delta_I(x) \sim \delta'(x)$ approximation of Eq. (5.38) to find

$$\frac{1}{L}\int_{-L}^{L} dr\ \Delta_I^*(r)e^{\frac{iq_0}{\nu}r} = -\Delta_I^{(1)}\int_{-L}^{L} dr\ \delta'(r)e^{\frac{iq_0}{\nu}r}. \tag{5.55}$$

Resolving the integral as shown in Eq. (5.32) yields

$$\frac{1}{L}\int_{-L}^{L} dr\ \Delta_I^*(r)e^{\frac{iq_0}{\nu}r} = \Delta_I^{(1)}\frac{\partial}{\partial r}\left(e^{\frac{iq_0}{\nu}r}\right)_{r=0}$$

$$= \frac{i\Delta_I^{(1)}q_0}{\nu}. \tag{5.56}$$

We thus find the pairing term

$$\boxed{H_p = \frac{i\Delta_p q_0^2 F^2}{4\pi\nu}\int_{-L/2}^{L/2} dX\ e^{2i(k_s-q_F)X-\frac{2i}{\sqrt{\nu}}\Phi(X)} + \text{h.\,c.}} \tag{5.57}$$

Inserting this result into the effective Hamiltonian Eq. (5.5),

$$H_{\text{eff}} = \frac{v}{4\pi\nu}\int dx\ [\partial_x\Phi(x)]^2 + \frac{i\Delta_p q_0^2 F^2}{4\pi\nu}\int_{-L/2}^{L/2} dx\ e^{2i(k_s-q_F)x}e^{-2i\Phi(x)/\sqrt{\nu}} + \text{h.\,c.} \tag{5.58}$$

we obtain the effective Hamiltonian of a proximitized segment of a fractional QH edge with filling factor ν in terms of the bosonic field $\Phi(x)$. In the above derivation we have performed first order expansion of the exponents and then applied the approximation $\Delta_I(x) \sim \delta'(x)$. Both steps result in lost information about the system, and thus applying them in the opposite order could possibly lead to a different result. That this is not the case is demonstrated in Appendix C. An interesting feature of the bosonized pairing term is that it appears that re-fermionization would lead to a vanishing term $H_p \propto \psi(x)\psi(x)$. This is not actually the case, as we will see in the next section.

Seeing as there is a oscillatory factor under the integral, we should consider the relevance of the pairing term to transport. In the continuum limit $L \to \infty$, the oscillatory factor $e^{2i(k_s-q_F)x}$ within the integral would average the pairing out for all cases but $k_s \simeq q_F$, corresponding to the resonance condition discussed in Chapter 3. That this

resonance condition shows up so explicitly in the Hamiltonian without reference to transport suggests that the pairing suppression is of a different nature than that found in the previous chapters. Since the pairing fundamentally happens between electrons, and the minimal excitation of the fractional QH edge is a fractional electron quasiparticle, the suppression can be interpreted as the competition between electron pairing and electron fractionalization.

For large but finite systems, the pairing will be weak but non-zero, with a dominant contribution for $k_s \simeq q_F$. In the case of large but finite L, we would then be justified in treating the pairing perturbatively in Δ_{p}/v, where v is the velocity associated with the system without pairing. We will use this to sketch out a calculation of transport properties of the proximitized fraction QH edge in Section 5.4.

5.3.4   Re-fermionization

To interpret Eq. (5.57), it is helpful to consider the re-fermionized version in the electron case $\nu = 1$. Using Eq. (5.53) we can write

$$H_p = \frac{i\Delta_{\mathrm{p}} q_0 F^2}{4\pi} \int_{-L/2}^{L/2} dx \, e^{2i(k_s - q_F)x} e^{-i\Phi(x)} \left(\frac{1}{2}[\Phi(x), \partial_x \Phi(x)] \right) e^{-i\Phi(x)} \tag{5.59}$$

Adding and subtracting the gradient of Φ we have

$$H_p = \frac{i\Delta_{\mathrm{p}} q_0 F^2}{8\pi} \int_{-L/2}^{L/2} dx \, e^{2i(k_s - q_F)x} \left(e^{-i\Phi(x)} \left(-i\partial_x \Phi(x) + \frac{1}{2}[\Phi(x), \partial_x \Phi(x)] \right) e^{-i\Phi(x)} \right.$$

$$\left. + e^{-i\Phi(x)} \left(i\partial_x \Phi(x) + \frac{1}{2}[\Phi(x), \partial_x \Phi(x)] \right) e^{-i\Phi(x)} \right) \tag{5.60}$$

As demonstrated in Appendix D, the derivative of an exponentiated operator obeys the relation

$$\partial_x e^{-i\Phi(x)} = - \left(i\partial_x \Phi(x) + \frac{1}{2}[\Phi(x), \partial_x \Phi(x)] \right) e^{-i\Phi(x)}. \tag{5.61}$$

Applying Eq. (5.46), we furthermore have that

$$\partial_x e^{i\Phi(x)} = -e^{i\Phi(x)} \left(i\partial_x \Phi(x) + \frac{1}{2}[\Phi(x), \partial_x \Phi(x)] - [\Phi(x), \partial_x \Phi(x)] \right)$$

$$= e^{i\Phi(x)} \left(-i\partial_x \Phi(x) + \frac{1}{2}[\Phi(x), \partial_x \Phi(x)] \right). \tag{5.62}$$

We can therefore rewrite Eq. (5.60) as

$$H_p = \frac{i\Delta_{\mathrm{p}} q_0 F^2}{8\pi} \int_{-L/2}^{L/2} dx \, e^{2i(k_s - q_F)x} \left[\left(\partial_x e^{-i\Phi(x)} \right) e^{-i\Phi(x)} - e^{-i\Phi(x)} \left(\partial_x e^{-i\Phi(x)} \right) \right]. \tag{5.63}$$

Re-fermionizing through the fermion field definition

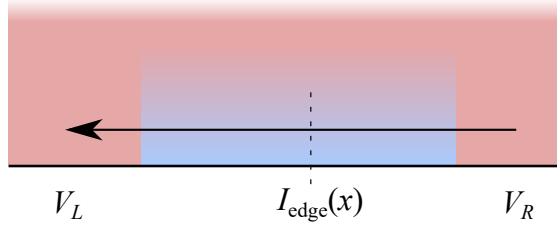$$\psi(x) = \frac{F}{\sqrt{2\pi/q_0}} e^{-iq_F x} e^{-i\Phi(x)}, \tag{5.64}$$

Figure 5.3: *We investigate the current $I_{edge}(x)$ at a point along the proximitized fractional QH edge (blue region). The current corresponds to a potential difference $V_R - V_L$ between the far right and far left regions.*

we find

$$H_p = \frac{i}{4}\Delta_{\text{P}} \int_{-L/2}^{L/2} dx \; e^{2ik_s x} \left[\Big(\partial_x \psi(x)\Big)\psi(x) - \psi(x)\Big(\partial_x \psi(x)\Big) \right].$$ (5.65)

Integrating by parts, and applying the Pauli principle $\psi(x)\psi(x) = 0$, we find

$$H_p = -\frac{i}{2}\Delta_{\text{P}} \int_{-L/2}^{L/2} dx \; e^{2ik_s x} \psi(x)\partial_x \psi(x).$$ (5.66)

This term can be understood through the definition of the derivative,

$$\partial_x \psi(x) = \lim_{a \to 0} \frac{\psi(x+a) - \psi(x)}{a},$$ (5.67)

from which we can see that $\psi(x)\partial_x \psi(x)$ corresponds to the two fields being separated by an infinitesimal distance. Since ψ is a fermionic field, this critically means that the term does not vanish due to the Pauli principle. As discussed in Section 5.2, at filling factors in the Laughlin sequence $\nu = 1/(2n+1)$, we also find fermionic behavior of the fields, and so this treatment can in principle be extended to Laughlin quasiparticles.

We would expect that at $\nu = 1$, the general bosonized pairing Hamiltonian would reduce to the electronic pairing Hamiltonian derived in Chapter 3. With the result in Eq. (5.66), we see that this is indeed the case for the bosonized pairing Hamiltonian in Eq. (5.57). In particular, we see that under the applied approximations, the bosonized pairing Hamiltonian reduces to the position space equivalent of the effective pairing Hamiltonian for electrons derived to linear order.

5.4 Transport

Now that we have found the Hamiltonian describing the proximitized fractional QH state, the next step is to use the Hamiltonian to predict the behavior of observable quantities as we did in Chapter 4. This problem was not addressed within the scope of this thesis, but here we provide an outline for how an observable transport signature could be predicted from the result in Eq. (5.57).

While the derivation of the effective Hamiltonian in Chapter 3 applies equally well to the integer and fractional QH edges, the same cannot be said for the transport calculations in Chapter 4. In particular, the scattering formalism used only applies to the case of free electrons, while in the fractional QH case, strong electron interaction is an essential element of the system. In this section we will outline another strategy with

which one use the derived Hamiltonian Eq. (5.57) to predict the outcome of transport measurements across a proximitized fractional QH edge.

Following Ref. [75], we can consider the current $I_{\text{edge}}(x)$ passing through a point x along the chiral, left-moving fractional QH edge in terms of its linear response to an applied electrostatic potential $V(x)$,

$$I_{\text{edge}}(x) = \int dx' D^R(x - x', \omega = 0) V(x'), \tag{5.68}$$

where $D^R(x, \omega)$ is the retarded response function for position x and frequency ω,

$$D^R(x - x', \omega) = -i \int_{-\infty}^{0} dt e^{-i\omega t} \frac{\nu e^2}{(2\pi)^2} \langle [\dot{\Phi}(x, 0), \partial_{x'} \Phi(x', t)] \rangle. \tag{5.69}$$

It can then be shown that for a potential $V(x)$ which has the constant value V_L far to the left, and the constant value V_R far to the right, see Fig. 5.3, the current becomes

$$I_{\text{edge}} = -\nu \frac{e^2}{2\pi} V_R, \tag{5.70}$$

corresponding to the expected fractional QH conductance.

We then add pairing by considering the above result as true for a system described by the Hamiltonian H_0, and then investigating the case where the system is described by the Hamiltonian $H_0 + H_p$, with H_p defined in Eq. (5.57). We can pull out the derivatives from the correlator inside the response function

$$\partial_t \partial_{x'} \langle [\Phi(x, t), \Phi(x', t')] \rangle_I |_{t=0, t'=t}, \tag{5.71}$$

where the I subscript indicated that it has induced pairing. To treat the pairing perturbatively, we take the standard approach of considering time evolution in the interaction picture [50], which lets us write up the well-defined sum to second order in Δ_{p}/v

$$\langle [\Phi(x, t), \Phi(x', t')] \rangle_I \simeq \langle [\Phi(x, t), \Phi(x', t')] \rangle_0 + \langle [\Phi(x, t), \Phi(x', t')] \rangle_I^{(2)}. \tag{5.72}$$

where the $\langle \ldots \rangle_0$ correlator is that of the system without pairing. The first order term must vanish under the following argument: any correlators in the context of bosonization in terms of $\Phi(x)$ must be invariant under a constant shift $\Phi(x) + C$ [71], and since the first order contribution would involve a correlator on the form $\langle \dot{\Phi} \partial_x \Phi H_p[\Phi] \rangle$, we see from Eq. (5.57) that it can only be invariant under a constant shift if it is zero.

The second order term will constitute a correction to the response function

$$D^R(x - x', \omega) = D_0^R(x - x', \omega) + D_p^R(x - x', \omega), \tag{5.73}$$

which in turn will modify the current as

$$I_{\text{edge}}(x) = \int dx' \left[D_0^R(x - x', \omega) + D_p^R(x - x', \omega) \right] V(x'). \tag{5.74}$$

Thus, we expect a direct observation of the induced superconductivity in the transport characteristics of the otherwise highly precisely quantized fraction QH edge, much like we saw with the integer QH case in Chapter 4. This contribution can be predicted by calculating $\langle [\Phi(x, t), \Phi(x', t')] \rangle_I^{(2)}$ by resolving time-ordered correlators of the bosonic Φ fields and the pairing Hamiltonian H_p.

Experimentally [27], results from a finger setup have found a reduction of the Hall resistance R_H for up to 10% at the $\nu = 1/3$ plateau, as well as strongly negative longitudinal resistance on the order of $k\Omega$. The reduction of R_H can, however, also be attributed to other reasons than induced superconductivity. A clearer signature of induced superconductivity would be negative longitudinal resistance, the prediction of which would require a different approach than that sketched out here.

5.5 Summary

We extend the effective Hamiltonian of an integer QH edge with induced superconductivity as derived in Chapter 3 to the case of a fractional QH edge. To account for the strong electron interactions causing the fractionalization, we apply the theory of a Tomonaga-Luttinger liquid to bosonize the Hamiltonian, and use the fact that this becomes an approximate low energy description of the fractional QH edge in the case where the interaction parameter equals the filling fraction $K = \nu$.

The bosonized theory has a large momentum cutoff q_0, and we show that for a large cutoff, the spatial pairing amplitude is approximately the derivative of a delta function, $\Delta_I(x) \sim \delta'(x)$. We expand the bosonized Hamiltonian for small pairing distances and apply the derivative-of-delta approximation to find the effective pairing Hamiltonian of the fractional QH edge in terms of the bosonic fields Φ

$$H_p = \frac{i\Delta_{\mathrm{p}} q_0 F^2}{4\pi\sqrt{\nu}} \int_{-L/2}^{L/2} dx \; e^{2i(k_s - q_F)x} e^{-2i\Phi(x)/\sqrt{\nu}} + \mathrm{h.\,c.} \tag{5.75}$$

We then refermionize the Hamiltonian at $\nu = 1$ to confirm that it has the expected behavior for p-wave paired electrons. A sketch is presented for how the Hamiltonian can be used to predict a modified Hall resistance in experiments, which is consistent with the relevant literature.

By deriving the effective pairing Hamiltonian for the fractional QH edge based on the results for the integer QH edge, we have demonstrated the general applicability of our model to both cases. Despite the fact that the minimal excitation of the fractional QH edge is a fractional electron quasiparticle, our results predict that electron pairing is still possible, as was also recently found experimentally.

CHAPTER 6

Current correlations of Cooper-pair point tunneling into the quantum Hall edge

In this chapter we consider a different model of a similar system, namely second-order tunneling of Cooper pairs across a quantum point contact into a quantum Hall (QH) edge at different integer and fractional filling factors. This model was introduced by M. P. A. Fisher in 1994 [58], and we expand upon the work by predicting the experimental signatures of the most notable effects in terms of tunneling current and finite-frequency noise. Since the paper by Fisher, the fractional nature of the quantum Hall edge at very high fields has been successfully probed through experimental investigations of tunneling current and noise signatures [76], and we will extend the results of the original paper in terms of those quantities. Only recently, however, has it become possible to couple the fractional QH edge to a superconductor (SC) due to the monumental challenge of developing a SC material whose superconducting state can survive magnetic fields up to $B \sim 14$ T, with Ref. [27] being the only experiment known to the author to report success in this regard. Since that experiment did not report on the tunneling current and noise quantities investigate in this chapter, theoretical predictions on this type of system remain untested for now.

The work in this chapter was published in Ref. [33]. This chapter will focus on my contribution to the paper, which, in contrast to the previous chapters, did not involve the full technical derivations. Therefore, some of the key results in this chapter will not be derived, but rather taken from the paper, as marked by a reference to Ref. [33]. In addition, while great care was taken in the previous chapters to rigorously derive a Hamiltonian of the coupled system, this chapter will involve a more loosely derived phenomenological Hamiltonian. Seeing as this Hamiltonian has already been treated in the literature [58], we satisfy ourselves with only briefly motivating it before discussing the resulting physical predictions. As a consequence of the loosely motivated Hamiltonian, we do not expect to derive accurate predictions beyond scaling relations, e.g. predicting which is the lowest non-zero order voltage contribution to the tunneling current.

Throughout the chapter we will be working in units of $|e| = k_B = \hbar = 1$.
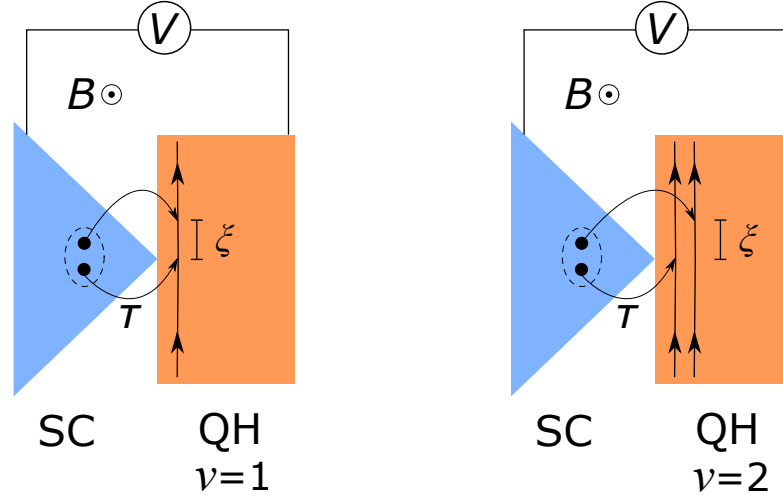
Figure 6.1: *A quantum point contact with tunneling amplitude τ connects a SC to the chiral edge states of an integer quantum Hall (QH) phase at filling factor ν. For $\nu = 1$, both electrons of the Cooper pair tunnel into the same state, leading to a Pauli blockade, while at $\nu = 2$ the electrons can tunnel into different states. The bias V is applied between the chiral edge channel and the superconductor.*

6.1 Quantum point contact

Compared to the extended interface with which we have become familiar over the previous chapters, the quantum point contact is different in a few key areas. The fact that tunneling only occurs at one point implies that we have broken translation invariance, and thus momentum conservation, along the interface. The description of the system will therefore be in position space, and we will not find the same momentum matching condition that played such a key role in the previous chapters.

Furthermore, where the extended interface saw hybridization between the SC surface states and the QH edge states, resulting in electron transport across the interface corresponding to an oscillation between particle-like and hole-like states in the QH edge, the quantum point contact has a more well-defined spatial electron transport. The electron transport due to an applied voltage across the interface will all happen at the point contact, and rather than looking for signatures of induced superconductivity downstream of the contact, we will be directly investigating the tunneling current passing through the point contact.

The geometry of the system and some key simplifying assumptions allow us to extend our analysis to filling factor $\nu = 2$, where two parallel states propagate along the QH edge, and we will see that this case is qualitatively different due to the possibility of a Cooper pair tunneling into separate edge states. Another extension compared to previous chapters is that into finite (non-zero) temperature, where we will see a dampening of quantum effects. Of course, while this system is different to the one treated in previous chapters, it is also similar, and the reader will recognize several elements of the treatment. In particular, we will see that the Pauli blockade, which completely suppressed Andreev reflection at zero bias as discussed in Chapter 4, will appear again.

6.1.1 Perturbative Hamiltonian

We consider a system consisting of a quantum point contact between a SC and a QH edge with an applied voltage V across the contact, as depicted in Fig. 6.1, using the Hamiltonian presented in Ref. [58]. In this section we will briefly outline the justification of the Hamiltonian, and refer the reader to the reference for more detail. Similarly to the total Hamiltonian treated in Chapter 3, it consists of a QH edge Hamiltonian, a SC Hamiltonian and a tunneling Hamiltonian

$$H = H_{QH} + H_{SC} + H_T. \tag{6.1}$$

We will be treating QH edges at different integer and fractional filling factors, which imply different forms of H_{QH} as detailed in the following sections. The SC will be assumed to be an s-wave SC described by a BCS Hamiltonian, which means that it hosts local pairing with an amplitude Δ between electrons of opposite spin, where Δ can be assumed real without loss of generality. We will assume all energies to be within the SC gap described by Δ, such that all tunneling involves only Cooper pairs, and no single electrons. Assuming that the QH edge states are spin polarized in the same direction, the s-wave nature of the SC implies that tunneling is only allowed in the presence of a spin-flip mechanism such as spin-orbit coupling, as discussed in Chapter 2. In contrast to the case in that chapter, however, we will not assume any particular source of the this mechanism, but simply include it in the tunneling Hamiltonian. This can be considered an effective model of relevant spin-orbit coupling at the SC surface or in the QH edge.

As we will see, the tunneling current can be described exclusively in terms of the tunneling Hamiltonian, and thus this is the only part of the total Hamiltonian in Eq. (6.1) which we will be describing explicitly. The simplest tunneling Hamiltonian removes one Cooper pair from the SC and adds two electrons to the QH edge, or vice versa. The point-like nature of the tunneling means that the resulting Hamiltonian will depend evenly on all momenta, and we can ignore momentum dependencies. In a mean field description [1], the Cooper pair operator can be replaced with the pairing amplitude Δ, and thus the tunneling Hamiltonian with included spin-flip takes the form

$$H_T = \int dx dx'\, t_1(x,x')\Big(\Delta \psi_\uparrow^\dagger(x)\psi_\downarrow^\dagger(x') + \mathrm{h.\,c.}\Big)$$
$$+ \int dx\, t_2(x)\Big(\psi_\uparrow^\dagger(x)\psi_\downarrow(x) + \mathrm{h.\,c.}\Big), \tag{6.2}$$

where $\psi_\uparrow(x)$ is the annihilation operator of the QH edge spin-up electron at position x while t_1 is the unitless Cooper pair tunneling amplitude and t_2 is the spin flip amplitude with units of energy. Note that the operator ψ is not tied to a particular edge state, and thus for $\nu > 1$ it represents a superposition of edge states as discussed below. The coordinates x, x' run along the QH edge, and we have assumed the point contact to be at $x = 0$, meaning that this is the only coordinate where Cooper pairs can tunnel to and from the SC.

Treating the tunneling Hamiltonian perturbatively in t_1 and t_2, the lowest order non-zero term must be a second order cross term involving both tunneling, as indicated by the presence of t_1, and spin-flip, as indicated by the presence of t_2. While the tunneling Hamiltonian is symmetric in spin, all spin-down fields will be highly energetic due to spin polarization, and can be integrated over in a low-energy theory. Under these

arguments, the dominating term can be shown to be describing pairing between parallel spins

$$\int dx\,dx'\, \tau(x, x')\Delta\left[\psi_\uparrow^\dagger(x)\psi_\uparrow^\dagger(x') + \text{h. c.}\right]. \tag{6.3}$$

with an effective unitless tunneling amplitude

$$\tau(x, x') \propto t_1(x, x')[t_2(x) - t_2(x')]. \tag{6.4}$$

We neglect all other terms and consider this the effective tunneling Hamiltonian. Following Ref. [58], we can simplify the description further by the following observation: for a single edge state, the tunneling will be suppressed at small distances $x - x' \to 0$ due to the Pauli principle forcing $\psi_\uparrow(x)\psi_\uparrow(x) = 0$. Furthermore, superconducting correlations are exponentially suppressed between electrons beyond the superconducting coherence length $\xi = v_{F,s}/\pi\Delta$ [77], with $v_{F,s}$ being the Fermi velocity of the SC. We thus find that the greatest contribution to the integral Eq. (6.3) must occur at distances on the order $x - x' \sim \xi$. We can then simplify the tunneling term by only considering the dominant contribution to the integral

$$H_T' = \tau\Delta\psi_\uparrow^\dagger(x = \xi)\psi_\uparrow^\dagger(x = 0) + \text{h. c.}, \tag{6.5}$$

where we have fixed the positions of the QH electrons involved in the tunneling. Going forward we will suppress the spin index since we will only be concerned with spin-up electrons. The Pauli principle argument clearly applies to the case of one edge state, but we can extend the validity of the argument, and thus the fixed distance tunneling approximation, to the case of two edge states with equal spin by defining different electron fields for the different states, ψ_1 and ψ_2, and writing

$$\psi(x) = \sqrt{p}\,\psi_1(x) + \sqrt{1-p}\,\psi_2(x). \tag{6.6}$$

Here we have introduced $0 \leq p \leq 1$ which is the probability of tunneling into edge state 1, and consequently $1 - p$ is the probability of tunneling into edge state 2. At a fixed QH edge Fermi energy, the two edge states will have a relative phase related to the strength of the external B-field and the distance between them, see Chapter 2. As we will see, this phase difference will lead to interference effects in the tunneling current. By assuming p real, we assume that no further phase differences are induced due to tunneling. To evaluate the finite distance approximation in Eq. (6.5) for two states, we can write

$$\psi(x)\psi(x) = \left(\sqrt{p}\,\psi_1(x) + \sqrt{1-p}\,\psi_2(x)\right)\left(\sqrt{p}\,\psi_1(x) + \sqrt{1-p}\,\psi_2(x)\right)$$
$$= p\psi_1(x)\psi_1(x) + (1-p)\psi_2(x)\psi_2(x) + \sqrt{p(1-p)}\left(\psi_1(x)\psi_2(x) + \psi_2(x)\psi_1(x)\right), \tag{6.7}$$

which must be zero under the Pauli principle. Thus, for two edges we can still consider Eq. (6.5) the dominant term.

Replacing the tunneling Hamiltonian in Eq. (6.1) by Eq. (6.5) gives us the total effective Hamiltonian of the system. By considering the effective tunneling term perturbatively we will calculate the tunneling current and noise for different filling factors.

6.1.2 Tunneling current

The first observable of interest we wish to calculate is the tunneling current across the quantum point contact. The corresponding operator measures the change in electron number in the QH edge over time,

$$J = \frac{dN_{\mathrm{QH}}}{dt} = i[H, N_{\mathrm{QH}}],$$ (6.8)

where $N_{\mathrm{QH}} = \int dx\,\psi^\dagger(x)\psi(x)$ is the number operator for electrons in the QH edge. Since the only term of the Hamiltonian in Eq. (6.1) which changes electron number in the QH edge is the tunneling term, this is the only term with a non-zero commutator

$$J = i[H'_T, N_{\mathrm{QH}}].$$ (6.9)

Evaluating the commutator lets us perform the integral within the number operator yielding

$$J = -2i\tau\Delta\Big(\psi^\dagger(\xi)\psi^\dagger(0) - \mathrm{h.\,c.}\Big).$$ (6.10)

We can calculate the current across the point contact at a time t under a dc bias perturbatively in the tunneling by applying the Keldysh formalism [78]. Then the current is the interaction picture expectation value with respect to the biased ground state of the system without tunneling

$$I(t) = \langle U^\dagger(t, -\infty)J(t)U(t, -\infty)\rangle,$$ (6.11)

where the time evolution operator $U(t_2, t_1)$ can be written to lowest order in the tunneling amplitude as

$$U(t, -\infty) \simeq 1 - i \int_{-\infty}^{t} dt'\, H'_T(t').$$ (6.12)

The steady state current at a given dc bias V can then be found in terms of the operator

$$A(t) = \psi(0, t)\psi(\xi, t)$$ (6.13)

as [79]

$$I_{dc}(V) = 2(\tau\Delta)^2 \int_{-\infty}^{\infty} dt \left\langle \Big[A^\dagger(t), A(0)\Big] \right\rangle.$$ (6.14)

Taking the center of the SC gap as zero energy, the applied bias V means that the QH edge fields are at energy V. Applying the unitary transform $U_V = e^{iVt}$ to the QH edge operators shifts the QH ground state energy down to zero, corresponding to the momentum shift discussed in Section 2.5.1, but for energy and time instead of momentum and space. We can apply this transformation to rewrite Eq. (6.14) as

$$I_{dc}(V) = 2(\tau\Delta)^2 \int_{-\infty}^{\infty} dt\, e^{2iVt} \left\langle \Big[A^\dagger(t), A(0)\Big] \right\rangle_0,$$ (6.15)

where the expectation value is now with respect to the unbiased ground state. Evaluating this expression at different filling factors will be one of the main original contributions of this chapter.

6.1.3 Noise

Beyond current and conductance, a common experimentally available quantity used to probe quantum mechanical effects of materials is noise [2]. Experiments on quantum systems involve many sources of noise, with some external which interfere with the experiments, and some which are inherent to the system which can be used to understand details about the system which are otherwise difficult to access. If we consider a well-isolated system we can focus on two interesting sources of noise: thermal fluctuations, and the Poissonian statistics of quantized charge transport across a tunneling junction, i.e. shot noise [76].

Specifically, we describe the noise through its power spectral density S at a finite frequency ω and dc bias voltage V, which is defined as

$$S_{\mathrm{dc}}(\omega, V) = \int_{-\infty}^{\infty} dt e^{i\omega t} \langle \delta J(t) \delta J(0) \rangle, \tag{6.16}$$

where $\delta J(t) = J(t) - \langle J(t) \rangle$ measures the deviation of the current from its average, which is taken with respect to the ground state of the QH and SC system without tunneling but with bias. Using the definition of the current operator Eq. (6.10), we can write up the noise to the lowest order in the tunneling amplitude

$$S_{\mathrm{dc}}(\omega, V) = 4(\tau\Delta)^2 \int_{-\infty}^{\infty} dt \left[e^{i(\omega+2V)t} + e^{i(\omega-2V)t} \right] \langle A^\dagger(t) A(0) \rangle_0. \tag{6.17}$$

From this expression, results relating to the shot noise can be found by assuming that the power spectral density is independent of frequency, corresponding to taking $S(\omega = 0, V)$. In that case, we can exploit time-translation invariance [33]

$$\left\langle A^\dagger(t) A(0) \right\rangle = \left\langle A^\dagger(0) A(-t) \right\rangle, \tag{6.18}$$

to express S through the anticommutator

$$\begin{aligned} S_{\mathrm{dc}}(0, V) &= 4(\tau\Delta)^2 \int_{-\infty}^{\infty} dt \left[e^{2iVt} \langle A^\dagger(t) A(0) \rangle_0 + e^{-2iVt} \langle A^\dagger(0) A(-t) \rangle_0 \right] \\ &= 4(\tau\Delta)^2 \int_{-\infty}^{\infty} dt e^{2iVt} \left\langle \left\{ A^\dagger(t), A(0) \right\} \right\rangle_0. \end{aligned} \tag{6.19}$$

Here we have made the substitution $t \to -t$ in the second term in the second step.

It can be shown through scattering calculations that the shot noise across a quantum point contact obeys the relation [76, 80, 81]

$$S(0, V) = q I_{\mathrm{dc}}(V), \tag{6.20}$$

where q is the charge involved in tunneling, i.e. for Cooper pair tunneling, which involves two electrons, we have $q = 2$, while for tunneling of fractional quasiparticles [73] at filling fraction ν we have $q = \nu$. By measuring the signal-to-noise ratio represented by the Fano factor[1] $S(0, V)/I_{\mathrm{dc}} = q$, one is then experimentally able to determine the charge involved in tunneling, a fact which cannot be extracted from the current itself.

---

[1]Depending on one's definition of noise, the Fano factor may be defined as $S(0, V)/2I(V)$ instead.

6.2 Tunneling current in the DC regime

In this section we present the tunneling currents at filling factors $\nu = 1, 2$ and the Laughlin sequence $\nu = 1/(2n + 1)$ with $n \in \mathcal{N}$. These are calculated by applying Eq. (6.15), and the section will focus on discussing the physical interpretations of the results in different experimentally relevant limits, foregoing the inclusion of the full derivations.

Note that several of the results in this section were already discussed in Ref. [58]. We present the calculations in greater detail and include interactions, and the next section adds to these results with noise calculations not found in the literature.

6.2.1 Filling factor $\nu = 1$

For a single QH edge state at filling factor $\nu = 1$, we can write the QH Hamiltonian in position space as

$$H_{QH} = -iv_F \int dx\, \psi^\dagger(x)\partial_x \psi(x), \tag{6.21}$$

where v_F is the Fermi velocity of the QH edge. We can assume $v_F > 0$ (right moving particles) and $V > 0$ without loss of generality. Resolving the integral in Eq. (6.15) in this case yields [33]

$$\frac{I_{\mathrm{dc}}(V)}{I_0} = \frac{\xi T}{v_F}\sinh\left(\frac{V}{T}\right)\left[\mathcal{F}\left(0, \frac{V}{\pi T}\right) - \mathcal{F}\left(\frac{2\pi \xi T}{v_F}, \frac{V}{\pi T}\right)\right], \tag{6.22}$$

where we have normalized by the factor $I_0 = (\tau\Delta)^2/\pi v_F \xi$ and the terms in square brackets are given by the dimensionless integral

$$\mathcal{F}(a, b) = \int_{-\infty}^{+\infty} dz\, \frac{\cos(bz)}{\cosh(a) + \cosh(z)}. \tag{6.23}$$

This integral has an analytic solution in terms of hypergeometric functions, but since we are primarily interested in the scaling of the current in terms of voltage and temperature, we will simplify the expression by considering it in different limits. First we consider the limit of low temperature compared to the SC gap, $\xi T/v_F \ll 1$, as well as low voltage compared to the temperature scale, $V/T \ll 1$, to find the lowest order result in V and T. To expand the integrals we note that for $a \ll 1$, $\cosh(a) \simeq 1 + a^2/2$, letting us expand the integrand as

$$\mathcal{F}(0, b) - \mathcal{F}(a, b) \simeq \frac{a^2}{2}\int_{-\infty}^{\infty} dz\, \frac{\cos(bz)}{\left(1 + \cosh(z)\right)^2} = \frac{\pi}{3}\frac{a^2 b(1 + b^2)}{\sinh(\pi b)}, \tag{6.24}$$

while for $b \ll 1$ we can further expand

$$\mathcal{F}(0, b) - \mathcal{F}(a, b) \simeq \frac{a^2}{3}\left[1 + \left(1 - \frac{\pi^2}{6}\right)b^2\right]. \tag{6.25}$$

Applying this expansion we find the current

$$\frac{I_{\mathrm{dc}}(V)}{I_0} \simeq \frac{\xi T}{v_F}\frac{V}{T}\left\{\frac{1}{3}\left(\frac{2\pi \xi T}{v_F}\right)^2\left[1 + \left(1 - \frac{\pi^2}{6}\right)\left(\frac{V}{\pi T}\right)^2\right]\right\}, \tag{6.26}$$
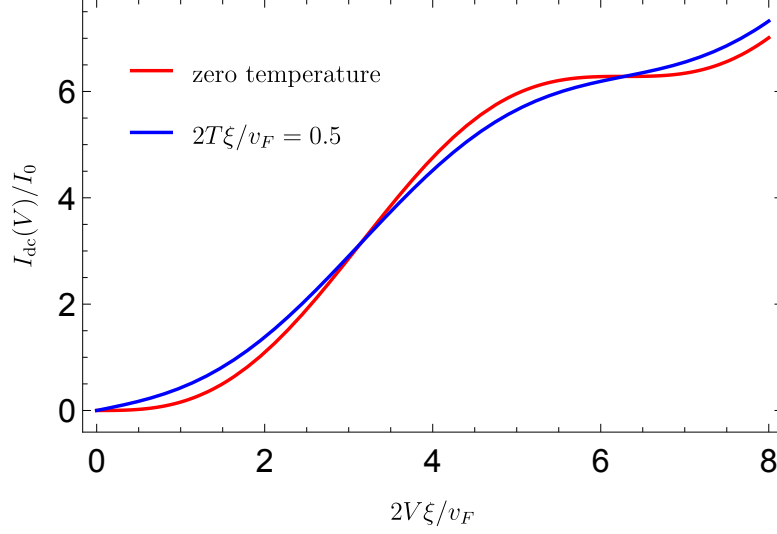
Figure 6.2: *The normalized tunneling current $I_{dc}(V)/I_0$ at filling factor $\nu = 1$ oscillates with the dimensionless bias $2V\xi/v_F$ around linear (Ohmic) behavior, with non-zero temperature damping out the oscillation (see Eqs. (6.22) and (6.28)).*

which to lowest order in V/T is

$$\frac{I_{dc}(V)}{I_0} \simeq \frac{4\pi^2}{3}\left(\frac{\xi T}{v_F}\right)^2 \frac{\xi V}{v_F}. \tag{6.27}$$

Resolving the integral Eq. (6.15) at $T = 0$ requires a slightly different strategy than at finite T to avoid dividing by zero, and in this case it is found that [33]

$$\frac{I_{dc}(V)}{I_0} = \frac{2\xi V}{v_F}\left[1 - \frac{\sin(2\xi V/v_F)}{2\xi V/v_F}\right], \tag{6.28}$$

which for small bias voltage $\xi V/v_F \ll 1$ can be approximated as

$$\frac{I_{dc}(V)}{I_0} \simeq \frac{4}{3}\left(\frac{\xi V}{v_F}\right)^3. \tag{6.29}$$

This limit can also be found by setting $T = 0$ in Eq. (6.26) which suppresses the linear dependence $I \propto V$, leaving the non-Ohmic $I \propto V^3$ behavior as the lowest non-vanishing order. The general results are plotted in Fig. 6.2, where it can be seen that the zero-temperature case oscillates around Ohmic behavior, with oscillations damped at higher temperatures.

The departure from Ohmic behavior at zero temperature means that the conductance $G = \frac{\partial I_{dc}}{\partial V}$ at $V \to 0$ goes from the finite T value

$$\frac{G(T)}{G_0} = 1 - \frac{2\pi\xi T/v_F}{\sinh(2\pi\xi T/v_F)}, \qquad G_0 = \frac{2(\tau\Delta)^2}{\pi v_F^2}, \tag{6.30}$$

to zero at zero temperature $G(T \to 0) = 0$. As discussed in Ref. [58], this behavior stems from the effect of the Pauli exclusion principle in a similar way to how the hole transmission probability P_h in Chapter 4 vanishes for vanishing V or I. Without an applied bias, the Cooper paired electrons would both tunnel into a single state, which is

94

not allowed. The time scale ξ/v_F can be understood as the time separation below which the tunneling events are suppressed, i.e. the second electron can tunnel after the first tunneling electron has been transported away from the point contact for a time $t \sim \xi/v_F$.

This Pauli blockade constitutes a strong experimental signature of pair-tunneling, and is also found for the extended surface treated in Chapter 3. We will hold off on calculating the noise, since it will be shown in the next section that the $\nu = 1$ filling factor is a special case of the $\nu = 2$ filling factor.

6.2.2 Filling factor $\nu = 2$

We now extend our discussion to filling factor $\nu = 2$, modeling a system where the QH edge hosts two edge states with parallel spin polarization, see Fig. 6.1. As discussed in Section 6.1.1, this system can be described within the same framework as for $\nu = 1$ by substituting the QH edge state electron operators in the tunneling Hamiltonian with

$$\psi \to \sqrt{p}\,\psi_1 + \sqrt{1-p}\,\psi_2. \tag{6.31}$$

where p is the probability of tunneling into state 1. For simplicity we can assume both edge states to have the same Fermi velocity – different velocities could be absorbed into a redefinition of p. Upon performing the substitution Eq. (6.31), the dc bias tunneling current at finite temperature is found to be [33]

$$\frac{I_{\mathrm{dc}}(V)}{I_0} = \frac{\xi T}{v_F} \sinh\left(\frac{V}{T}\right) \left[\mathcal{F}\left(0, \frac{V}{\pi T}\right) - \mathcal{N}(p, k\xi)\mathcal{F}\left(\frac{2\pi\xi T}{v_F}, \frac{V}{\pi T}\right)\right], \tag{6.32}$$

with $\mathcal{F}$ and I_0 defined as in Eq. (6.22). Shifting to filling factor $\nu = 2$ has introduced the interference factor

$$\mathcal{N}(p, k\xi) = 1 - 2p(1-p)[1 - \cos(k\xi)], \tag{6.33}$$

where $k = k_2 - k_1$ is the difference in edge state momenta. Without going into details of the derivation of Eq. (6.32), we can attempt an interpretation of $\mathcal{N}$ in terms of the amplitudes of the different correlators involved in calculating $\langle A^\dagger(t)A(0)\rangle$ for two edge states. These are four point correlators of the form

$$\left\langle \psi_a^\dagger(\xi, t)\psi_b^\dagger(0, t)\psi_c(0, 0)\psi_d(\xi, 0) \right\rangle, \tag{6.34}$$

where the indices a, b, c, d indicate either state 1 or state 2, with either all indices equal or each state index appearing twice. Since we know from Chapter 2 that an edge state is proportional to a plane wave along the interface $\psi_a(x, t) \propto e^{-ik_a x}$, we anticipate momentum differences coming out of the correlator when $a = c$ and $b = d$. In particular, the expectation value $\langle A^\dagger(t)A(0)\rangle$ will involve the two terms

$$\left\langle A^\dagger(t)A(0) \right\rangle = p(1-p) \left\langle \psi_1^\dagger(\xi, t)\psi_2^\dagger(0, t)\psi_1(0, 0)\psi_2(\xi, 0) \right\rangle$$
$$+ p(1-p) \left\langle \psi_2^\dagger(\xi, t)\psi_1^\dagger(0, t)\psi_2(0, 0)\psi_1(\xi, 0) \right\rangle + \dots \tag{6.35}$$

The former term involves the phase difference $e^{-i(k_2-k_1)\xi}$, while the latter involves the phase difference $e^{i(k_2-k_1)\xi}$. The correlators with $a = d$ and $b = c$ will carry no phase, but still contribute with an amplitude $p(1-p)$, while the remaining correlators with all

indices equal correspond to tunneling into one edge state only. We can then see that $\mathcal{N}$ corresponds to one minus the sum of amplitudes of cross-tunneling correlators

$$\mathcal{N} = 1 - 2p(1-p) - 2p(1-p)\left(e^{i(k_2-k_1)\xi} + e^{-i(k_2-k_1)\xi}\right)$$
$$= 1 - 2p(1-p)[1 - \cos(k\xi)]. \tag{6.36}$$

This simple argument is not meant as a derivation of the source of $\mathcal{N}$, but rather meant to facilitate some intuitive understanding of its appearance at filling $\nu = 2$.

As discussed in Chapter 2, the momentum of an edge state depends on the choice of gauge, however by taking the difference the gauge dependence cancels. Indeed, due to the inherent relationship between an edge state's momentum and position, the momentum difference becomes $k = Bl$ where B is the B-field strength and l is the spatial separation between the edge states. As expected, we recover the $\nu = 1$ current for $p = 0$ or $p = 1$ where only one edge state is involved in the tunneling, but interestingly it is also recovered for $\cos(k\xi) = 1$, due to destructive interference between the two tunneling events. This can be experimentally accessed by tuning the applied magnetic field to $B = 2\pi n/(\xi l)$ for an integer n.

The zero-temperature current is found to be [33]

$$\frac{I_{dc}(V)}{I_0} = \frac{2V\xi}{v_F}\left[1 - \mathcal{N}(p, k\xi)\frac{\sin(2V\xi/v_F)}{2V\xi/v_F}\right], \tag{6.37}$$

where we see that for $\xi V/v_F \ll 1$ we again have Ohmic behavior in the leading order,

$$\frac{I_{dc}(V)}{I_0} \simeq [1 - \mathcal{N}(p, k\xi)]\frac{2\xi V}{v_F} + \frac{4}{3}\mathcal{N}(p, k\xi)\left(\frac{\xi V}{v_F}\right)^3, \tag{6.38}$$

as long as $\mathcal{N}(p, k\xi) < 1$. Correspondingly, the zero bias conductance for finite temperature is

$$\frac{G(T)}{G_0} = 1 - \frac{2\pi\xi T\mathcal{N}(p, k\xi)}{v_F \sinh(2\pi\xi T/v_F)}, \tag{6.39}$$

with the zero temperature limit $G \propto 1 - \mathcal{N}(p, k\xi)$, which is no longer necessarily vanishing.

The recovery of Ohmic behavior is expected, since allowing the electrons to tunnel into different edge states allows the circumvention of the Pauli blockade. What is more interesting is that tuning the B-field across the values yielding $\cos(k\xi) = 1$ while staying at filling factor $\nu = 2$ should allow for the experimental observation of the Pauli blockade turning on and off. This result lets us interpret $\mathcal{N}$ as the amplitude of destructive interference between the tunneling modes.

The current in Eq. (6.32) is plotted in Fig. 6.3, where the Pauli blockade is recovered for $k\xi = 2\pi n$ with $n \in \mathcal{N}$, resulting in more pronounced oscillations along the V axis.

Interacting electrons

We now further generalize our model by including electron interactions both within an edge state and between edge states. In particular we will consider the model of a Coulomb potential suppressed on all but extremely short range compared to ξ by the surrounding material such that it is effectively a delta function in space [82–84]. As
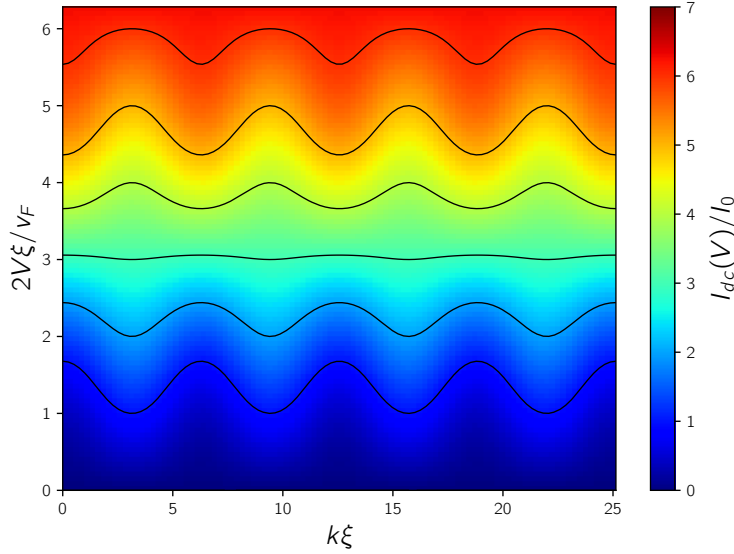
Figure 6.3: *At filling factor $\nu = 2$, we have oscillations of the normalized tunneling current both with the dimensionless bias $2V\xi/v_F$ as well as the interference factor argument $k\xi$. Here, the oscillations are shown at a finite temperature of $2\xi T/v_F = 0.5$, with tunneling probability $p = 0.5$, see Eq. (6.32). Black lines indicate integer values of the current ratio I_{dc}/I_0.*

discussed in Section 5.2, we can exploit the one-dimensional nature of the QH edge to include interactions of arbitrary strength in a low energy effective field theory [46,70]. We assume that tunneling is only allowed into one of the edge states, corresponding to $p = 1$ or $p = 0$. The excitations of the interacting electron system can be described as collective fluctuations of the charge density of the edge state with index $j = 1, 2$

$$\rho_j(x) = \frac{1}{2\pi}\partial_x\phi_j(x), \tag{6.40}$$

where $\phi_j(x)$ is a bosonic field operator with commutator

$$[\phi_i(x), \phi_j(y)] = i\pi\delta_{ij}\,\mathrm{sgn}(x - y). \tag{6.41}$$

In terms of this field, the free electron Hamiltonian for two edge states is as in Section 5.2

$$H_0 = \frac{v_F}{4\pi}\sum_{j=1,2}\int dx\Big[\partial_x\phi_j(x)\Big]^2, \tag{6.42}$$

where we recall the assumption that both edge states have the same velocity. We then introduce the screened Coulomb interaction between electron densities $U\delta(x - y)$, where $U > 0$ is the interaction strength. Defining the matrix

$$V_{ij}(x, y) = (U + 2\pi v_F\delta_{ij})\delta(x - y), \tag{6.43}$$

we can write up the total Hamiltonian

$$\begin{aligned} H_{\mathrm{QH}} &= \frac{1}{2}\sum_{ij=1,2}\int dx\int dy\rho_i(x)V_{ij}(x, y)\rho_j(y) \\ &= \frac{1}{8\pi^2}\sum_{ij=1,2}\int dx\int dy[\partial_x\phi_i(x)]V_{ij}(x, y)[\partial_y\phi_j(y)], \end{aligned} \tag{6.44}$$
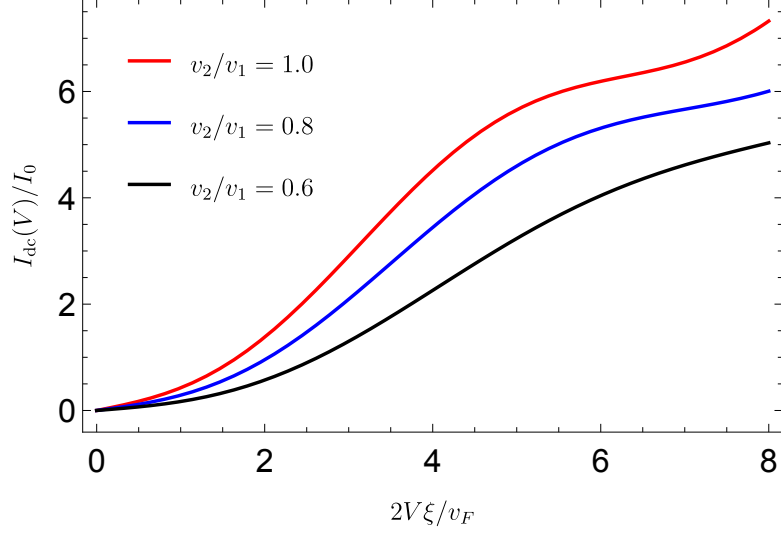
97

Figure 6.4: *The dc bias tunneling current for interacting electrons tunneling into a single edge, see Eq. (6.47). We have $\nu = 2$ and $2\xi T/v_F = 0.5$ and the interaction is parametrized by v_2/v_1, with $v_2/v_1 = 1$ being the non-interacting case. Stronger interactions (i.e. smaller v_2/v_1) mean decreased magnitude of the normalized tunneling current, as well as longer oscillation periods with the applied bias.*

which becomes H_0 for $U = 0$. This Hamiltonian is diagonalized by the unitary transformation

$$\phi_1 = \frac{1}{\sqrt{2}}(\chi_1 + \chi_2), \qquad \phi_2 = \frac{1}{\sqrt{2}}(\chi_1 - \chi_2) \tag{6.45}$$

which preserves bosonic commutation relations and yields the chiral bosonized Hamiltonian,

$$H_{\text{QH}} = \frac{1}{4\pi} \sum_{j=1,2} v_j \int dx \left[\partial_x \chi_j(x) \right]^2. \tag{6.46}$$

where j no longer represents the edge modes, but rather two effective bosonic modes with velocities $v_1 = U/\pi + v_F$ and $v_2 = v_F$.

Given this model of interacting electrons, the integral in Eq. (6.15) can be resolved to find [33]

$$\frac{I_{\text{dc}}(V)}{I_0'} = \frac{v_2}{v_1} \frac{2\xi T}{v_2} \sinh\left(\frac{V}{T}\right) \prod_{j=1,2} \left[\sinh\left(\frac{\pi \xi T}{v_j}\right)\right] \mathcal{J}\left(\frac{2\pi \xi T}{v_1}, \frac{2\pi \xi T}{v_2}, \frac{2V}{\pi T}\right), \tag{6.47}$$

where the normalization factor is now $I_0' = (\tau\Delta)^2/\pi\sqrt{v_1 v_2}\xi$ and we have the unitless integral

$$\mathcal{J}(a_1, a_2, b) = \int_{-\infty}^{\infty} dy \frac{\cos(by)}{\cosh^2(y) \prod_{i=1,2} \sqrt{\cosh(2y) + \cosh(a_i)}}. \tag{6.48}$$

Assuming low temperature $\xi T/v_2 \ll 1$, we can employ similar strategies as in Section 6.2.1 to find the zero bias conductance as

$$\frac{G(T)}{G_0'} \simeq \frac{2\pi^2}{3} \frac{(\xi T)^2}{v_1 v_2}, \qquad G_0' = \frac{2(\tau\Delta)^2}{\pi v_1 v_2}, \tag{6.49}$$

98

while for zero temperature and $V\xi/v_2 \ll 1$ we have $I_{\mathrm{dc}} \propto (2/3\pi)(V^3\xi^2)/(v_1v_2)^2$, meaning the zero bias conductance vanishes. In other words, the Pauli blockade persists in the presence of cross-channel interactions, making it a robust result for experimental investigation.

The behavior of Eq. (6.47) at finite temperature is shown in Fig. 6.4 for different interaction strengths, with $v_2/v_1 = 1$ corresponding to the non-interacting case. As can be seen, non-zero interactions reduce the tunneling current while increasing the oscillation period around Ohmic behavior.

Noise

We first consider the case of non-interacting electrons at filling factor $\nu = 2$ with tunneling into both edges, which reduces to the $\nu = 1$ case for $p = 0$ or $p = 1$. Applying Eq. (6.17) to this system yields the finite temperature noise

$$\frac{S_{\mathrm{dc}}(\omega, V)}{I_0} = \sum_{\sigma=\pm} \frac{\xi T}{v_F} \exp\left(\frac{\omega + 2\sigma V}{2T}\right)$$
$$\times \left[\mathcal{F}\left(0, \frac{\omega + 2\sigma V}{2\pi T}\right) - \mathcal{N}(p, k\xi)\mathcal{F}\left(\frac{2\pi\xi T}{v_F}, \frac{\omega + 2\sigma V}{2\pi T}\right)\right], \quad (6.50)$$

with the normalization factor I_0 defined after Eq. (6.22) and with the dimensionless integral $\mathcal{F}(a, b)$ defined in Eq. (6.23). The corresponding result at zero temperature is

$$\frac{S_{\mathrm{dc}}(\omega, V)}{I_0} = \sum_{\sigma=\pm} 2\theta\left(\frac{\xi(\omega + 2\sigma V)}{v_F}\right) \left\{ \frac{|\omega + 2\sigma V|\xi}{v_F} - \mathcal{N}(p, k\xi)\sin\left(\frac{|\omega + 2\sigma V|\xi}{v_F}\right)\right\},$$
$$(6.51)$$

where $\theta(x)$ is the Heaviside step function and the interference factor $\mathcal{N}(p, k\xi)$ is defined in Eq. (6.33). The noise at finite and zero temperature is shown in Fig. 6.5. At frequencies $\omega = \pm 2V$ the zero-temperature noise changes with a discontinuous derivative. For Cooper pair transport, these frequencies are known as Josephson frequencies, and the characteristic behavior at these frequencies is due to the difference in chemical potential [85]. Notably, in the case of tunneling between chiral Tomonaga-Luttinger liquids, the noise exhibits a singularity at these frequencies, which is absent in our system [85].

We can expand the zero-temperature noise for small frequencies $0 < \omega \ll 2V$

$$\frac{S_{\mathrm{dc}}(\omega, V)}{I_0} \simeq 2\left[\frac{2\xi V}{v_F} - \mathcal{N}(p, k\xi)\sin\left(\frac{2\xi V}{v_F}\right)\right] + 2\left[1 - \mathcal{N}(p, k\xi)\cos\left(\frac{2\xi V}{v_F}\right)\right]\left(\frac{\xi\omega}{v_F}\right),$$
$$(6.52)$$

where we see that the frequency dependence appears linearly in a sub-leading term, while for large frequencies $\omega \gg 2V > 0$ we find

$$\frac{S_{\mathrm{dc}}(\omega, V)}{I_0} \simeq \frac{4\xi\omega}{v_F}, \quad (6.53)$$

i.e. that the linear frequency dependency leads. By measuring the shot noise we can also observe the Pauli blockade behavior we found for the conductance measurements,

$$G_0^{-1}\frac{\partial S_{\mathrm{dc}}(0, V)}{\partial V}\bigg|_{V\to 0} = 2[1 - \mathcal{N}(p, k\xi)], \quad (6.54)$$
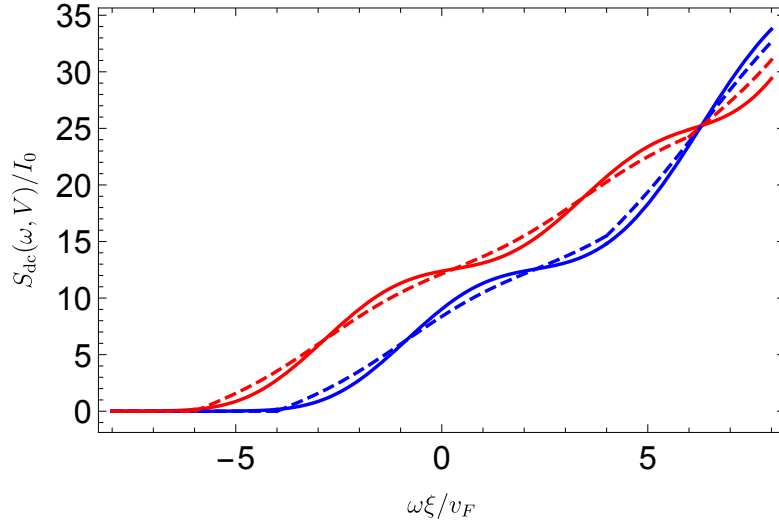
Figure 6.5: *The normalized finite frequency noise at dc bias $S_{dc}(\omega, V)/I_0$ with filling factor $\nu = 2$, plotted as a function of the dimensionless frequency $\omega\xi/v_F$ at applied voltages $2V\xi/v_F = 4$ (blue lines) and $2V\xi/v_F = 6$ (red lines). The solid lines correspond to finite temperature $2T\xi/v_F = 0.5$, see Eq. (6.50), and the dashed lines correspond to zero temperature, see Eq. (6.51). We have $p = 0.5$ and $k\xi = 2\pi/3$.*

where G_0 is defined in Eq. (6.30). The signature oscillations of the interference factor can thus be found in shot noise measurements as well. At low, non-zero temperatures $\xi T/v_F \ll 1$ we find a sub-leading correction to Eq. (6.54) of $(4/3)\mathcal{N}(p, k\xi)(\pi\xi T/v_F)^2$, and so the temperature independence of the derivative of the shot noise is only found to leading order.

Using Eqs. (6.32) and (6.50) and the fact that $\mathcal{F}(a, -b) = \mathcal{F}(a, b)$, we can directly evaluate the fraction of shot noise and current at finite temperature

$$\frac{S_{dc}(0, V)}{I_{dc}(V)} = 2 \coth\left(\frac{V}{T}\right), \tag{6.55}$$

which shows that the tunneling current exhibits the typical Poissonian shot noise form [76]. In the limit of zero temperature, we recover the Fano factor $S_{dc}(0, V)/I_{dc}(V) = 2$, which is consistent with the tunneling of Cooper pairs. Explicitly considering filling factor $\nu = 1$, i.e. setting $p = 1$ or $p = 0$, we have that at low temperature $\xi T/v_F \ll 1$ and bias voltage $V/T \ll 1$ we find

$$\frac{S_{dc}(0, V)}{I_0} \simeq \frac{8\xi V}{3v_F}\left(\frac{\pi\xi T}{v_F}\right)^2. \tag{6.56}$$

Including electron-electron interactions and assuming tunneling into only one channel, we find the noise

$$\frac{S_{dc}(\omega, V)}{I_{dc}(V)} = \sum_{\sigma=\pm} \frac{v_2}{v_1} \frac{2\xi T}{v_2} \exp\left(\frac{\omega + 2\sigma V}{2T}\right) \prod_{i=1,2} \sinh\left(\frac{\pi\xi T}{v_i}\right) \mathcal{J}\left(\frac{2\pi\xi T}{v_1}, \frac{2\pi\xi T}{v_2}, \frac{\omega + 2\sigma V}{\pi T}\right). \tag{6.57}$$

The Fano factor for this noise is unchanged from the result in Eq. (6.55), which is expected since interactions should have no effect on the tunneling charge. The zero temperature

100

shot noise for $V\xi/v_i \ll 1$ with $i = 1, 2$ becomes

$$\frac{S_{\text{dc}}(0, V)}{I_0} \simeq \frac{8v_2^2}{3v_1^2}\frac{V^3\xi^3}{v_2^3},$$ (6.58)

where again the Pauli blockade is recovered as $\partial S_{\text{dc}}(0, V)\partial V = 0$ at $V \to 0$.

6.2.3 Filling factor $\nu = 1/(2n + 1)$

Finally we consider the fractional filling factors belonging to the Laughlin sequence $\nu = 1/(2n + 1)$ with $n \in \mathcal{N}$. Once again we can construct an effective field theory in terms of bosonic fields, this time considering a single channel of free bosonic fields $\phi(x)$ propagating with velocity v. This field relates to the electron operator through $\psi(x) \propto e^{i\phi(x)/\nu}$ as discussed in Chapter 5. Repeating the steps of the previous sections, the tunneling current can be shown to be [33]

$$\frac{I_{\text{dc}}(V)}{I_0''} = 2^{1/\nu}\frac{\xi T}{v}\left(\frac{aT}{2v}\right)^{2/\nu-2}\sinh^{2/\nu}\left(\frac{\pi\xi T}{v}\right)\sinh\left(\frac{V}{T}\right)\mathcal{Q}\left(\frac{2\pi\xi T}{v}, \frac{2V}{\pi T}\right),$$ (6.59)

where a is an ultraviolet (short distance) cutoff and we have the normalization factor $I_0'' = (\tau\Delta)^2/\pi v\xi$. We have also introduced the dimensionless integral

$$\mathcal{Q}(a, b) = \int_{-\infty}^{\infty} dy\frac{\cos(by)}{\cosh^{-2/\nu}(2y)[\cosh(2y) + \cosh(a)]^{1/\nu}}.$$ (6.60)

For low temperatures $\xi T/v \ll 1$, the zero bias conductance becomes

$$\frac{G(T)}{G_0''} \simeq \frac{\sqrt{\pi}}{2}\frac{\Gamma(2/\nu)}{\Gamma(1/2 + 2/\nu)}\left(\frac{rT}{2v}\right)^{2/\nu-2}\left(\frac{\pi\xi T}{v}\right)^{2/\nu}, \qquad G_0'' = \frac{2(\tau\Delta)^2}{\pi v^2}$$ (6.61)

where $\Gamma(x)$ is the gamma function. At zero temperature and small bias $\xi V/v \ll 1$, the current becomes

$$\frac{I_{\text{dc}}}{I_0''} \simeq \frac{2\pi^2\xi v}{r^2}\left(\frac{2r\xi}{\pi v^2}\right)^{2/\nu}\frac{V^{4/\nu-2}}{\Gamma(4/\nu)}.$$ (6.62)

This means that the zero bias conductance vanishes, and we once again recover the Pauli blockade.

There are several interesting things to note here, as pointed out in Ref. [58]. First of all, the powers of V and T involved are very large: the $\nu = 1/3$ state leads to a conductance scaling of $G(T) \sim T^{10}$ and a zero temperature tunneling current scaling of $I_{\text{dc}}(V) \sim V^{10}$. Furthermore, despite the fact that both the SC state and the fractional QH edge state can be accurately described as bosonic states, the Pauli blockade persists due to the fundamental electronic nature of the tunneling.

Noise

Resolving Eq. (6.17) in this context, the noise at fractional filling factors is found to be [33]

$$\frac{S_{\text{dc}}(\omega, V)}{I_0''} = \sum_{\sigma=\pm}2^{1/\nu}\frac{\xi T}{v}\left(\frac{rT}{2v}\right)^{2/\nu-2}\sinh^{2/\nu}\left(\frac{\pi\xi T}{v}\right)$$
$$\times \exp\left(\frac{\omega + 2\sigma V}{2T}\right)\mathcal{Q}\left(\frac{2\pi\xi T}{v}, \frac{\omega + 2\sigma V}{\pi T}\right).$$ (6.63)

At zero temperature and frequency, assuming a small bias $V\xi/v \ll 1$ yields the approximation

$$\frac{S_{\mathrm{dc}}(0,V)}{I_0''} \simeq \frac{4\pi^2}{\Gamma(4/\nu)} \frac{v\xi}{r^2 V} \left(\frac{2r\xi V^2}{\pi v^2}\right)^{2/\nu},\tag{6.64}$$

with vanishing shot noise derivative $\partial S_{\mathrm{dc}}(0,V)/\partial V$ at $V \to 0$. Interestingly, the Fano factor Eq. (6.55) is unchanged despite the fractionalization of the edge state charges, indicating that the tunneling current consists of Cooper pairs no matter the filling factor of the edge state.

6.3 Tunneling current and finite frequency noise in the AC regime

Finally, we place our results so far into the context of a quantum point contact with an applied ac bias, i.e. a time-dependent voltage $\tilde{V}(t)$. We assume a periodic bias of the form

$$\tilde{V}(t) = V + V_1 \cos(\Omega t),\tag{6.65}$$

with a low driving frequency Ω allowing adiabatic treatment and constant voltages V, V_1. We will not assume any particular filling factor, but rather express our results in terms of the I_{dc} and S_{dc} results from the previous sections.

The time-dependent part averaged over one period $\mathcal{T} = 2\pi/\Omega$ gives zero, and the average tunneling current is given by [79]

$$I = \frac{2}{\mathcal{T}} \int_0^{\mathcal{T}} dt \int_{-\infty}^{t} dt' \mathrm{Re}\left\{e^{i\int_{t'}^{t} dt'' \tilde{V}(t'')} \langle[\hat{A}^\dagger(t), \hat{A}(t')]\rangle\right\}.\tag{6.66}$$

Applying the correlators calculated previously and using an expansion in terms of Bessel functions of the first kind J_n for integer n,

$$e^{i\lambda \sin\varphi} = \sum_{n=-\infty}^{\infty} J_n(\lambda)e^{in\varphi},\tag{6.67}$$

we find

$$I = \sum_{n=-\infty}^{+\infty} J_n^2(2V_1/\Omega)\, I_{\mathrm{dc}}(V + n\Omega/2),\tag{6.68}$$

where $I_{\mathrm{dc}}(V + n\Omega/2)$ is the relevant tunneling current calculated in the previous sections. At $\Omega \to 0$ or $V_1 \to 0$ the bias is constant, and we can use the Bessel function sum rule [86]

$$\sum_{n=-\infty}^{\infty} J_n^2(\lambda) = 1\tag{6.69}$$

for any λ, meaning we recover the dc bias results. To treat the noise under an ac-bias [79] we consider the time domain correlator $S(t,t') = \langle \delta J(t)\delta J(t')\rangle$ in terms of the "center of mass" variables

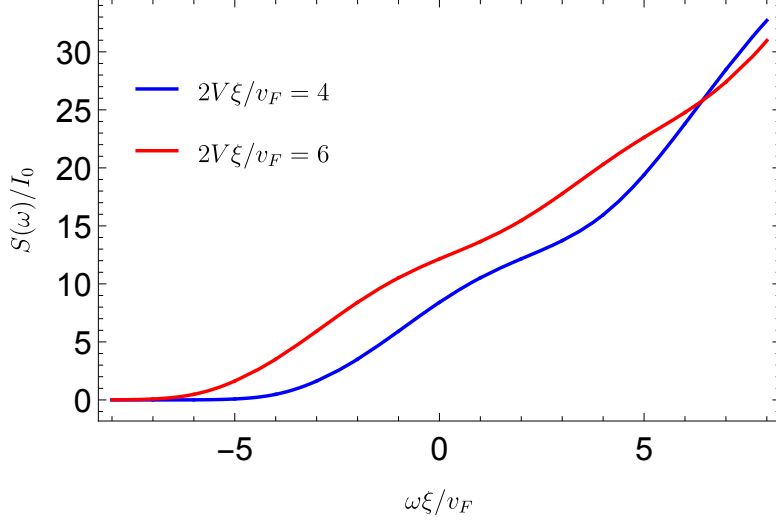$$\tau = \frac{t+t'}{2}, \qquad \tau' = t - t',\tag{6.70}$$

Figure 6.6: *The normalized finite frequency noise of the tunneling current in presence of adiabatic ac bias, $\tilde{V}(t) = V + V_1 \cos(\Omega t)$, at zero temperature for different $2V\xi/v_F$, see Eq. (6.72). The plot shows the case of $S_{dc}(\omega, V)$ at filling factor $\nu = 1$, i.e. with $\mathcal{N} = 1$. We set $2V_1\xi/v_F = 2$ and $\Omega\xi/v_F = 1$.*

yielding the one-period average noise

$$S(\omega) = \frac{1}{\mathcal{T}} \int_0^{\mathcal{T}} d\tau \int_{-\infty}^{\infty} d\tau' S(\tau + \tau'/2, \tau - \tau'/2) e^{i\omega\tau'}. \tag{6.71}$$

Applying the same methods as when calculating the ac-bias current, as well as the identity $J_{-n}^2(\lambda) = J_n^2(\lambda)$ we arrive at the result

$$S(\omega) = \sum_{n=-\infty}^{\infty} J_n^2(2V_1/\Omega) S_{\text{dc}}(\omega, V + n\Omega/2), \tag{6.72}$$

where $S_{\text{dc}}(\omega, V + n\Omega/2)$ is the relevant dc-bias noise as calculated in previous sections. At filling factor $\nu = 1$, the ac-bias noise $S(\omega)$ is shown in Fig. 6.6. The result is similar to the case of dc bias, and again we see no singularities in the noise.

An analogous relation to Eq. (6.72) was experimentally tested for quasiparticle tunneling between fractional QH edge states Ref. [87], and found to hold for electron current, heat current and shot noise in a quantum point contacted fractional QH edge under AC bias. According to Eq. (6.72), the relation holds for the tunneling current and the finite frequency noise of a tunneling contact to a SC, indicating that the relation might be universal for systems point contacted with a QH edge, and that the relation may also hold for finite frequency noise across a point contact between QH edges. Further work to find if Eq. (6.72) holds for tunneling between fractional QH edges would allow probing of such a system, and the anyonic quasiparticles it is predicted to host, beyond the regime of shot noise, but that is beyond the scope of this thesis.

6.4 Summary

We consider an effective model of Cooper pairs performing local tunneling from across a SC-QH edge quantum point contact as presented in Ref. [58], which lets us predict

tunneling current and noise for applied ac and dc biases across the point contact. Only recently has a similar system been realized experimentally, motivated by which we expand on the known theoretical predictions of such a system by considering interactions and noise.

The main experimental signature is the Pauli blockade, which causes vanishing zero-bias conductance in the zero temperature limit. This blockade is found both for interacting and non-interacting electrons, as well as for a single integer QH edge state at $\nu = 1$ and for a fractional QH edge state in the Laughlin sequence $\nu = 1/(2n + 1)$. For two integer QH edge states, we find a zero bias conductance $G \propto 1 - \mathcal{N}$, with $0 \leq \mathcal{N} \leq 1$ measuring the amplitude of destructive interference between tunneling modes which involve both edge states. We predict a recovery of the Pauli blockade for an applied magnetic field $B = 2\pi n/(\xi l)$, in which case $\mathcal{N} = 1$.

The finite frequency noise is predicted to have discontinuous derivatives in its frequency dependence at the Josephson frequencies $\omega = \pm 2V$, where singularities have been predicted in the case of tunneling between chiral Tomonaga Luttinger liquids. The Pauli blockade can also be seen in the shot noise, whose derivative vanishes with the conductance.

At small bias and low but finite temperatures, tunneling involving the fractional QH edge involves remarkable scaling of the conductance $G \propto T^{4/\nu-2}$, while at zero temperature we find similar scaling of the current $I_{\mathrm{dc}} \propto V^{4/\nu-2}$ and the noise $S_{\mathrm{dc}} \propto V^{4/\nu-1}$.

Investigating the point contact under an ac bias, we find that current and noise are expressed as sums over their dc bias counterparts, weighted by squared Bessel functions. This result is analogous to an experimental result for tunneling between point contacted fractional QH systems, indicating that finite frequency noise would show the same behavior in that system.

CHAPTER 7

Conclusion

In this thesis we have developed a model of a superconductor (SC) tunnel-coupled to an integer or fractional quantum Hall (QH) edge. By integrating out the superconductor, we have arrived at an effective QH edge Hamiltonian with induced pairing, and derived an analytical prediction of the induced pairing amplitude in terms of externally determined parameters of the separate systems. We have derived the effects of the induced pairing on transport in a typical experimental setup where a segment of the edge of a Hall bar is proximitized. This includes an analytical expression of the probability that an electron is transmitted as a hole when passing the proximitized segment, as well as an analytical expression of the effect of this hole transmission on the resistance measured downstream of the proximitized segment. We have predicted the negative downstream resistance found in experiments in terms of applied voltage and current, as well as its dependence on Fermi energy, induced pairing and interface length. The analytical descriptions of pairing amplitude, hole transmission probability and downstream resistance constitute a central contribution to the literature, advancing the qualitative understanding of the interplay of physical effects in this composite system.

This model has been extended to the fractional QH edge, where we predict that pairing is induced despite the effective fractionalization of the electronic edge states. Finally, applying an alternative, phenomenological model to the problem of a quantum point contact between a SC and an integer or fractional QH edge, we have predicted a number of experimental signatures of the induced superconductivity. The most robust of these is the Pauli blockade, which causes vanishing zero temperature conductance and shot noise, and persists in the presence of interactions and fractionalization. We predict that this blockade can be continuously tuned across in the case of filling factor $\nu = 2$ by inducing constructive interference through the externally applied magnetic field.

Taking into account the presence of the strong magnetic field needed to induce the QH phase, we have found that the Meissner effect, which leads to a supercurrent at the SC surface, has a surprisingly profound effect on the induced superconductivity. In particular, the resonance condition that the QH edge fermi momentum matches the supercurrent momentum $q_F = k_s$, corresponding to the QH system Fermi energy matching the cyclotron frequency $E_F = \omega_c$, plays a key role in our predictions:

- it marks the topological phase transition where the induced p-wave pairing crosses

between the weak and strong pairing phases.

- it marks the point of maximum hole transmission amplitude, where perfect hole conversion is predicted even for a weak induced pairing amplitude,

- in the competition between fractionalization and pairing in the proximitized fractional QH edge, it marks the point where pairing is most significant.

Predicting the key role of the Meissner effect is another central contribution of the thesis. The resonance condition is clearly linked to experimentally tunable parameters, making it both a critical test of the applicability of the presented theory, and an indicator that accounting for the Meissner could be an important step on the way to ever-improving fabrication of SC-QH systems and ultimately the encoding of quantum information in anyonic zero modes.

Outlook

Considering the interesting physics contained in the different experimental geometries presented in Chapter 4, it would be very interesting to extend the transport calculations to predict the behavior of experimental signatures in those geometries. Since the trench and finger setups involve the coupling of counter-propagating edge states, these states can couple directly into the SC bulk states with zero center-of-mass momentum, and it would be interesting to see the impact of the Meissner effect in this case.

Naturally, a complete transport calculation for the fractional QH edge is of great interest, in particular to predict if there are qualitative differences between the integer and fractional QH cases. Furthermore, considering higher order tunneling terms in the model would allow for the investigation of how the tunneling case and the transparent case converge in the semi-transparent case. Another approach to model the semi-transparent case would be to generalize the surface current to include a wide range of momenta k_s, modeling induced surface currents from the evanescent penetration of QH edge states into the superconductor.

A

The renormalized Numerov method

This appendix is based on a more in-depth explanation in Ref. [88]. We reintroduce $\hbar \neq 1$ for clarity. The Numerov method integrates one-dimensional second order differential equations with no first order derivative. Assume that such an equation is of the form

$$\left[\frac{\partial^2}{\partial x^2} + Q(x)\right]\psi(x) = 0, \tag{A.1}$$

which is the Schrödinger equation when

$$Q(x) = \frac{2m}{\hbar^2}(E - V(x)). \tag{A.2}$$

We discretize space into N small intervals of length a starting at a point x_0, continuing in points $x_n = x_0 + na$ with $n \in \mathbb{N}$ and ending at a point x_N. The discretized wave function is then $\psi_n = \psi(x_n)$, and $Q_n = Q(x_n)$. The Numerov formula, which is derived through a Taylor expansion in a, says that

$$\left(1 + \frac{a^2}{12}Q_{n+1}\right)\psi_{n+1} + \left(1 + \frac{a^2}{12}Q_{n-1}\right)\psi_{n-1} - \left(2 - \frac{5a^2}{6}Q_n\right)\psi_n + \mathcal{O}(a^6) = 0 \tag{A.3}$$

where Q_n is known for all n. For increased numerical stability we introduce the ratio

$$R_n = \frac{\psi_{n+1}}{\psi_n} \tag{A.4}$$

which is usually on order one. If we ignore terms of order a^6 and higher, we find

$$R_n = \left(1 + \frac{a^2}{12}Q_{n+1}\right)^{-1}\left[\left(2 - \frac{5a^2}{6}Q_n\right) - \left(1 + \frac{a^2}{12}Q_{n-1}\right)R_{n-1}^{-1}\right]. \tag{A.5}$$

Given $R_0 = \psi_1/\psi_0$, we can use this formula to iteratively construct the wave function forwards from x_0. We can also construct the wave function backwards from x_N by defining

$$\tilde{R}_n = \frac{\psi_{n-1}}{\psi_n} \tag{A.6}$$

and use the formula

$$\tilde{R}_n = \left(1 + \frac{a^2}{12}Q_{n-1}\right)^{-1}\left[\left(2 - \frac{5a^2}{6}Q_n\right) - \left(1 + \frac{a^2}{12}Q_{n+1}\right)R_{n+1}^{-1}\right]. \tag{A.7}$$

The numerically optimal strategy is to choose a point x_c between x_0 and x_N. The wave function is then iterated from left and right up to x_c. At this point, the matching function

$$G(E) = \left(\frac{\psi(x_N + a)}{\psi(x_N)}\right)_{\text{right}} - \left(\frac{\psi(x_N + a)}{\psi(x_N)}\right)_{\text{left}} \tag{A.8}$$

is evaluated. G is zero if and only if E is an eigenvalue of the Hamiltonian $\hat{H}$ corresponding to $Q(x, E)$. While the choice of x_c is arbitrary, it can be advantageous to use the first extremum of the wave function as evaluated from x_N when the more complex behaviour occurs in x_0.

The task is then to choose x_0 and x_N as points with well known wave function behaviour (and thus $R_0, \tilde{R}_N$). Then a root of $G(E)$ can be found through optimization in E, with the resulting energy being an eigenvalue of the Hamiltonian. The wave function can then be reconstructed from the boundary conditions and the ratios R and $\tilde{R}$.

B

Commutators

We have the general operator identities

$$[A, B] = 2AB - \{A, B\} = \{A, B\} - 2BA, \tag{B.1}$$
$$[AB, C] = A[B, C] + [A, C]B. \tag{B.2}$$

For fermionic operators ψ we generally have [50]

$$\{\psi_m, \psi_n\} = \{\psi_m^\dagger, \psi_n^\dagger\} = 0, \tag{B.3}$$
$$\{\psi_m, \psi_n^\dagger\} = \delta_{m,n}, \tag{B.4}$$
$$[\psi_m, \psi_n] = 2\psi_m\psi_n, \tag{B.5}$$
$$[\psi_m, \psi_n^\dagger] = 2\psi_m\psi_n - \delta_{m,n}. \tag{B.6}$$

These identities will be applied in the following proofs.

B.1   Density-density commutator

The commutator of two different density operators at two different points is

$$\left[\psi_m^\dagger(x)\psi_m(x), \psi_n^\dagger(y)\psi_n(y)\right] = \psi_m^\dagger(x)\psi_m(x)\psi_n^\dagger(y)\psi_n(y) - \psi_n^\dagger(y)\psi_n(y)\psi_m^\dagger(x)\psi_m(x). \tag{B.7}$$

We can apply Eqs. (B.3) and (B.4) to re-arrange the fields such that

$$\begin{aligned}
&\left[\psi_m^\dagger(x)\psi_m(x), \psi_n^\dagger(y)\psi_n(y)\right] \\
&= \psi_m^\dagger(x)\psi_m(x)\psi_n^\dagger(y)\psi_n(y) - \psi_n^\dagger(y)\Big(\delta_{m,n}\delta(x-y) - \psi_m^\dagger(x)\psi_n(y)\Big)\psi_m(x) \\
&= \psi_m^\dagger(x)\psi_m(x)\psi_n^\dagger(y)\psi_n(y) \\
&\qquad - \psi_n^\dagger(y)\delta_{m,n}\delta(x-y)\psi_m(x) + \psi_n^\dagger(y)\psi_m^\dagger(x)\psi_n(y)\psi_m(x) \\
&= \psi_m^\dagger(x)\psi_m(x)\psi_n^\dagger(y)\psi_n(y) \\
&\qquad - \psi_n^\dagger(y)\delta_{m,n}\delta(x-y)\psi_m(x) + \psi_m^\dagger(x)\psi_n^\dagger(y)\psi_m(x)\psi_n(y) \\
&= \psi_m^\dagger(x)\psi_m(x)\psi_n^\dagger(y)\psi_n(y) \\
&\qquad - \psi_n^\dagger(y)\delta_{m,n}\delta(x-y)\psi_m(x) + \psi_m^\dagger(x)\Big(\delta_{m,n}\delta(x-y) - \psi_m(x)\psi_n^\dagger(y)\Big)\psi_n(y). \tag{B.8}
\end{aligned}$$

Writing out the parenthesis we see that the first and last term cancel,

$$\left[\psi_m^\dagger(x)\psi_m(x),\psi_n^\dagger(y)\psi_n(y)\right]$$
$$= \cancel{\psi_m^\dagger(x)\psi_m(x)\psi_n^\dagger(y)\psi_n(y)}$$
$$- \psi_n^\dagger(y)\delta_{m,n}\delta(x-y)\psi_m(x) + \psi_m^\dagger(x)\delta_{m,n}\delta(x-y)\psi_n(y) - \cancel{\psi_m^\dagger(x)\psi_m(x)\psi_n^\dagger(y)\psi_n(y)}. \tag{B.9}$$

The remaining terms are zero when $m \neq n$ or $x \neq y$, while for $m = n$ and $x = y$ they cancel,

$$\left[\psi_m^\dagger(x)\psi_m(x),\psi_n^\dagger(y)\psi_n(y)\right] = -\psi_n^\dagger(y)\delta_{m,n}\delta(x-y)\psi_m(x) + \psi_m^\dagger(x)\delta_{m,n}\delta(x-y)\psi_n(y)$$
$$= 0. \tag{B.10}$$

B.2   Current operator

In the derivation of a current operator, the commutator

$$[\psi_r^\dagger(y)\partial_y\psi_s(y), \psi_m^\dagger(x)\psi_m(x)], \tag{B.11}$$

must be evaluated. Applying Eq. (B.2) we have

$$[\psi_r^\dagger(y)\partial_y\psi_s(y), \psi_m^\dagger(x)\psi_m(x)]$$
$$= \psi_r^\dagger(y)[\partial_y\psi_s(y), \psi_m^\dagger(x)\psi_m(x)] + [\psi_r^\dagger(y), \psi_m^\dagger(x)\psi_m(x)]\partial_y\psi_s(y). \tag{B.12}$$

In the first term we can move out the derivative to find

$$[\psi_r^\dagger(y)\partial_y\psi_s(y), \psi_m^\dagger(x)\psi_m(x)]$$
$$= \psi_r^\dagger(y)\partial_y[\psi_s(y), \psi_m^\dagger(x)\psi_m(x)] + [\psi_r^\dagger(y), \psi_m^\dagger(x)\psi_m(x)]\partial_y\psi_s(y). \tag{B.13}$$

Applying Eq. (B.2) we have

$$[\psi_s(y), \psi_m^\dagger(x)\psi_m(x)] = -[\psi_m^\dagger(x), \psi_s(y)]\psi_m(x) + \psi_m^\dagger(x)[\psi_s(y), \psi_m(x)]$$
$$= -\left(2\psi_m^\dagger(x)\psi_s(y) - \{\psi_m^\dagger(x), \psi_s(y)\}\right)\psi_m(x) + \psi_m^\dagger(x)\left(2\psi_s(y)\psi_m(x) - \cancel{\{\psi_s(y),\psi_m(x)\}}\right)$$
$$= -2\psi_m^\dagger(x)\psi_s(y)\psi_m(x) + 2\psi_m^\dagger(x)\psi_s(y)\psi_m(x) + \delta_{m,s}\delta(y-x)\psi_m(x)$$
$$= \delta_{m,s}\delta(y-x)\psi_m(x), \tag{B.14}$$

and

$$[\psi_r^\dagger(y), \psi_m^\dagger(x)\psi_m(x)] = [\psi_r^\dagger(y), \psi_m^\dagger(x)]\psi_m(x) + \psi_m^\dagger(x)[\psi_r^\dagger(y), \psi_m(x)]$$
$$= \left(2\psi_r^\dagger(y)\psi_m^\dagger(x) - \cancel{\{\psi_r^\dagger(y),\psi_m^\dagger(x)\}}\right)\psi_m(x) + \psi_m^\dagger(x)\left(2\psi_r^\dagger(y)\psi_m(x) - \delta_{m,r}\delta(x-y)\right)$$
$$= 2\psi_r^\dagger(y)\psi_m^\dagger(x)\psi_m(x) + 2\psi_m^\dagger(x)\psi_r^\dagger(y)\psi_m(x) - \psi_m^\dagger(x)\delta_{m,r}\delta(y-x)$$
$$= 2\psi_r^\dagger(y)\psi_m^\dagger(x)\psi_m(x) - 2\psi_r^\dagger(y)\psi_m^\dagger(x)\psi_m(x) - \psi_m^\dagger(x)\delta_{m,r}\delta(y-x)$$
$$= -\delta_{m,r}\delta(y-x)\psi_m^\dagger(x), \tag{B.15}$$

Putting these results together we have

$$[\psi_r^\dagger(y)\partial_y\psi_s(y), \psi_m^\dagger(x)\psi_m(x)]$$
$$= \delta_{m,s}\psi_r^\dagger(y)\partial_y\left(\delta(y-x)\psi_m(x)\right) - \delta_{m,r}\delta(y-x)\psi_m^\dagger(x)\partial_y\psi_s(y). \tag{B.16}$$

110

Exponent expansion for bosonic pairing

We will do the approximations in opposite order and show that we find the same result. We start from the $\Delta \sim \delta'$ approximation in Eq. (5.38)

$$
\begin{aligned}
H_p &= \frac{q_0 F^2}{4\pi L} \int_{-L/2}^{L/2} dX \, e^{2i(k_s - \delta q_F)X} \int_{-L}^{L} dr \, \Delta_I^*(r) e^{-i\Phi(X+r/2)/\sqrt{\nu}} e^{-i\Phi(X-r/2)/\sqrt{\nu}} + \text{h. c.} \\
&= -\frac{q_0 \Delta_p F^2}{4\pi} \int_{-L/2}^{L/2} dX \, e^{2i(k_s - \delta q_F)X} \int_{-L}^{L} dr \, \delta'(r) e^{-i\Phi(X+r/2)/\sqrt{\nu}} e^{-i\Phi(X-r/2)/\sqrt{\nu}} + \text{h. c.}
\end{aligned}
$$

$$(\text{C.1})$$

Using Eq. (5.52) we expand the exponentials to find

$$
\begin{aligned}
\int_{-L}^{L} dr \, \delta'(r) e^{-i\Phi(X+r/2)/\sqrt{\nu}} e^{-i\Phi(X-r/2)/\sqrt{\nu}} &= -\frac{\partial}{\partial r} \left(e^{-i\Phi(X+r/2)/\sqrt{\nu}} e^{-i\Phi(X-r/2)/\sqrt{\nu}} \right)_{r=0} \\
&= -\frac{\partial}{\partial r} \left(e^{-\frac{2i}{\sqrt{\nu}}\Phi(X)} e^{\frac{i}{\nu} r q_0} \right)_{r=0}
\end{aligned}
$$

$$(\text{C.2})$$

We evaluate the derivative to find the expected pairing term

$$
H_p = \frac{i\Delta_p q_0 F^2}{4\pi\sqrt{\nu}} \int_{-L/2}^{L/2} dX \, e^{2i(k_s - \delta q_F)X} e^{-2i\Phi(X)/\sqrt{\nu}} \left[\frac{q_0}{\sqrt{\nu}} \right] + \text{h. c.} \qquad (\text{C.3})
$$

Evaluating $\partial_x e^{i\Phi(x)}$

We wish to derive the result of taking the derivative

$$\partial_x e^{i\Phi(x)}. \tag{D.1}$$

Naively, one might take

$$\partial_x e^{i\Phi(x)} \stackrel{?}{=} i\partial_x \left(\Phi(x)\right) e^{i\Phi(x)}, \tag{D.2}$$

but that assumes a specific ordering of operators not present in the original expression. Let us instead derive the result by replacing the exponential with its series representation,

$$\partial_x e^{i\Phi(x)} \stackrel{\text{def}}{=} \sum_{n=1}^{\infty} \frac{i^n}{n!} \left(\partial_x \Phi^n(x)\right). \tag{D.3}$$

The constant term evaluates to zero, and is skipped. Of course, taking the derivative inside the sum is simple,

$$\partial_x \Phi^n(x) = \Phi^{n-1}(x)\left(\partial_x \Phi(x)\right) + \Phi^{n-2}(x)\left(\partial_x \Phi(x)\right)\Phi(x) + \Phi^{n-3}(x)\left(\partial_x \Phi(x)\right)\Phi^2(x) + \dots$$
$$= \sum_{m=1}^{n} \Phi^{n-m}(x)\left(\partial_x \Phi(x)\right)\Phi^{m-1}(x), \tag{D.4}$$

and thus

$$\partial_x e^{i\Phi(x)} = \sum_{n=1}^{\infty} \frac{i^n}{n!} \sum_{m=1}^{n} \Phi^{n-m}(x)\left(\partial_x \Phi(x)\right)\Phi^{m-1}(x). \tag{D.5}$$

We can propagate the derivative to the left to find

$$\sum_{n=1}^{\infty} \frac{i^n}{n!} \sum_{m=1}^{n} \Phi^{n-m}(x)\left(\partial_x \Phi(x)\right)\Phi^{m-1}(x)$$
$$= \sum_{n=1}^{\infty} \frac{i^n}{n!} \sum_{m=1}^{n} \left\{ \left(\partial_x \Phi(x)\right)\Phi^{n-m}(x) + \left[\Phi^{n-m}(x), \partial_x \Phi(x)\right] \right\} \Phi^{m-1}(x). \tag{D.6}$$

Using the identity

$$\left[\Phi^{n-m}(x), \partial_x \Phi(x)\right] = (n-m)\left[\Phi(x), \partial_x \Phi(x)\right]\Phi^{n-m-1}(x) \tag{D.7}$$

we find

$$\sum_{n=1}^{\infty} \frac{i^n}{n!} \sum_{m=1}^{n} \left\{ (\partial_x \Phi(x))\,\Phi^{n-m}(x) + \left[\Phi^{n-m}(x), \partial_x \Phi(x)\right] \right\} \Phi^{m-1}(x)$$

$$= \sum_{n=1}^{\infty} \frac{i^n}{n!} \sum_{m=1}^{n} \left\{ (\partial_x \Phi(x))\,\Phi^{n-m}(x) + (n-m)\left[\Phi(x), \partial_x \Phi(x)\right]\Phi^{n-m-1}(x) \right\} \Phi^{m-1}(x)$$

$$= \sum_{n=1}^{\infty} \frac{i^n}{n!} \sum_{m=1}^{n} \left\{ (\partial_x \Phi(x))\,\Phi^{n-1}(x) + (n-m)\left[\Phi(x), \partial_x \Phi(x)\right]\Phi^{n-2}(x) \right\}$$

$$= \sum_{n=1}^{\infty} \frac{i^n}{n!} \left\{ n\,(\partial_x \Phi(x))\,\Phi^{n-1}(x) + \frac{n(n-1)}{2}\left[\Phi(x), \partial_x \Phi(x)\right]\Phi^{n-2}(x) \right\} \tag{D.8}$$

The first term can be evaluated by shifting the index by one to $k = n - 1$

$$\partial_x \Phi(x) \sum_{n=1}^{\infty} \frac{i^n n}{n!}\Phi^{n-1}(x) = \partial_x \Phi(x) \sum_{n=1}^{\infty} \frac{i^n}{(n-1)!}\Phi^{n-1}(x)$$

$$= i\partial_x \Phi(x) \sum_{k=0}^{\infty} \frac{i^k}{(k)!}\Phi^k(x)$$

$$= i\partial_x \Phi(x)e^{i\Phi(x)}. \tag{D.9}$$

In the second term we see that due to the factor $(n-1)$, the $n=1$ term drops out, and we can form the exponential by shifting the index by two to $j = n - 2$

$$\left[\Phi(x), \partial_x \Phi(x)\right] \sum_{n=1}^{\infty} \frac{i^n}{n!} \frac{n(n-1)}{2}\Phi^{n-2}(x) = \frac{i^2}{2}\left[\Phi(x), \partial_x \Phi(x)\right]\sum_{n=2}^{\infty} \frac{i^{n-2}}{(n-2)!}\Phi^{n-2}(x)$$

$$= -\frac{1}{2}\left[\Phi(x), \partial_x \Phi(x)\right]\sum_{j=0}^{\infty} \frac{i^j}{j!}\Phi^j(x)$$

$$= -\frac{1}{2}\left[\Phi(x), \partial_x \Phi(x)\right]e^{i\Phi(x)}. \tag{D.10}$$

In conclusion, we find

$$\partial_x e^{i\Phi(x)} = \left(i\partial_x \Phi(x) - \frac{1}{2}\left[\Phi(x), \partial_x \Phi(x)\right] \right)e^{i\Phi(x)}, \tag{D.11}$$

which is the correct way of evaluating the derivative of an exponentiated operator.

Bibliography

[1] C. Timm, *Theory of Superconductivity*. Germany: TU Dresden, 2022.

[2] L. Vanucci, "Electron quantum optics at fractional filling factor: Minimal excitation states and interferometry," Ph.D. dissertation, Universit'a degli Studi di Genova, 2018.

[3] B. I. Halperin, "Statistics of Quasiparticles and the Hierarchy of Fractional Quantized Hall States," *Physical Review Letters*, vol. 52, no. 18, pp. 1583–1586, Apr. 1984.

[4] D. Arovas, J. R. Schrieffer, and F. Wilczek, "Fractional Statistics and the Quantum Hall Effect," *Physical Review Letters*, vol. 53, no. 7, pp. 722–723, Aug. 1984.

[5] H. Bartolomei, M. Kumar, R. Bisognin, A. Marguerite, J.-M. Berroir, E. Bocquillon, B. Plaçais, A. Cavanna, Q. Dong, U. Gennser, Y. Jin, and G. Fève, "Fractional statistics in anyon collisions," *Science*, vol. 368, no. 6487, pp. 173–177, Apr. 2020.

[6] J. M. Leinaas and J. Myrheim, "On the theory of identical particles," *Il Nuovo Cimento B (1971-1996)*, vol. 37, no. 1, pp. 1–23, Jan. 1977.

[7] C. Nayak, S. H. Simon, A. Stern, M. Freedman, and S. Das Sarma, "Non-Abelian anyons and topological quantum computation," *Reviews of Modern Physics*, vol. 80, no. 3, pp. 1083–1159, Sep. 2008.

[8] A. Y. Kitaev, "Fault-tolerant quantum computation by anyons," *Annals of Physics*, vol. 303, no. 1, pp. 2–30, Jan. 2003.

[9] M. Aghaee, A. Akkala, Z. Alam, R. Ali, A. A. Ramirez, M. Andrzejczuk, A. E. Antipov, P. Aseev, M. Astafev, B. Bauer, J. Becker, S. Boddapati, F. Boekhout, J. Bommer, E. B. Hansen, T. Bosma, L. Bourdet, S. Boutin, P. Caroff, L. Casparis, M. Cassidy, A. W. Christensen, N. Clay, W. S. Cole, F. Corsetti, A. Cui, P. Dalampiras, A. Dokania, G. de Lange, M. de Moor, J. C. E. Saldaña, S. Fallahi, Z. H. Fathabad, J. Gamble, G. Gardner, D. Govender, F. Griggio, R. Grigoryan, S. Gronin, J. Gukelberger, S. Heedt, J. H. Zamorano, S. Ho, U. L. Holgaard, W. H. P. Nielsen, H. Ingerslev, P. J. Krogstrup, L. Johansson, J. Jones, R. Kallaher, F. Karimi, T. Karzig, C. King, M. E. Kloster, C. Knapp, D. Kocon, J. Koski, P. Kostamo, M. Kumar, T. Laeven, T. Larsen, K. Li, T. Lindemann, J. Love, R. Lutchyn, M. Manfra, E. Memisevic, C. Nayak, B. Nijholt, M. H. Madsen, S. Markussen, E. Martinez, R. McNeil, A. Mullally, J. Nielsen, A. Nurmohamed, E. O'Farrell, K. Otani, S. Pauka, K. Petersson, L. Petit, D. Pikulin, F. Preiss, M. Q. Perez, K. Rasmussen, M. Rajpalke, D. Razmadze, O. Reentila, D. Reilly, R. Rouse, I. Sadovskyy, L. Sainiemi, S. Schreppler, V. Sidorkin, A. Singh, S. Singh, S. Sinha, P. Sohr, T. Stankevic, L. Stek, H. Suominen, J. Suter,

V. Svidenko, S. Teicher, M. Temuerhan, N. Thiyagarajah, R. Tholapi, M. Thomas, E. Toomey, S. Upadhyay, I. Urban, S. Vaitiekėnas, K. Van Hoogdalem, D. V. Viazmitinov, S. Waddy, D. Van Woerkom, D. Vogel, J. Watson, J. Weston, G. W. Winkler, C. K. Yang, S. Yau, D. Yi, E. Yucelen, A. Webster, R. Zeisel, and R. Zhao, "InAs-Al Hybrid Devices Passing the Topological Gap Protocol," *arXiv:2207.02472 [cond-mat]*, Jul. 2022.

[10] A. Y. Kitaev, "Unpaired Majorana fermions in quantum wires," *Physics-Uspekhi*, vol. 44, no. 10S, pp. 131–136, Oct. 2001.

[11] L. Fu and C. L. Kane, "Superconducting Proximity Effect and Majorana Fermions at the Surface of a Topological Insulator," *Physical Review Letters*, vol. 100, no. 9, Mar. 2008.

[12] T. M. Klapwijk, "Proximity Effect From an Andreev Perspective," *Journal of Superconductivity*, vol. 17, no. 5, pp. 593–611, Oct. 2004.

[13] H. Hoppe, U. Zülicke, and G. Schön, "Andreev Reflection in Strong Magnetic Fields," *Physical Review Letters*, vol. 84, no. 8, pp. 1804–1807, Feb. 2000.

[14] F. Giazotto, M. Governale, U. Zülicke, and F. Beltram, "Andreev reflection and cyclotron motion at superconductor—normal-metal interfaces," *Physical Review B*, vol. 72, no. 5, p. 054518, Aug. 2005.

[15] J. A. M. van Ostaay, A. R. Akhmerov, and C. W. J. Beenakker, "Spin-triplet supercurrent carried by quantum Hall edge states through a Josephson junction," *Physical Review B*, vol. 83, no. 19, p. 195441, May 2011.

[16] S. Groenendijk, A. Calzona, H. Tschirhart, E. G. Idrisov, and T. L. Schmidt, "Parafermion braiding in fractional quantum Hall edge states with a finite chemical potential," *Physical Review B*, vol. 100, no. 20, Nov. 2019.

[17] J. Alicea and P. Fendley, "Topological Phases with Parafermions: Theory and Blueprints," *Annual Review of Condensed Matter Physics*, vol. 7, no. 1, pp. 119–139, Mar. 2016.

[18] V. E. Calado, S. Goswami, G. Nanda, M. Diez, A. R. Akhmerov, K. Watanabe, T. Taniguchi, T. M. Klapwijk, and L. M. K. Vandersypen, "Ballistic Josephson junctions in edge-contacted graphene," *Nature Nanotechnology*, vol. 10, no. 9, pp. 761–764, Sep. 2015.

[19] Z. Wan, A. Kazakov, M. J. Manfra, L. N. Pfeiffer, K. W. West, and L. P. Rokhinson, "Induced superconductivity in high-mobility two-dimensional electron gas in gallium arsenide heterostructures," *Nature Communications*, vol. 6, no. 1, p. 7426, Jun. 2015.

[20] F. Amet, C. T. Ke, I. V. Borzenets, J. Wang, K. Watanabe, T. Taniguchi, R. S. Deacon, M. Yamamoto, Y. Bomze, S. Tarucha, and G. Finkelstein, "Supercurrent in the quantum Hall regime," *Science*, vol. 352, no. 6288, pp. 966–969, May 2016.

[21] M. Ben Shalom, M. J. Zhu, V. I. Fal'ko, A. Mishchenko, A. V. Kretinin, K. S. Novoselov, C. R. Woods, K. Watanabe, T. Taniguchi, A. K. Geim, and J. R. Prance,

"Quantum oscillations of the critical current and high-field superconducting proximity in ballistic graphene," *Nature Physics*, vol. 12, no. 4, pp. 318–322, Apr. 2016.

[22] G.-H. Lee, K.-F. Huang, D. K. Efetov, D. S. Wei, S. Hart, T. Taniguchi, K. Watanabe, A. Yacoby, and P. Kim, "Inducing superconducting correlation in quantum Hall edge states," *Nature Physics*, vol. 13, no. 7, pp. 693–698, Apr. 2017.

[23] A. Seredinski, A. W. Draelos, E. G. Arnault, M.-T. Wei, H. Li, T. Fleming, K. Watanabe, T. Taniguchi, F. Amet, and G. Finkelstein, "Quantum Hall–based superconducting interference device," *Science Advances*, vol. 5, no. 9, Sep. 2019.

[24] L. Zhao, E. G. Arnault, A. Bondarev, A. Seredinski, T. F. Q. Larson, A. W. Draelos, H. Li, K. Watanabe, T. Taniguchi, F. Amet, H. U. Baranger, and G. Finkelstein, "Interference of chiral Andreev edge states," *Nature Physics*, vol. 16, no. 8, pp. 862–867, Aug. 2020.

[25] M. Hatefipour, J. J. Cuozzo, J. Kanter, W. M. Strickland, C. R. Allemang, T.-M. Lu, E. Rossi, and J. Shabani, "Induced Superconducting Pairing in Integer Quantum Hall Edge States," *Nano Letters*, vol. 22, no. 15, pp. 6173–6178, Aug. 2022.

[26] M. R. Sahu, A. K. Paul, J. Sutradhar, K. Watanabe, T. Taniguchi, V. Singh, S. Mukerjee, S. Banerjee, and A. Das, "Quantized conductance with nonzero shot noise as a signature of Andreev edge state," *Physical Review B*, vol. 104, no. 8, p. L081404, Aug. 2021.

[27] Ö. Gül, Y. Ronen, S. Y. Lee, H. Shapourian, J. Zauberman, Y. H. Lee, K. Watanabe, T. Taniguchi, A. Vishwanath, A. Yacoby, and P. Kim, "Andreev Reflection in the Fractional Quantum Hall State," *Physical Review X*, vol. 12, no. 2, p. 021057, Jun. 2022.

[28] A. L. R. Manesco, I. M. Flór, C.-X. Liu, and A. R. Akhmerov, "Mechanisms of Andreev reflection in quantum Hall graphene," *arXiv:2103.06722 [cond-mat]*, Mar. 2021.

[29] Y. Tang, C. Knapp, and J. Alicea, "Vortex-enabled Andreev processes in quantum Hall-superconductor hybrids," *arXiv:2207.10687 [cond-mat, physics:quant-ph]*, Jul. 2022.

[30] T. H. Galambos, F. Ronetti, B. Hetényi, D. Loss, and J. Klinovaja, "Crossed Andreev reflection in spin-polarized chiral edge states due to the Meissner effect," *Physical Review B*, vol. 106, no. 7, p. 075410, Aug. 2022.

[31] N. Schiller, B. A. Katzir, A. Stern, E. Berg, N. H. Lindner, and Y. Oreg, "Interplay of superconductivity and dissipation in quantum Hall edges," *arXiv:2202.10475 [cond-mat]*, Feb. 2022.

[32] V. D. Kurilovich, Z. M. Raines, and L. I. Glazman, "Disorder in Andreev reflection of a quantum Hall edge," *arXiv:2201.00273 [cond-mat]*, Jan. 2022.

[33] A. B. Michelsen, T. L. Schmidt, and E. G. Idrisov, "Current correlations of Cooper-pair tunneling into a quantum Hall system," *Physical Review B*, vol. 102, no. 12, p. 125402, Sep. 2020.

[34] A. B. Michelsen, P. Recher, B. Braunecker, and T. L. Schmidt, "Supercurrent-enabled Andreev reflection in a chiral quantum Hall edge state," *arXiv:2203.13384 [cond-mat]*, Mar. 2022.

[35] A. B. Michelsen, M. Valiente, N. T. Zinner, and A. Negretti, "Ion-induced interactions in a Tomonaga-Luttinger liquid," *Physical Review B*, vol. 100, no. 20, p. 205427, Nov. 2019.

[36] J. Bardeen, L. N. Cooper, and J. R. Schrieffer, "Theory of Superconductivity," *Physical Review*, vol. 108, no. 5, pp. 1175–1204, Dec. 1957.

[37] K. von Klitzing, "Essay: Quantum Hall Effect and the New International System of Units," *Physical Review Letters*, vol. 122, no. 20, p. 200001, May 2019.

[38] J. Jain, *Composite Fermions*. Cambridge University Press, 2007.

[39] B. I. Halperin, "Quantized Hall conductance, current-carrying edge states, and the existence of extended states in a two-dimensional disordered potential," *Physical Review B*, vol. 25, no. 4, pp. 2185–2190, Feb. 1982.

[40] W. N. Mei and Y. C. Lee, "Harmonic oscillator with potential barriers-exact solutions and perturbative treatments," *Journal of Physics A: Mathematical and General*, vol. 16, no. 8, pp. 1623–1632, Jun. 1983.

[41] T. Patlatiuk, C. P. Scheller, D. Hill, Y. Tserkovnyak, G. Barak, A. Yacoby, L. N. Pfeiffer, K. W. West, and D. M. Zumbühl, "Evolution of the quantum Hall bulk spectrum into chiral edge states," *Nature Communications*, vol. 9, no. 1, pp. 1–8, Sep. 2018.

[42] S. Datta, *Electronic Transport in Mesoscopic Systems*, ser. Cambridge Studies in Semiconductor Physics and Microelectronic Engineering. Cambridge: Cambridge University Press, 1995.

[43] H. L. Stormer, "Nobel Lecture: The fractional quantum Hall effect," *Reviews of Modern Physics*, vol. 71, no. 4, pp. 875–889, Jul. 1999.

[44] M. E. Cage, R. F. Dziuba, and B. F. Field, "A test of the quantum Hall effect as a resistance standard," *IEEE Transactions on Instrumentation Measurement*, vol. 34, pp. 301–303, Jun. 1985.

[45] R. B. Laughlin, "Anomalous Quantum Hall Effect: An Incompressible Quantum Fluid with Fractionally Charged Excitations," *Physical Review Letters*, vol. 50, no. 18, pp. 1395–1398, May 1983.

[46] X.-G. Wen, "Edge transport properties of the fractional quantum Hall states and weak-impurity scattering of a one-dimensional charge-density wave," *Physical Review B*, vol. 44, no. 11, pp. 5708–5719, Sep. 1991.

[47] M. Tinkham, *Introduction to Superconductivity*, 2nd ed. McGraw-Hill, 1996.

[48] G. E. Blonder, M. Tinkham, and T. M. Klapwijk, "Transition from metallic to tunneling regimes in superconducting microconstrictions: Excess current, charge imbalance, and supercurrent conversion," *Physical Review B*, vol. 25, no. 7, pp. 4515–4532, Apr. 1982.

[49] D. J. Griffiths, *Introduction to Quantum Mechanics*. Cambridge University Press, 2017.

[50] J. J. Sakurai and J. Napolitano, "Modern Quantum Mechanics," Sep. 2017.

[51] F. London, "On the Problem of the Molecular Theory of Superconductivity," *Physical Review*, vol. 74, no. 5, pp. 562–573, Sep. 1948.

[52] N. B. Kopnin, *Theory of Superconductivity*, Helsinki University, Finland, 2006.

[53] P. F. Bagwell, "Critical current of a one-dimensional superconductor," *Physical Review B*, vol. 49, no. 10, pp. 6841–6846, Mar. 1994.

[54] R. Hu, G. L. Kerber, J. Luine, E. Ladizinsky, and J. Bulman, "Sputter deposition conditions and penetration depth in NbN thin films," *IEEE Transactions on Applied Superconductivity*, vol. 13, no. 2, pp. 3288–3291, Jun. 2003.

[55] A. Kamlapure, M. Mondal, M. Chand, A. Mishra, J. Jesudasan, V. Bagwe, L. Benfatto, V. Tripathi, and P. Raychaudhuri, "Measurement of magnetic penetration depth and superconducting energy gap in very thin epitaxial NbN films," *Applied Physics Letters*, vol. 96, no. 7, p. 072509, Feb. 2010.

[56] K. Makise, Y. Mizokami, T. Nogami, G. Sawada, T. Asano, B. Shinozaki, and F. Ichikawa, "Estimations of superconducting fluctuation effects in amorphous MoRu and MoRe alloy thin films," *Materials Research Express*, vol. 5, no. 9, p. 096406, Aug. 2018.

[57] L. M. Joshi, A. Verma, A. Gupta, P. K. Rout, S. Husale, and R. C. Budhani, "Superconducting properties of NbN film, bridge and meanders," *AIP Advances*, vol. 8, no. 5, p. 055305, May 2018.

[58] M. P. A. Fisher, "Cooper-pair tunneling into a quantum Hall fluid," *Physical Review B*, vol. 49, no. 20, pp. 14 550–14 553, May 1994.

[59] Y. A. Bychkov and E. I. Rashba, "Oscillatory effects and the magnetic susceptibility of carriers in inversion layers," *Journal of Physics C: Solid State Physics*, vol. 17, no. 33, pp. 6039–6045, Nov. 1984.

[60] Y. Kim, J. Zhang, E. Rossi, and R. M. Lutchyn, "Impurity-induced bound states in superconductors with spin-orbit coupling," *Physical Review Letters*, vol. 114, no. 23, p. 236804, Jun. 2015.

[61] F. Rohlfing, G. Tkachov, F. Otto, K. Richter, D. Weiss, G. Borghs, and C. Strunk, "Doppler shift in Andreev reflection from a moving superconducting condensate in Nb/InAs Josephson junctions," *Physical Review B*, vol. 80, no. 22, p. 220507, Dec. 2009.

[62] A. Altland and B. Simons, *Condensed Matter Field Theory*, 2nd ed. Cambridge: Cambridge Univ. Press, 2010.

[63] T. Lancaster and S. Blundell, *Quantum Field Theory for the Gifted Amateur*, 1st ed. Oxford: Oxford Univ. Press, 2014.

[64] J. Linder and A. V. Balatsky, "Odd-frequency superconductivity," *Reviews of Modern Physics*, vol. 91, no. 4, p. 045005, Dec. 2019, publisher: American Physical Society.

[65] N. Read and D. Green, "Paired states of fermions in two dimensions with breaking of parity and time-reversal symmetries and the fractional quantum Hall effect," *Physical Review B*, vol. 61, no. 15, pp. 10 267–10 297, Apr. 2000.

[66] M. R. Geller and W. Kohn, "Quantum mechanics of electrons in crystals with graded composition," *Physical Review Letters*, vol. 70, no. 20, pp. 3103–3106, May 1993.

[67] N. M. R. Peres, "Scattering in one-dimensional heterostructures described by the Dirac equation," *Journal of Physics: Condensed Matter*, vol. 21, no. 9, p. 095501, Jan. 2009.

[68] G.-H. Park, M. Kim, K. Watanabe, T. Taniguchi, and H.-J. Lee, "Propagation of superconducting coherence via chiral quantum-Hall edge channels," *Scientific Reports*, vol. 7, no. 1, Dec. 2017.

[69] T. Wakamura, N. Hasegawa, K. Ohnishi, Y. Niimi, and Y. Otani, "Spin Injection into a Superconductor with Strong Spin-Orbit Coupling," *Physical Review Letters*, vol. 112, no. 3, p. 036602, Jan. 2014.

[70] X.-G. Wen, "Topological orders and edge excitations in fractional quantum Hall states," *Advances in Physics*, vol. 44, no. 5, pp. 405–473, Oct. 1995.

[71] T. Giamarchi, *Quantum Physics in One Dimension*, 1st ed. Oxford University Press, 2003.

[72] X.-G. Wen, *Quantum Field Theory of Many-Body Systems: From the Origin of Sound to an Origin of Light and Electrons*, ser. Oxford Graduate Texts. Oxford: Oxford University Press, 2007.

[73] K. T. Law, D. E. Feldman, and Y. Gefen, "Electronic Mach-Zehnder interferometer as a tool to probe fractional statistics," *Physical Review B*, vol. 74, no. 4, Jul. 2006.

[74] E. Miranda, "Introduction to bosonization," *Brazilian Journal of Physics*, vol. 33, no. 1, Mar. 2003.

[75] C. L. Kane and M. P. A. Fisher, "Impurity scattering and transport of fractional quantum Hall edge states," *Physical Review B*, vol. 51, no. 19, pp. 13 449–13 466, May 1995.

[76] D. C. Glattli, "Tunneling Experiments in the Fractional Quantum Hall Effect Regime," in *The Quantum Hall Effect*, ser. Progress in Mathematical Physics, B. Douçot, V. Pasquier, B. Duplantier, and V. Rivasseau, Eds. Birkhäuser, Basel, 2005, vol. 45, ch. Tunneling experiments in the fractional Quantum Hall effect regime, pp. 163–197.

[77] A. Larkin and A. Varlamov, *Theory of Fluctuations in Superconductors*, ser. International Series of Monographs on Physics. Oxford: Oxford University Press, 2005.

[78] J. Rammer and H. Smith, "Quantum field-theoretical methods in transport theory of metals," *Reviews of Modern Physics*, vol. 58, no. 2, pp. 323–359, Apr. 1986.

[79] E. G. Idrisov, "Finite frequency noise in a chiral Luttinger liquid coupled to phonons," *Physical Review B*, vol. 100, no. 15, p. 155422, Oct. 2019.

[80] Y. M. Blanter and M. Büttiker, "Shot noise in mesoscopic conductors," *Physics Reports*, vol. 336, no. 1, pp. 1–166, Sep. 2000.

[81] G. B. Lesovik and I. A. Sadovskyy, "Scattering matrix approach to the description of quantum electron transport," *Physics-Uspekhi*, vol. 54, no. 10, p. 1007, Oct. 2011.

[82] I. Levkivskyi, *Mesoscopic Quantum Hall Effect*, ser. Springer Theses. Berlin, Heidelberg: Springer, 2012.

[83] I. P. Levkivskyi and E. V. Sukhorukov, "Shot-Noise Thermometry of the Quantum Hall Edge States," *Physical Review Letters*, vol. 109, no. 24, p. 246806, Dec. 2012.

[84] A. O. Slobodeniuk, E. G. Idrisov, and E. V. Sukhorukov, "Relaxation of an electron wave packet at the quantum Hall edge at filling factor two," *Physical Review B*, vol. 93, no. 3, p. 035421, Jan. 2016.

[85] C. de C. Chamon, D. E. Freed, and X. G. Wen, "Tunneling and quantum noise in one-dimensional Luttinger liquids," *Physical Review B*, vol. 51, no. 4, pp. 2363–2379, Jan. 1995.

[86] G. Dattoli and A. Dipace, "Remarks on the derivation of sum rules of special functions," *Il Nuovo Cimento B (1971-1996)*, vol. 87, no. 1, pp. 50–54, May 1985.

[87] M. Kapfer, P. Roulleau, M. Santin, I. Farrer, D. A. Ritchie, and D. C. Glattli, "A Josephson relation for fractionally charged anyons," *Science (New York, N.Y.)*, vol. 363, no. 6429, pp. 846–849, 2019.

[88] H. Doerk, "An atom-ion quantum gate," Ph.D. dissertation, Universität Ulm, 2008.